




2022

On Flow Polytopes, nu -Associahedra, and the Subdivision Algebra

Matias von Bell

University of Kentucky, matias.vonbell@gmail.com

Author ORCID Identifier:

 <https://orcid.org/0000-0003-4288-4329>

Digital Object Identifier: <https://doi.org/10.13023/etd.2022.184>

[Right click to open a feedback form in a new tab to let us know how this document benefits you.](#)

Recommended Citation

von Bell, Matias, "On Flow Polytopes, nu -Associahedra, and the Subdivision Algebra" (2022). *Theses and Dissertations--Mathematics*. 90.

https://uknowledge.uky.edu/math_etds/90

This Doctoral Dissertation is brought to you for free and open access by the Mathematics at UKnowledge. It has been accepted for inclusion in Theses and Dissertations--Mathematics by an authorized administrator of UKnowledge. For more information, please contact UKnowledge@lsv.uky.edu.

STUDENT AGREEMENT:

I represent that my thesis or dissertation and abstract are my original work. Proper attribution has been given to all outside sources. I understand that I am solely responsible for obtaining any needed copyright permissions. I have obtained needed written permission statement(s) from the owner(s) of each third-party copyrighted matter to be included in my work, allowing electronic distribution (if such use is not permitted by the fair use doctrine) which will be submitted to UKnowledge as Additional File.

I hereby grant to The University of Kentucky and its agents the irrevocable, non-exclusive, and royalty-free license to archive and make accessible my work in whole or in part in all forms of media, now or hereafter known. I agree that the document mentioned above may be made available immediately for worldwide access unless an embargo applies.

I retain all other ownership rights to the copyright of my work. I also retain the right to use in future works (such as articles or books) all or part of my work. I understand that I am free to register the copyright to my work.

REVIEW, APPROVAL AND ACCEPTANCE

The document mentioned above has been reviewed and accepted by the student's advisor, on behalf of the advisory committee, and by the Director of Graduate Studies (DGS), on behalf of the program; we verify that this is the final, approved version of the student's thesis including all changes required by the advisory committee. The undersigned agree to abide by the statements above.

Matias von Bell, Student

Dr. Martha Yip, Major Professor

Dr. Benjamin Braun, Director of Graduate Studies

On Flow Polytopes, ν -Associahedra, and the Subdivision Algebra

DISSERTATION

A dissertation submitted in partial
fulfillment of the requirements for
the degree of Doctor of Philosophy
in the College of Arts and Sciences
at the University of Kentucky

By
Matias K. von Bell
Lexington, Kentucky

Director: Dr. Martha Yip, Professor of Mathematics
Lexington, Kentucky
2022

Copyright©Matias K. von Bell 2022
<https://orcid.org/0000-0003-4288-4329>

ABSTRACT OF DISSERTATION

On Flow Polytopes, ν -Associahedra, and the Subdivision Algebra

This dissertation studies the geometry and combinatorics related to a flow polytope $\mathcal{F}_{\text{car}(\nu)}$ constructed from a lattice path ν , whose volume is given by the ν -Catalan numbers. It begins with a study of the ν -associahedron introduced by Ceballos, Padrol, and Sarmiento in 2019, but from the perspective of Schröder combinatorics. Some classical results for Schröder paths are extended to the ν -setting, and insights into the geometry of the ν -associahedron are obtained by describing its face poset with two ν -Schröder objects. The ν -associahedron is then shown to be dual to a framed triangulation of $\mathcal{F}_{\text{car}(\nu)}$, which is a geometric realization of the ν -Tamari complex. The dual graph of this triangulation is the Hasse diagram of the ν -Tamari lattice due to Préville-Ratelle and Viennot. The dual graph of a second framed triangulation of $\mathcal{F}_{\text{car}(\nu)}$ is shown to be the Hasse diagram of a principal order ideal of Young's lattice generated by ν , and is used to show that the h^* -vector of $\mathcal{F}_{\text{car}(\nu)}$ is given by ν -Narayana numbers. This perspective serves to unify these two important lattices associated with ν -Dyck paths through framed triangulations of a flow polytope. Via an integral equivalence between $\mathcal{F}_{\text{car}(\nu)}$ and a subpolytope $\mathcal{U}_{I,\bar{J}}$ of a product of two simplices $\Delta_a \times \Delta_b$, subdivisions of $\mathcal{U}_{I,\bar{J}}$ are shown to be obtainable with Mészáros' subdivision algebra, which answers a question of Ceballos, Padrol, and Sarmiento. Building on this result, the subdivision algebra is extended to encode subdivisions of $\Delta_a \times \Delta_b$, giving a new tool for their future study.

KEYWORDS: Flow polytope, triangulation, subdivision algebra, associahedron

Matias K. von Bell

May 3, 2022

On Flow Polytopes, ν -Associahedra, and the Subdivision Algebra

By
Matias K. von Bell

Dr. Martha Yip

Director of Dissertation

Dr. Benjamin Braun

Director of Graduate Studies

May 3, 2022

Date

ACKNOWLEDGMENTS

My deepest gratitude goes to all of my mathematics teachers and professors throughout the years, whose time invested in me I do not take for granted.

I thank all of my elementary school teachers, in particular 冯老师 and 李老师 at 衡阳路小学 for memorable lessons on the multiplication table and for teaching the use of an abacus.

I thank all my secondary school teachers. Micah Gurley for making Algebra 1/2 fun. Timothy Robuck for teaching me about sequences, and for letting me marry his daughter many years later. Ritva Heino at Lumon Lukio for introducing me to differential and integral calculus. Matti Kuosmanen for his generous tutoring and for preparing me for my Finnish matriculation exam in mathematics.

I thank all my undergraduate professors. David Coulliette for bringing joy and humor into the mathematics classroom, and encouraging me after failing his calculus exam. Duk Lee for his high standards and expectations, and for teaching me the need to work hard. I want to express my deepest gratitude to Kenneth Rietz, who's *Logic and Sets* course ignited my passion for mathematics. His continued mentorship, encouragement, and guidance have been of incalculable value to me ever since. I also thank him for encouraging me to apply to graduate school, and believing in my ability to succeed.

I thank my professors during my time at the University of Helsinki, in particular Erik Elfving and Anne-Maria Ernvall-Hytönen for their teaching and guidance.

I thank all of my professors at the University of Kentucky. Benjamin Braun for his helpful advice and for facilitating an enjoyable atmosphere in the department as the Director of Graduate Studies. I thank Richard Ehrenborg for several inspiring

conversations and helpful suggestions. I am deeply grateful to Martha Yip for her excellent advising. Her guidance, encouragement, and support have been invaluable.

I wish to thank each member of my doctoral committee: Benjamin Braun, Richard Ehrenborg, Renee Fatemi, Timothy Gorringer, and Martha Yip.

I thank all of my research collaborators, from whom I have learned so much, and with whom doing mathematics has been a true joy: Caroline Bang, Benjamin Braun, Kaitlin Bruegge, Eric Culver, Mark Denker, Jessica Dickson, Stoyan Dimitrov, Rafael González D'León, Derek Hanely, Paul Horn, Kate Lorenzen, Rachel Perrier, Zachary Peterson, Khrystyna Serhiyenko, Sheila Sundaram, Julie Vega, Andrés Vindas-Meléndez, and Martha Yip.

I thank all of my friends, for their generous friendship and support.

I wish to convey a special gratitude to my parents, Carl von Bell and Ritva Lehonkoski, for teaching me to pursue truth, and for instilling in me a deep curiosity about the world.

I am deeply indebted to my wife, Evelyn von Bell, especially for carrying our first child during the writing of this dissertation. Although I am unable to count the ways in which I am grateful, I have always been able to count on her tremendous love, patience, and support.

Above all $IX\Theta Y\Sigma$.

Thank you! Kiitos! Tack ska du ha! 谢谢!

TABLE OF CONTENTS

Acknowledgments iii

List of Tables vii

List of Figures viii

Chapter 1 Introduction 1

Chapter 2 Background 5

 2.1 Lattice polytopes and their triangulations 5

 2.2 Root polytopes 10

 2.3 Flow polytopes 11

 2.4 The subdivision algebra 16

 2.5 The ν -associahedron and ν -Tamari lattice 20

 2.5.1 The ν -associahedron 21

 2.5.2 The ν -Tamari lattice 23

 2.6 The ν -cyclohedron 26

Chapter 3 The ν -associahedron and Schröder combinatorics 28

 3.1 ν -Schröder objects 28

 3.1.1 ν -Schröder paths 28

 3.1.2 ν -Schröder trees 33

 3.1.3 The posets of ν -Schröder paths and trees 36

 3.2 The face poset of the ν -associahedron 41

 3.2.1 Contractibility of the ν -associahedron 43

Chapter 4 The family of ν -caracol flow polytopes 47

 4.1 The ν -caracol flow polytope 47

 4.1.1 The volume of $\mathcal{F}_{\text{car}(\nu)}$ 48

 4.2 Framed triangulations of $\mathcal{F}_{\text{car}(\nu)}$ 50

 4.2.1 The length-framed triangulation 51

 4.2.2 The planar-framed triangulation 54

 4.2.3 Comparing the length-framed and planar-framed triangulations 56

 4.2.4 The h^* -vector of the ν -caracol flow polytope 57

 4.2.5 A connection with order polytopes 59

 4.3 The polytope $\mathcal{U}_{I, \bar{J}}$ 62

 4.3.1 The graph $G(I, \bar{J})$ 62

 4.3.2 A subdivision algebra for $\mathcal{U}_{I, \bar{J}}$ 65

 4.3.3 The ν -Tamari complex via the subdivision algebra 69

Chapter 5 A subdivision algebra for $\Delta_a \times \Delta_b$ via flow polytopes 72

5.1	Flow polytopes and negative flows	73
5.2	The flow polytope $\mathcal{F}_{\tilde{G}_B(\nu)}$ and its simplex subdivisions	76
5.2.1	The flow polytope $\mathcal{F}_{\tilde{G}_B(\nu)}$	76
5.2.2	The simplex subdivision	77
5.3	A subdivision algebra for $\Delta_a \times \Delta_b$	79
5.3.1	The ν -cyclohedra triangulations of $\mathcal{F}_{\tilde{G}_B(\nu)}$	83
Chapter 6	Future directions	86
6.1	Maximal clique posets	86
6.2	ν -Permutohedra	86
6.3	Applications of the subdivision algebra for $\Delta_a \times \Delta_b$	87
	Bibliography	88
	Vita	93

LIST OF TABLES

4.1 ν -Catalan objects and their role in the combinatorial structure of the two framed triangulations.	51
--	----

LIST OF FIGURES

1.1	A lattice path.	1
1.2	Three ν -Dyck paths.	2
2.1	Some polytopes in dimensions 1, 2, and 3.	6
2.2	A 2-simplex and its face lattice.	7
2.3	Three affinely equivalent polytopes.	8
2.4	The root polytope \mathcal{R}_2^+ is contained in \mathcal{R}_2	11
2.5	An a -flow (left) and a u -flow (right) on a graph G	12
2.6	A graph G and its flow polytope \mathcal{F}_G (visualized in \mathbb{R}^3).	13
2.7	The graph $\text{car}(6)$ and the associated vector partitions.	14
2.8	The correspondence between vector partitions and Dyck paths.	15
2.9	A framing at a vertex and coherent routes.	15
2.10	A graphical representation of a reduction.	16
2.11	A reduction tree corresponding to the reductions in Example 2.4.2.	17
2.12	The subdivision of \mathcal{R}_2^+ encoded by $x_{12}x_{13} + x_{13}x_{23} + \beta x_{13}$	18
2.13	Partial and full augmentations of a graph G	19
2.14	A visualization of the integral equivalences in Lemma 2.4.7.	19
2.15	The correspondence between the routes not shared by \tilde{H} and \tilde{G}	20
2.16	The 2-associahedron with faces labeled using three different objects.	21
2.17	Three (I, \bar{J}) -forests. The two left-most graphs are also covering (I, \bar{J}) -forests, while the left-most graph is the only (I, \bar{J}) -tree.	22
2.18	Various paths ν and their corresponding ν -associahedra.	23
2.19	Three corresponding ν -Catalan objects.	24
2.20	A ν -Tamari lattice arising from three combinatorial objects.	24
2.21	The six configurations of cyclically crossing arcs.	26
2.22	Two cyclic (I, J) -trees. The left tree is also an (I, J) -tree.	27
2.23	A cyclic ν -Tamari poset.	27
3.1	Various ν -Schröder paths.	29
3.2	High peaks and valley points determine ν -Dyck paths.	30
3.3	A ν -tree (left) and a ν -Schröder tree (right), where $\nu = \nu(3, 5)$	34
3.4	Rotations in a ν -tree.	35
3.5	A diagonal contraction at the node (1,2).	35
3.6	The right and left flushing maps.	38
3.7	A right and left contraction.	40
3.8	A diagonal contraction.	40
3.9	An (I, \bar{J}) -forest and the corresponding ν -Schröder tree.	41
3.10	A ν -associahedron with its faces indexed by ν -Schröder paths.	43
3.11	A contraction poset of ν -Schröder paths.	45
4.1	A lattice path and its associated ν -caracol graph.	48
4.2	Correspondence between a gravity diagram and a ν -Dyck path.	50

4.3	The edge labeling for source and sink edges in $\text{car}(\nu(5, 3))$	50
4.4	A maximal clique in the length framing and its corresponding (I, \bar{J}) -tree.	52
4.5	A maximal clique in the length framing and its corresponding ν -tree.	54
4.6	A maximal clique in the length framing and its corresponding ν -Dyck path.	56
4.7	A ν -Tamari lattice and a principal order ideal in Young's lattice.	57
4.8	The graph $\text{car}(\nu)$ and its truncated dual.	60
4.9	Various graphs associated to the valid pair $I = \{1, 2, 3, 5, 9\}$ and $\bar{J} = \{\bar{2}, \bar{7}, \bar{8}, \bar{9}\}$	64
4.10	Contracting idle edges in $\widehat{G}(I, \bar{J})$ and $\text{car}(\nu)$ gives the graph H up to relabeling of the vertices. Here $I = \{1, 2, 3, 5, 9\}$ and $\bar{J} = \{\bar{2}, \bar{7}, \bar{8}, \bar{9}\}$	66
4.11	The (I, \bar{J}) -tree corresponding to the monomial $x_{12}x_{17}x_{37}x_{18}x_{19}$	69
5.1	A lattice path encoding a simplex in the staircase triangulation of $\Delta_3 \times \Delta_2$. The six vertices of the simplex (right) are given by the six lattice points on the lattice path.	72
5.2	Two graphs with integrally equivalent flow polytopes.	73
5.3	A graph $G_B(\nu)$ with its partially augmented counterpart $\widehat{G}_B(\nu)$	77
5.4	A decomposition of $G_B(\nu)$ into the possible $G(\nu, i)$	78
5.5	A reordering of the inner vertices of $\widehat{G}(\nu, 2)$ gives $\widehat{G}(\bar{\nu}(2), w)$ up to a relabeling of inner vertices.	80
5.6	The dual graph of the triangulation obtained in Example 5.3.5.	82
5.7	Two graphs and their corresponding cyclic (I, \bar{J}) -trees.	84
5.8	Obtaining the cyclohedron via the subdivision algebra.	85

Chapter 1 Introduction

The use of combinatorial objects is ubiquitous in modern mathematics. Graphs, trees, tableaux, posets, partitions, permutations, etc., although fascinating in and of themselves, can serve as information encoding devices for succinctly capturing complex mathematical ideas. This power of combinatorial objects has contributed to the thriving fields of algebraic combinatorics and discrete geometry. Algebraic combinatorics is concerned with employing algebraic techniques for solving combinatorial problems, and conversely, using combinatorial objects to study algebraic structures. For instance, Young tableaux have proven to be of great utility in Schubert calculus and representation theory, as they conveniently encode group representation of the symmetric group and general linear groups. Discrete geometry on the other hand is concerned with the study of enumerative and combinatorial properties of geometric objects, including convex polytopes, hyperplane arrangements, and simplicial complexes. Many combinatorial objects also give rise to interesting geometric structures. For example, permutations give rise to permutohedra, graphs to symmetric edge polytopes, posets to order polytopes, etc. The topics of this dissertation lie in the intersection of algebraic combinatorics and discrete geometry, and we will witness their delicate interplay.

The primary combinatorial objects we will encounter in this dissertation are lattice paths. Given a point (a, b) where a and b are nonnegative integers, by a **lattice path** we will mean a sequence of steps beginning at the origin and ending at (a, b) . In general, the steps can be vectors $(i, j) \in \mathbb{Z}_{\geq 0}^2$, although we will mainly consider two types of steps: **east steps** $E := (1, 0)$ and **north steps** $N := (0, 1)$. Therefore we will generally use “lattice path” to mean a path consisting only of E and N steps, unless stated otherwise.

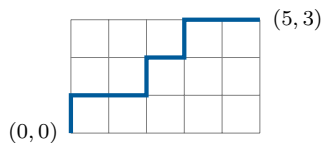


Figure 1.1: A lattice path.

A lattice path can then be written as a word in the alphabet $\{E, N\}$. For example, the lattice path in Figure 1.1 can be written as the word $NEENENE$. A lattice path to the point (a, b) has a total of $a + b$ steps, with the number of east and north steps given by a and b respectively. We can therefore enumerate the lattice paths to (a, b) by counting the words of length $a + b$ with a copies of the letter E and b copies of the letter N . As a result, there are $\binom{a+b}{a} = \binom{a+b}{b} = \frac{(a+b)!}{a!b!}$ lattice paths to the point (a, b) .

Perhaps the most well-known set of lattice paths are the **Dyck paths**, which are lattice paths staying weakly above the line $y = x$. The number of Dyck paths to a point (n, n) is given by the n -th **Catalan number** $\text{Cat}(n) = \frac{1}{n+1} \binom{2n}{n}$. Catalan

numbers have been of great interest for combinatorialists, and they are known to count over two hundred different combinatorial objects. A collection of these objects was compiled by Stanley [65].

A Dyck path to the point (n, n) can equivalently be defined as a lattice path using steps E and N which stays weakly above the staircase shaped path $(NE)^n$. From this perspective it is natural to consider generalizations of Dyck paths by replacing the staircase path with some other fixed path ν , leading to the following definition. A ν -**Dyck path** is a lattice path using steps E and N staying weakly above a fixed path ν , and the ν -**Catalan number** $\text{Cat}(\nu)$ is the number of ν -Dyck paths.

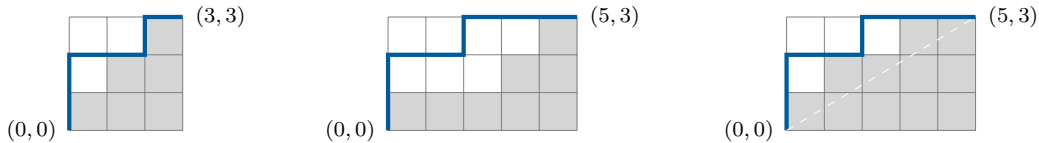


Figure 1.2: Three ν -Dyck paths.

Note that the number of initial N steps and terminal E steps in ν does not change the number of ν -Dyck paths. When enumerating ν -Dyck paths, we can therefore assume that ν begins with an N step, in which case the ν -Catalan number $\text{Cat}(\nu)$ can be calculated by the following determinantal formula

$$\text{Cat}(\nu) = \det \left(\begin{pmatrix} 1 + \sum_{k=1}^{b-j} \nu_k \\ 1 + j - i \end{pmatrix} \right)_{1 \leq i, j \leq b-1},$$

where ν_k denotes the number of E steps immediately following the k -th N step of ν . This formula is derived by an application of the Gessel–Viennot Lemma [37], but no closed-form positive formula is known for general ν . For certain special cases, such formulas do exist. An important such case is when a and b are coprime and ν is the lattice path to (a, b) that borders the squares intersecting the line $y = \frac{b}{a}x$. In this case, we write $\nu(a, b)$ to denote the path ν determined by (a, b) . Any $\nu(a, b)$ -Dyck path is then referred to as a **rational (a, b) -Dyck path**. For example, the right-most ν -Dyck path in Figure 1.2 is a rational $(5, 3)$ -Dyck path. The classical Dyck paths are not rational Dyck paths, as a and b are not coprime when $a = b$. However, since $\nu(n, n + 1) = (NE)^n E$, the rational $(n, n + 1)$ -Dyck paths can be identified with the classical Dyck paths by removing the final E step. In this sense, the rational (a, b) -Dyck paths include the classical case. Rational (a, b) -Dyck paths are enumerated by the **rational Catalan number** $\text{Cat}(a, b) = \frac{1}{a+b} \binom{a+b}{a}$. For more on rational Dyck paths, we refer the reader to the work of Armstrong, Rhoades, and Williams [7], and Armstrong, Loehr, and Warrington [6].

Lattice paths are closely related to integer partitions. In particular, a lattice path ν in the rectangular grid defined by $(0, 0)$ to (a, b) naturally corresponds with an integer partition $\lambda(\nu) = (\lambda_1, \dots, \lambda_b)$, where λ_k is the number of E steps appearing before the $(b-k+1)$ -th N step in ν . The Young diagram for $\lambda(\nu)$ may be visualized as

the region within the rectangle from $(0, 0)$ to (a, b) which lies NW of ν . For example, the regions of white boxes above each ν in Figure 1.2 are the Young diagrams of the partitions $(2, 1, 0)$, $(4, 3, 0)$, and $(3, 1, 0)$ respectively. The set of boxes above a ν -Dyck path then encodes a partition whose Young diagram is contained in the Young diagram determined by ν . Each of the ν -Dyck paths in Figure 1.2 corresponds with the Young diagram of the partition $(2, 0, 0)$. The set of ν -Dyck paths can thus be studied as the set of Young diagrams contained in the region above ν . As lattice paths, however, ν -Dyck paths have been studied in various contexts [56, 16, 15].

Lattice paths and their corresponding words will appear throughout this dissertation, although our primary interest will not be in the lattice paths themselves. Instead, our focus will be on the geometric structures which they can encode, including various polytopes and their triangulations, along with simplicial and polytopal complexes. Without the ability to visualize these objects beyond the third dimension, their study quickly becomes difficult. However, by encoding them using lattice paths, we obtain a window into their geometric and combinatorial properties. The lattice path ν will play a key role throughout this dissertation. It will determine the set of ν -Schröder paths in Chapter 3, which capture the combinatorial structure of the ν -associahedron, giving insight into its geometry. In Chapter 4, the path ν gives rise to a flow polytope whose volume is given by $\text{Cat}(\nu)$, which has two triangulations related to known lattice structures on ν -Dyck paths. In Chapter 5, the path ν gives rise to a subdivision of a product of two simplices. With a generalization of Mészáros' subdivision algebra, these subdivisions can be refined to triangulations, one of which is a geometric realization of the cyclic ν -Tamari complex. In this way, the path ν encodes a multitude of beautiful geometric structures throughout our story. Perhaps put most simply, this dissertation is a study of the geometry encoded in a path ν .

An overview of this dissertation is as follows.

In Chapter 2 we introduce the main actors of the dissertation along with the necessary background. We first provide general background on the theory of polytopes, their triangulations, and polytopal complexes. We will also discuss specific families of polytopes, including flow polytopes, root polytopes, and techniques relevant to their study. In particular, we discuss an algebraic setting for obtaining subdivisions of these polytopes introduced by Mészáros [44, 45] known as the subdivision algebra. Certain flow polytopes and root polytopes can be encoded with a monomial in this subdivision algebra, with a reduction operation on the monomial encoding subdivisions of these polytopes. Further background on ν -Dyck paths and the relevant geometric objects associated to them is also provided. This includes background on the ν -Tamari lattice introduced by Préville-Ratelle and Viennot [56], and its connection to the ν -associahedron and ν -cyclohedron introduced by Ceballos, Padrol, and Sarmiento [16].

Chapter 3 details a study of the ν -associahedron from a lattice path perspective, conducted by the present author in collaboration with Martha Yip [11]. We introduce and study ν -Schröder paths and trees, extending some classical results for Schröder paths to the ν -setting. We then show that ν -Schröder paths and trees give an alternate description of the face poset of the ν -associahedron. Using ν -Schröder

paths, we obtain further insight into the geometric structure of the ν -associahedron, including a proof that it is contractible via discrete Morse theory.

In Chapter 4, we establish a connection between the ν -associahedron and flow polytopes. This work was done in collaboration with Rafael González D’León, Francisco Mayorga Cetina, and Martha Yip [10]. We construct a family of flow polytopes from a lattice path ν , which we call ν -caracol flow polytopes. This family of flow polytopes is combinatorially interesting, and their volumes are given by the ν -Catalan numbers. Using a triangulation technique developed for flow polytopes by Danilov, Karzanov, and Koshevoy [24], we proceed to study two triangulations of the ν -caracol flow polytope, each of which is related to known ν -Catalan objects. The first triangulation is a geometric realization of the ν -Tamari complex, which is dual to the ν -associahedron. The second triangulation is related to filters of Young’s lattice generated by ν , and we use it to compute the h^* -polynomial of the ν -caracol flow polytope. The chapter concludes with an extension of this work by the present author and Martha Yip making explicit the connection between ν -caracol flow polytopes, acyclic root polytopes, and a subpolytope $\mathcal{U}_{I,\bar{J}}$ of a product of two simplices. These connections allow the subdivision algebra to be used to obtain triangulations of $\mathcal{U}_{I,\bar{J}}$, answering a question of Ceballos et al. [16]. We then demonstrate how to obtain the ν -Tamari complex using the subdivision algebra.

The objects of study in Chapters 3 and 4 can be broadly classified as belonging under the umbrella of type A Coxeter combinatorics. With this perspective, Chapter 5 studies their type B counterparts. For any lattice path ν , we construct a flow polytope which is integrally equivalent to the product of two simplices $\Delta_a \times \Delta_b$. We show that $\Delta_a \times \Delta_b$ can be subdivided into a union of “type A” flow polytopes, each of which can be encoded with a polynomial in the subdivision algebra. This allows for an extended subdivision algebra for $\Delta_a \times \Delta_b$, which we use to obtain the cyclic ν -Tamari complex as a special case. In this chapter, lattice paths play the role of inducing subdivisions of $\Delta_a \times \Delta_b$, which can then be refined to triangulations with the subdivision algebra.

We conclude the dissertation in Chapter 6 with a brief discussion of future directions. Three potential directions of further investigation are identified, and possible methods of studying them are considered.

Chapter 2 Background

In this chapter, we give the necessary prerequisites on the theory of polytopes and their triangulations, along with background on the geometry associated with the ν -Tamari lattice. After some general discussion of polytopes, we focus on two families of polytopes central to the remainder of this dissertation, namely flow polytopes and root polytopes. We then discuss the subdivision algebra, which is an algebraic setting in which certain flow polytopes and root polytopes can be triangulated. Finally, we give background on the ν -associahedron, ν -Tamari lattice, along with their cyclic counterparts.

2.1 Lattice polytopes and their triangulations

Polytopes play an important role in mathematics, and their study dates back to ancient times. In combinatorics, they generate a wealth of interesting enumerative questions, and their structure can be studied with the aid of combinatorial objects such as graphs and posets. Our study of polytopes will be limited to convex polytopes, and we will henceforth simply refer to them as polytopes for brevity. To further simplify matters, the polytopes of interest will all be lattice polytopes. Our overview of the background will cover only the topics and results necessary for our purposes, and we refer the interested reader to [38] and [71] for more background on polytopes, and to [27] for more background on their triangulations.

Definition 2.1.1. A polytope can be defined in either of the following two ways:

- (**\mathcal{H} -description**) A **polytope** \mathcal{P} is the solution set to a finite system of linear inequalities, which is bounded. In other words,

$$\mathcal{P} := \{\mathbf{x} \in \mathbb{R}^n \mid \mathbf{A}\mathbf{x} \leq \mathbf{b}\},$$

where $\mathbf{A} \in \mathbb{R}^{m \times n}$ is a real matrix and $\mathbf{b} \in \mathbb{R}^m$ is real a vector.

- (**\mathcal{V} -description**) A **polytope** \mathcal{P} is the convex hull of finitely many points $\mathbf{v}_1, \dots, \mathbf{v}_k \in \mathbb{R}^n$, in other words

$$\mathcal{P} := \text{conv}(\mathbf{v}_1, \dots, \mathbf{v}_k) = \left\{ \sum_{i=1}^k \lambda_i \mathbf{v}_i \mid \lambda_i \geq 0 \text{ and } \sum_{i=1}^k \lambda_i = 1 \right\}.$$

The fact that the \mathcal{H} -description and \mathcal{V} -description are equivalent definitions is not obvious, and is a well-known result in the theory of polytopes (see for example [71, Theorem 1.1]). The following definition captures much of the basic terminology for polytopes that we will use throughout this dissertation.

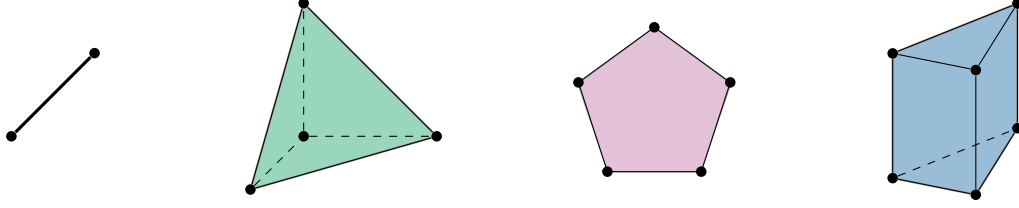


Figure 2.1: Some polytopes in dimensions 1, 2, and 3.

Definition 2.1.2. Let $\mathcal{P} \subseteq \mathbb{R}^n$ be a polytope.

- The **dimension** of \mathcal{P} is the dimension of its affine hull

$$\text{aff}(\mathcal{P}) = \left\{ \sum_{i=1}^k \lambda_i \mathbf{x}_i \mid \lambda_i \in \mathbb{R}, \mathbf{x}_i \in \mathcal{P}, \sum_{i=1}^k \lambda_i = 1 \right\}.$$

If \mathcal{P} has dimension d , then it is a **d -polytope**.

- The **normalized volume** of \mathcal{P} , denoted $\text{vol } \mathcal{P}$, is $d!$ times its Euclidean volume. Henceforth when speaking of volume, we mean the normalized volume.
- A **face** F of \mathcal{P} is any set of the form $F := \mathcal{P} \cap \{\mathbf{x} \in \mathbb{R}^n \mid \mathbf{c}^T \mathbf{x} \leq c_0\}$, where $c_0 \in \mathbb{R}$ and $\mathbf{c}^T \mathbf{x} \leq c_0$ is satisfied for all $\mathbf{x} \in \mathcal{P}$. Faces of polytopes are themselves polytopes. Note that choosing $\mathbf{c} = \mathbf{0}$ with $c_0 = 0$ gives \mathcal{P} itself, and with $c_0 = -1$ gives the **empty face**. By convention, the dimension of the empty face is chosen to be -1 .
- A **k -face** of \mathcal{P} is a k -dimensional face of \mathcal{P} . The 0-, 1-, and $(d-1)$ -faces of a d -polytope are respectively known as **vertices**, **edges**, and **facets**.
- The **face lattice** of \mathcal{P} is the lattice induced by ordering the face of \mathcal{P} by inclusion. The face lattice is ranked by the dimensions of the faces.
- \mathcal{P} is **simple** if each vertex in \mathcal{P} is adjacent to d edges (and facets), where d is the dimension of \mathcal{P} .
- \mathcal{P} is a **lattice polytope** if all of its vertices have integer coordinates.
- \mathcal{P} is a **d -simplex** if it is a d -polytope with $d+1$ vertices.

Definition 2.1.3. Two polytopes are said to be **combinatorially isomorphic** or **of the same combinatorial type** if their face lattices are isomorphic as partially ordered sets. The equivalence classes of combinatorially isomorphic polytopes are known as **combinatorial types**.

When the geometric realization of a polytope is important, we have the following notions of equivalence for polytopes.

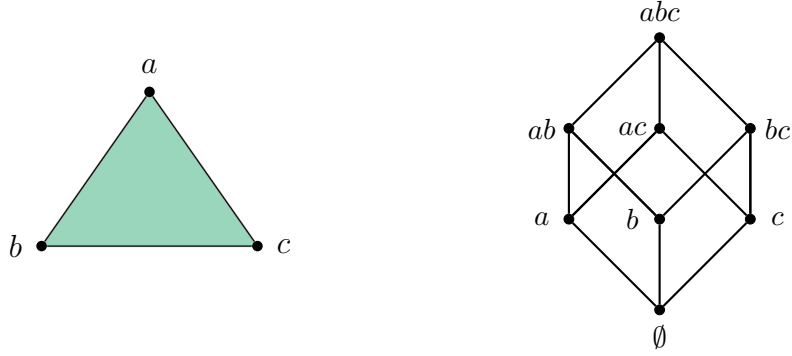


Figure 2.2: A 2-simplex and its face lattice.

Definition 2.1.4. An **affine isomorphism** between two polytopes $\mathcal{P} \subseteq \mathbb{R}^n$ and $\mathcal{Q} \subseteq \mathbb{R}^m$ is an affine transformation $\varphi : \mathbb{R}^n \rightarrow \mathbb{R}^m$ which restricts to a bijection between \mathcal{P} and \mathcal{Q} . If φ further restricts to a bijection between $\text{aff}(\mathcal{P}) \cap \mathbb{Z}^n$ and $\text{aff}(\mathcal{Q}) \cap \mathbb{Z}^m$, we say that it is an **integral equivalence**. If there is an affine isomorphism between \mathcal{P} and \mathcal{Q} , we say that they are **affinely isomorphic** and write $\mathcal{P} \cong \mathcal{Q}$. If there is an integral equivalence between \mathcal{P} and \mathcal{Q} , we say that they are **integrally equivalent** and write $\mathcal{P} \equiv \mathcal{Q}$.

Affinely isomorphic polytopes share the same face lattice, and so they are of the same combinatorial type. The notion of integral equivalence is important when we wish to preserve lattice point counts between the polytopes and their dilates, which is of primary concern in Ehrhart theory. In particular, integrally equivalent polytopes have the same Ehrhart polynomial. Our focus will not be on Ehrhart theory, and for our purposes affine isomorphisms suffice. However, since the extra condition is easy to check and our important maps will also be integral equivalences, we will use the stronger notion.

Any affine map $\psi : \mathbb{R}^n \rightarrow \mathbb{R}^n$ which restricts to a bijection from \mathbb{Z}^n to itself is an integral equivalence. A non-trivial scaling is not an integral equivalence, but the following are some easy to verify examples of integral equivalences $\mathbb{R}^n \rightarrow \mathbb{R}^n$:

- A translation $\mathbf{x} \mapsto \mathbf{x} + k\mathbf{e}_i$ where $1 \leq i \leq n$ and $k \in \mathbb{Z}$.
- A reflection across a hyperplane $\{\mathbf{x} \mid x_i = k/2\}$ where $1 \leq i \leq n$ and $k \in \mathbb{Z}$.
- A rotation of $\pi/2$ radians about a coordinate axis.

Certain projections are also integral equivalences, as shown by the following lemma.

Lemma 2.1.5. *Let $\mathcal{P} \subseteq \mathbb{R}^n$ be a lattice polytope. The projection $\varphi : \mathbb{R}^n \rightarrow \mathbb{R}^{n-1}$ given by $(x_1, \dots, x_k, \dots, x_n) \mapsto (x_1, \dots, \widehat{x}_k, \dots, x_n)$ is an integral equivalence between \mathcal{P} and its image $\varphi(\mathcal{P})$ if and only if φ restricts to a bijection between $\text{aff}(\mathcal{P}) \cap \mathbb{Z}^n$ and $\text{aff}(\varphi(\mathcal{P})) \cap \mathbb{Z}^{n-1}$.*

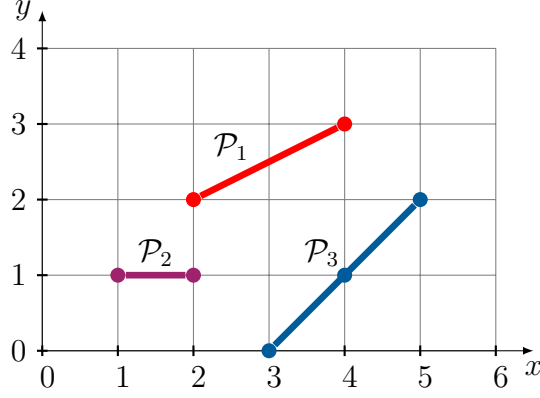


Figure 2.3: Three affinely (and combinatorially) isomorphic polytopes \mathcal{P}_1 , \mathcal{P}_2 , and \mathcal{P}_3 , of which only \mathcal{P}_1 and \mathcal{P}_2 are integrally equivalent.

Proof. Let $\mathbf{v}_1, \dots, \mathbf{v}_k$ denote the vertices of \mathcal{P} . Any point \mathbf{x} in \mathcal{P} can then be written as a convex combination of $\mathbf{v}_1, \dots, \mathbf{v}_k$, that is $\mathbf{x} = \sum_{i=1}^k \lambda_i \mathbf{v}_i$ with $0 \leq \lambda_i \leq 1$ for each i and $\sum_{i=1}^k \lambda_i = 1$. Since φ restrict to a bijection between $\text{aff}(\mathcal{P}) \cap \mathbb{Z}^n$ and $\text{aff}(\varphi(\mathcal{P})) \cap \mathbb{Z}^{n-1}$, it is a bijection between the vertices of \mathcal{P} and the vertices of $\varphi(\mathcal{P})$, and the restriction extends linearly to a bijection between \mathcal{P} and $\varphi(\mathcal{P})$. \square

Projecting the polytope \mathcal{P}_1 in Figure 2.3 to the y -axis, we see that it is integrally equivalent to \mathcal{P}_2 by a translation and rotation of $\pi/2$ radians. The polytope \mathcal{P}_3 , however, is not integrally equivalent to \mathcal{P}_1 (or \mathcal{P}_2) since any affine equivalence restricting to a bijection between them cannot be a bijection between lattice points.

Definition 2.1.6. A **triangulation** \mathcal{T} of a d -dimensional lattice polytope \mathcal{P} is a finite collection of d -simplices such that

- (i) $\mathcal{P} = \bigcup_{\Delta \in \mathcal{T}} \Delta$; and
 - (ii) $\Delta_1 \cap \Delta_2$ is a common face of Δ_1 and Δ_2 for any pair of simplices $\Delta_1, \Delta_2 \in \mathcal{T}$.
- The d -simplices are referred to as **facets** of the triangulation.

The combinatorial structure of a triangulation of a polytope is encoded in its **dual graph**, that is, the graph on the set of facets in the triangulation, with edges between facets sharing a common face of codimension one.

Definition 2.1.7. A lattice simplex $\Delta \subseteq \mathbb{R}^n$ with vertices $\mathbf{v}_1, \dots, \mathbf{v}_{k+1}$ is said to be **unimodular** if the vectors $\mathbf{v}_{k+1} - \mathbf{v}_1, \mathbf{v}_k - \mathbf{v}_1, \dots, \mathbf{v}_2 - \mathbf{v}_1$ form a lattice basis for $\text{aff}(\Delta) \cap \mathbb{Z}^n$. A triangulation \mathcal{T} is **unimodular** if all of its facets are unimodular.

Unimodular simplices have normalized volume one, so given a unimodular triangulation of a lattice polytope \mathcal{P} , the volume computation becomes an enumeration problem for simplices. For a non-unimodular simplex consider the central simplex in a unit cube formed by taking the convex hull of vertices $(0, 0, 0)$, $(1, 1, 0)$, $(1, 0, 1)$, and $(0, 1, 1)$.

Another important type of triangulation is the following.

Definition 2.1.8. A triangulation of $\mathcal{P} \subseteq \mathbb{R}^n$ is said to be **regular** if it can be obtained by projecting the lower envelope of a lifting of \mathcal{P} to \mathbb{R}^{n+1} .

Proposition 2.1.9 ([27, Proposition 2.2.4]). *Every polytope admits a regular triangulation.*

A triangulation can be thought of as a simplicial complex, which is defined as follows.

Definition 2.1.10. A **simplicial complex** \mathcal{S} is a collection of simplices such that

- (i) every face of a simplex is also in \mathcal{S} ; and
- (ii) $\sigma_1 \cap \sigma_2$ is a face of σ_1 and σ_2 for any simplices $\sigma_1, \sigma_2 \in \mathcal{S}$.

A **polytopal complex** is defined similarly by replacing the words simplex/simplices above with polytope/polytopes.

Definition 2.1.11. A simplicial complex is said to be **flag** if the cardinality of its minimal non-faces is 2. A **flag triangulation** is a triangulation that is flag as a simplicial complex.

Definition 2.1.12. The **f -vector** of a d -dimensional polytopal complex \mathcal{K} is the vector $(f_{-1}, f_0, f_1, \dots, f_d)$ where f_k is the number of k -faces in \mathcal{K} .

For simplicial complexes, it is often useful to encode the f -vector using the h -vector, which is defined as follows.

Definition 2.1.13. The **h -vector** of a d -dimensional simplicial complex \mathcal{S} is the vector (h_0, h_1, \dots, h_d) whose entries are given by

$$h_k := \sum_{i=0}^k (-1)^{k-i} \binom{d-i}{d-k} f_{i-1},$$

where f_i denotes the number of i -faces of \mathcal{S} .

An important problem in discrete geometry is the enumeration of lattice points contained in a polytope, which is the primary focus of Ehrhart theory. We give some important definitions from Ehrhart theory that we will encounter in our story, and point the interested reader to [9] for an introduction to Ehrhart theory.

Definition 2.1.14. The **t -th dilate** of a polytope $\mathcal{P} \subseteq \mathbb{R}^n$ is the polytope $t\mathcal{P} := \{t\mathbf{x} \mid \mathbf{x} \in \mathcal{P}\}$, for $t \in \mathbb{Z}_{>0}$. The **Ehrhart series** $\text{Ehr}_{\mathcal{P}}(z)$ of a polytope \mathcal{P} is the generating function whose t -th coefficient gives the lattice point count in the t -th dilate of \mathcal{P} , i.e.

$$\text{Ehr}_{\mathcal{P}}(z) = 1 + \sum_{t \geq 1} L_{\mathcal{P}}(t) z^t,$$

where $L_{\mathcal{P}}(t) := |t\mathcal{P} \cap \mathbb{Z}^n|$. When \mathcal{P} is a lattice polytope of dimension d , the Ehrhart series has the form

$$\text{Ehr}_{\mathcal{P}}(z) = \frac{h^*(z)}{(1+z)^{d+1}},$$

where $h^*(z)$ is a polynomial of degree d . The polynomial $h^*(z)$ is known as the **h^* -polynomial** of \mathcal{P} and its sequence of coefficients $(h_0^*, h_1^*, \dots, h_d^*)$ is known as the **h^* -vector** of \mathcal{P} . $L_{\mathcal{P}}(t)$ is also a polynomial of degree d known as the **Ehrhart polynomial** of \mathcal{P} . In particular, Ehrhart [33] showed that there are rational values c_1, c_2, \dots, c_d , such that

$$L_{\mathcal{P}}(t) = \sum_{i=0}^d h_i^* \binom{t+d-i}{d} = \sum_{i=0}^d c_i t^i.$$

For lattice polytopes, Stanley [61] showed that $h^*(z)$ has nonnegative coefficients. He showed further in [63] that the h^* -vector of a lattice polytope coincides with the h -vector of any of its unimodular triangulations.

2.2 Root polytopes

Root polytopes were first considered in [35], although the name was introduced later by Postnikov in [54] for the type A_n Coxeter system. Their triangulations were studied in [44]. Type C_n and D_n root polytopes and their triangulations have since also been considered [2, 19, 45]. For the purposes of our story, however, we will only consider the type A_n case.

Recall that a **root** in the type A_n root system is a vector of the form

$$\alpha_{ij} := \mathbf{e}_i - \mathbf{e}_j$$

where $1 \leq i, j \leq n+1, i \neq j$, and \mathbf{e}_k denotes the k -th standard basis vector in \mathbb{R}^{n+1} . A root α_{ij} is a **positive root** if $i < j$ and a **simple root** if $j = i + 1$. We use Φ_n to denote the set of roots in type A_n , and Φ_n^+ for the set of positive roots.

Definition 2.2.1. For $S \subseteq \Phi_n$, the associated (type A_n) **root polytope** is the polytope

$$\mathcal{R}(S) := \text{conv}\{\mathbf{0}, \alpha \mid \alpha \in S\}.$$

Choosing $S = \Phi_n^+$ gives the **positive root polytope** \mathcal{R}_n^+ , and choosing $S = \Phi_n$ gives the **full root polytope** \mathcal{R}_n .

The positive root polytope has also been called the full root polytope in the work of Mészáros [44] and Postnikov [54], but since we are not restricting ourselves to positive roots, we follow Ardila–Beck–Hoşten–Pfeifle–Seashore [2] and use “full root polytope” to mean the convex hull of all roots in Φ_n . The full root polytope was studied by Cho in [21] and also appears under the name *Legendre polytope* in the work of Hetyei [40] and Ehrenborg–Hetyei–Readdy [32].

Another special class of root polytopes are the acyclic root polytopes defined by Mészáros in [44]. Given an acyclic (undirected) graph G on vertex set $[n+1]$, each

edge (i, j) in $E(G)$ can be identified with the positive root α_{ij} . Let $\Phi_G^+ := \{\alpha_{ij} \mid (i, j) \in E(G)\}$ be the set of positive roots associated with the edges in G , and let $L(\Phi_G^+)$ denote the set of positive roots obtainable as nonnegative linear combinations of roots in Φ_G^+ . The **acyclic root polytope** is the root polytope $\mathcal{R}_G^+ := \mathcal{R}(L(\Phi_G^+))$. Letting P_n denote the path graph on n vertices, the acyclic root polytope $\mathcal{R}_{P_{n+1}}^+$ is the positive root polytope \mathcal{R}_n^+ .

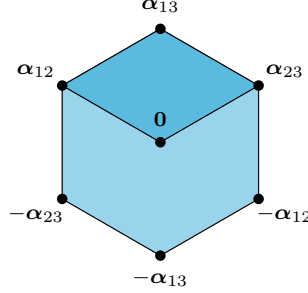


Figure 2.4: The root polytope \mathcal{R}_2^+ is contained in \mathcal{R}_2 .

2.3 Flow polytopes

Flow polytopes are a rich family of polytopes whose geometric and combinatorial study began with Baldoni and Vergne in [8] along with unpublished work by Postnikov and Stanley. Flow polytopes have received much recent attention due to their close connections to many areas, including representation theory [8], diagonal harmonics [50], Schubert polynomials [52], and toric geometry [41]. The class of flow polytopes includes (in some cases up to integral equivalence) many well-known polytopes, such as the Chan–Robbins–Yuen polytope [20], the Pitman–Stanley polytope [66], Tesler polytopes [50], certain order polytopes and faces of the alternating sign matrix polytope [51].

Definition 2.3.1. Let G be a connected directed graph on vertex set $V(G) = [n]$ and edge multiset $E(G)$ with m edges directed toward their larger vertex. At each vertex $i \in V(G)$ we assign a netflow $a_i \in \mathbb{Z}$ satisfying the balance condition $\sum_{i=1}^n a_i = 0$, and hence $a_n = -\sum_{i=1}^{n-1} a_i$. Vertices with positive, negative, and zero netflow are respectively referred to as **sources**, **sinks**, and **inner vertices**. For $\mathbf{a} = (a_1, \dots, a_{n-1}, -\sum_{i=1}^n a_i) \in \mathbb{Z}^n$, an **\mathbf{a} -flow on G** is a tuple $(x_e)_{e \in E(G)} \in \mathbb{R}^m$ satisfying

$$\sum_{e \in \text{In}(j)} x_e - \sum_{e \in \text{Out}(j)} x_e = a_j, \quad (2.1)$$

where $\text{In}(j)$ and $\text{Out}(j)$ respectively denote the set of incoming and outgoing edges at j . The **flow polytope** $\mathcal{F}_G(\mathbf{a})$ is the set of all \mathbf{a} -flows on G . A **unit flow** on G is a \mathbf{u} -flow on G where $\mathbf{u} = \mathbf{e}_1 - \mathbf{e}_n$.

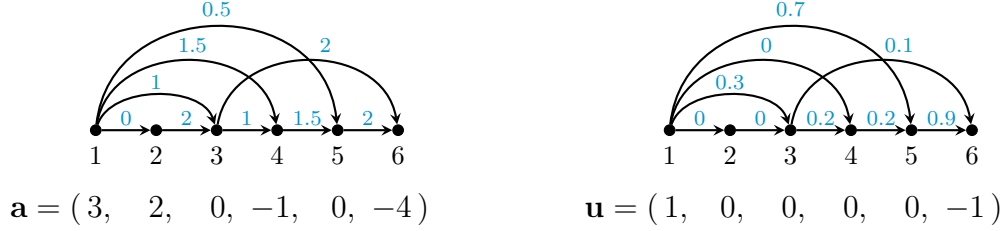


Figure 2.5: An \mathbf{a} -flow (left) and a \mathbf{u} -flow (right) on a graph G .

The fact that $\mathcal{F}_G(\mathbf{a})$ is a polytope is well-known in discrete optimization. Let \mathbf{M}_G denote the incidence matrix of the digraph G whose rows correspond to the vertices of G and columns correspond to the edges of G . Then

$$\mathcal{F}_G(\mathbf{a}) = \{\mathbf{x} \in \mathbb{R}^m \mid \mathbf{M}_G \mathbf{x} = \mathbf{a}, \mathbf{0} \leq \mathbf{x}\}. \quad (2.2)$$

In this context, $\mathcal{F}_G(\mathbf{a})$ is a lattice polytope by the Hoffman-Kruskal theorem (see [23, Theorem 4.5]) and the fact that an incidence matrix of a digraph is totally unimodular [23, Theorem 4.9]. From (2.2) we see that the dimension of $\mathcal{F}_G(\mathbf{a})$ depends only on \mathbf{M}_G and hence only the graph G . More specifically, we have the following result, which also appears in [24, Proposition 1] and [8, 51].

Lemma 2.3.2. *The dimension of a flow polytope $\mathcal{F}_G(\mathbf{a})$ is given by*

$$\dim(\mathcal{F}_G(\mathbf{a})) = |E(G)| - |V(G)| + 1.$$

Proof. We induct on the number of vertices. Let G be a graph on vertex set $[n]$. The result holds for $n = 1$, so we consider the case when $n > 1$. Deleting the vertex n and its k incident edges, we obtain a graph $G \setminus \{n\}$. We see that

$$\mathbf{M}_G = \begin{bmatrix} \mathbf{M}_{G \setminus \{n\}} & \mathbf{B} \\ \mathbf{0}^T & \mathbf{1}^T \end{bmatrix},$$

where $\mathbf{B} \in \mathbb{R}^{(n-1) \times k}$, $\mathbf{0} \in \mathbb{R}^{m-k}$ and $\mathbf{1} \in \mathbb{R}^k$. All but one of the last k columns of \mathbf{M}_G are free, so $\dim(\mathcal{F}_G(\mathbf{a})) = \dim(\mathcal{F}_{G \setminus \{n\}}(\mathbf{a})) + k - 1$. By the inductive hypothesis $\dim(\mathcal{F}_{G \setminus \{n\}}(\mathbf{a})) = |E(G)| - k + |V(G)| + 2$, and the result follows. \square

The \mathcal{V} -description of $\mathcal{F}_G(\mathbf{a})$ can be given as follows.

Proposition 2.3.3 ([49, Proposition 2.5],[41, Lemma 3.1]). *The vertices of $\mathcal{F}_G(\mathbf{a})$ are the set of \mathbf{a} -flows supported on subgraphs of G with no undirected cycles.*

Our focus will be on flow polytopes obtained as the set of all unit flows on a graph G , namely $\mathcal{F}_G(\mathbf{u})$. For this reason we will suppress notation to $\mathcal{F}_G := \mathcal{F}_G(\mathbf{u})$ for brevity. In this case, the vertices of \mathcal{F}_G are easier to describe, as they are given by paths from the source to the sink in G called **routes**. Letting \mathcal{R}_G denote the set of routes in G , we obtain the following.

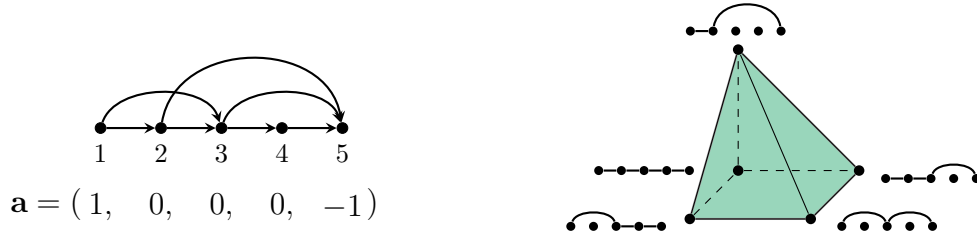


Figure 2.6: A graph G and its flow polytope \mathcal{F}_G (visualized in \mathbb{R}^3).

Corollary 2.3.4. *The flow polytope \mathcal{F}_G is a lattice polytope with \mathcal{V} -description*

$$\mathcal{F}_G = \text{conv}\{\mathbf{x}_R \mid R \in \mathcal{R}_G\}.$$

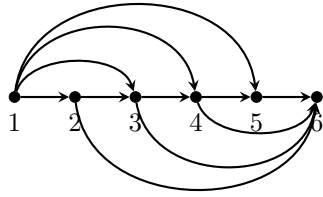
Example 2.3.5. Let G be the path graph P_5 on 5 vertices with added edges $(1, 3)$, $(2, 5)$, and $(3, 5)$. The flow polytope \mathcal{F}_G is a three dimensional polytope in \mathbb{R}^7 , and its vertices correspond to the possible routes in G (see Figure 2.6).

An edge (i, j) is said to be **idle** if it is the only outgoing edge from i , or it is the only incoming edge to j . In the graph of Figure 2.6, the edges $(1, 2)$, $(3, 4)$, and $(4, 5)$ are all idle edges. The following lemma is useful for altering the underlying graph while preserving the flow polytope up to integral equivalence.

Lemma 2.3.6 ([31, Corollary 2.13], [52, Lemma 2.2]). *If G' is obtained from G by contracting idle edges, then $\mathcal{F}_{G'} \equiv \mathcal{F}_G$.*

The volume of a flow polytope can be computed using the Lidksii formula given by Baldoni and Vergne [8], which is a sum of Kostant partition functions. Their proof is based on residue computations, while a proof revealing the underlying geometry and combinatorics was given by Mészáros and Morales in [49]. Based on the Lidksii formula, computing the volume of a flow polytope was shown in [12, Theorem 4.4] to be equivalent to enumerating combinatorial objects which they called “unified diagrams”. To state the Lidksii formula, we first need to state a few definitions and establish some notation.

Recall from Section 2.2, that the edges in a graph G can be associated with a subset Φ_G^+ of the positive roots Φ_{n-1}^+ in the type A_{n-1} root system. The **Kostant partition function** $K_G(\mathbf{a})$ is the number vector partitions of \mathbf{a} using vectors in Φ_G^+ . In other words, it is the number of ways of writing \mathbf{a} as a nonnegative integer combination of vectors in Φ_G^+ . The **shifted out-degree vector** $\mathbf{s} = (s_1, \dots, s_{n-1})$ of G is the vector where s_i is one less than the out-degree of vertex i . Note that $\sum_{i=1}^{n-1} s_i = m - n + 1$. A **weak composition** of $\ell \in \mathbb{Z}_{\geq 0}$ is a sequence of nonnegative integers whose sum is ℓ . A weak composition $\mathbf{d} = (d_1, \dots, d_\ell)$ is said to **dominate** $\mathbf{s} = (s_1, \dots, s_\ell)$, denoted by $\mathbf{d} \triangleright \mathbf{s}$, if $\sum_{i=1}^k d_i \geq \sum_{i=1}^k s_i$ for all $k \geq 1$. We use the notation $\hat{\mathbf{a}}$ to denote the vector consisting of all but the last coordinate of \mathbf{a} , and the multiexponent notation $\mathbf{x}^{\mathbf{y}} := x_1^{y_1} x_2^{y_2} \dots x_\ell^{y_\ell}$.



1. $[\alpha_1 + \alpha_2 + \alpha_3] + [\alpha_1 + \alpha_2] + [\alpha_1]$
2. $[\alpha_1 + \alpha_2 + \alpha_3] + 2[\alpha_1] + [\alpha_2]$
3. $2[\alpha_1 + \alpha_2] + [\alpha_3] + [\alpha_1]$
4. $2[\alpha_1] + [\alpha_1 + \alpha_2] + [\alpha_2] + [\alpha_3]$
5. $3[\alpha_1] + 2[\alpha_2] + [\alpha_3]$

Figure 2.7: The graph $\text{car}(6)$ (left) and the five vector partitions of $(3, -1, -1, -1, 0, 0)$ using vectors in $\Phi_{\text{car}(6)}^+$ (right).

Theorem 2.3.7 (Lidskii volume formula [12, 8, 49]). *Let G be a graph with n vertices, m edges, shifted out-degree vector $\mathbf{s} = (s_1, \dots, s_{n-1})$, and net-flow vector \mathbf{a} . Then*

$$\text{vol } \mathcal{F}_G(\mathbf{a}) = \sum_{\mathbf{d} \triangleright \mathbf{s}} \binom{m-n+1}{\mathbf{d}} \cdot \hat{\mathbf{a}}^{\mathbf{d}} \cdot K_{G|_{n-1}}(\mathbf{d} - \mathbf{s}),$$

where the sum is taken over the weak compositions $\mathbf{d} = (d_1, \dots, d_{n-1})$ of $m - n + 1$ that dominate \mathbf{s} .

An analog of Theorem 2.3.7 can be given in terms of in-degrees (see [49, Corollary 1.3]), which is obtained by reversing the directions of the edges in G , and using the **shifted in-degree vector** $\mathbf{t} = (t_2, \dots, t_n)$ where t_i is one less than the in-degree of vertex i . In the unit flow case, when $\mathbf{a} = \mathbf{u}$, the only nonzero term in the sum occurs when $\mathbf{d} = (m - n + 1, 0, \dots, 0)$, and the Lidskii formula simplifies to the following special case due to Stanley and Postnikov [49, Theorem 2.2].

Corollary 2.3.8. *Let G be a graph with n vertices, m edges, shifted out-degree vector $\mathbf{s} = (s_1, \dots, s_{n-1})$, and shifted in-degree vector $\mathbf{t} = (t_2, \dots, t_n)$. Then*

$$\text{vol } \mathcal{F}_G = K_G(\mathbf{v}_{\text{out}}) = K_G(\mathbf{v}_{\text{in}}),$$

where $\mathbf{v}_{\text{out}} = (m - n + 1 - s_1, -s_2, \dots, -s_{n-1}, 0)$ and $\mathbf{v}_{\text{in}} = (0, t_2, t_3, \dots, t_n - (m - n + 1))$.

In general, the problem of enumerating vector partitions is difficult. In the following example we compute the volume of a flow polytope with this method.

Example 2.3.9. Two flow polytopes with combinatorially notable volumes are the following.

1. The **caracol graph** $\text{car}(n)$ is constructed from the path graph on vertex set $[2, n - 1]$ by adding vertices 1 and n , along with the edges $\{(1, i), (i, n) \mid 1 < i < n\}$. The volume computation of the **caracol flow polytope** $\mathcal{F}_{\text{car}(n)}$ by the Lidskii formula amounts to finding $K_{\text{car}(n)|_{n-1}}(n - 3, -1, \dots, -1, 0)$. The positive roots of $\Phi_{\text{car}(n)}^+$ that can be used in the vector partition are of the form $[\alpha_1 + \dots + \alpha_k]$, where $1 \leq k \leq n - 2$. These vector partitions are in bijection with Dyck paths, as visualized in Figure 2.8 using the vector partitions in Figure 2.7. For a proof of this bijection, we point the reader to [12, Proposition 3.3]. As a result, the volume of $\mathcal{F}_{\text{car}(n)}$ is $\text{Cat}(n - 3)$.

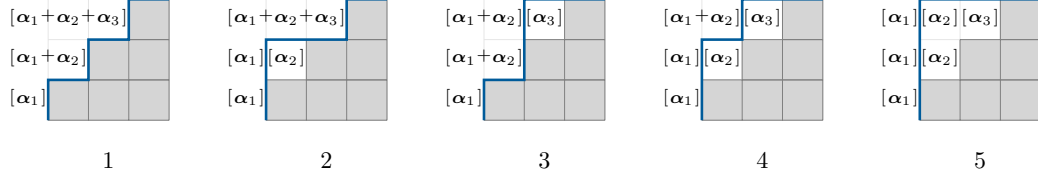


Figure 2.8: The correspondence between vector partitions and Dyck paths.

- The flow polytope \mathcal{F}_{K_n} , where K_n denotes the complete graph on n vertices, has been of particular interest and is called the Chan–Robbins–Yuen polytope. Its volume was conjectured by Chan, Robbins, and Yuen in [20] to be a product of consecutive Catalan numbers, namely $\text{vol } \mathcal{F}_{K_n} = \prod_{i=1}^{n-2} \text{Cat}(i)$. This was proven by Zeilberger [70] using a special case of the Morris constant term identity equivalent to the Selberg integral, but no combinatorial proof is known.

Framed triangulations of flow polytopes

A well-known class of triangulations of a flow polytope \mathcal{F}_G are induced by framings of the graph G . A **framing** at the vertex i is a pair of linear orders $(\prec_{\text{In}(i)}, \prec_{\text{Out}(i)})$ on the incoming and outgoing edges at i . A **framed graph**, denoted (G, \prec) , is a graph with a framing at every inner vertex. For a route R containing an inner vertex i , let Ri (respectively iR) denote the maximal subpath of R ending (respectively beginning) at i . Furthermore, let $\mathcal{I}(i) = \{Ri \mid R \in \mathcal{R}_G\}$ and $\mathcal{O}(i) = \{iR \mid R \in \mathcal{R}_G\}$. We then define linear orders $\prec_{\mathcal{I}(i)}$ and $\prec_{\mathcal{O}(i)}$ on $\mathcal{I}(i)$ and $\mathcal{O}(i)$ as follows. Given paths $Ri, Qi \in \mathcal{I}(i)$, let $j \leq i$ be the first vertex after which Ri and Qi coincide. Let e_R be the edge of R entering j and let e_Q be the edge of Q entering j . Then $Ri \prec_{\mathcal{I}(i)} Qi$ if and only if $e_R \prec_{\text{In}(j)} e_Q$. Similarly for $iR, iQ \in \mathcal{O}(i)$, let $j' \geq i$ be the last vertex before which iR and iQ coincide. Let e'_R be the edge of R leaving j' and let e'_Q be the edge of Q leaving j' . Then $iR \prec_{\mathcal{O}(i)} iQ$ if and only if $e'_R \prec_{\text{Out}(j')} e'_Q$. Two routes R and Q containing an inner vertex i are **coherent at i** if $Ri \prec_{\mathcal{I}(i)} Qi$ and $iR \prec_{\mathcal{O}(i)} iQ$, or if $Qi \prec_{\mathcal{I}(i)} Ri$ and $iQ \prec_{\mathcal{O}(i)} iR$. Routes R and Q are then said to be **coherent** if they are coherent at each common inner vertex. A set of mutually coherent routes is a **clique**. For a maximal clique C , let Δ_C denote the convex hull of the vertices of \mathcal{F}_G corresponding to the unitary flows along the routes in C . A framing on G then induces a triangulation of \mathcal{F}_G by the following theorem due to Danilov–Karzanov–Koshevoy [24].

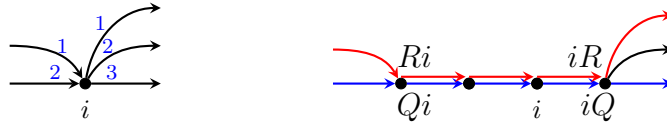


Figure 2.9: A framing at a vertex and coherent routes.

Theorem 2.3.10. *Let (G, \prec) be a framed graph and let \mathcal{T} be the collection of all simplices Δ_C such that C is a maximal clique in (G, \prec) . Then \mathcal{T} is a regular unimodular triangulation of \mathcal{F}_G .*

The triangulation given in Theorem 2.3.10 is known as the **Danilov–Karzanov–Koshevoy (DKK) triangulation** of \mathcal{F}_G (induced by \prec). Another triangulation of \mathcal{F}_G arising from (G, \prec) called the **framed Postnikov–Stanley (PS) triangulation** also appears in the literature. However, Mészáros–Morales–Striker [51, Theorem 7.8] showed that the PS triangulation and the DKK triangulation induced by the framed graph (G, \prec) are equal.

2.4 The subdivision algebra

The subdivision algebra is an algebraic setting in which subdivisions of certain root polytopes and flow polytopes can be encoded algebraically using a reductions of polynomials. It was first introduced by Mészáros [44, 45] for acyclic root polytopes, and has since been used extensively to study subdivisions of flow polytopes [46, 48, 52]. We will describe the subdivision algebra for both families of polytopes.

Definition 2.4.1. The **subdivision algebra** $\mathcal{S}(\beta)$ is an associative and commutative¹ algebra over the ring of polynomials $\mathbb{Q}[\beta]$, generated by $\{x_{ij} \mid 1 \leq i < j \leq n\}$, and subject to the relation $x_{ij}x_{jk} = x_{ik}x_{ij} + x_{jk}x_{ik} + \beta x_{ik}$, if $1 \leq i < j < k \leq n$.

Given a polynomial p in $\mathcal{S}(\beta)$, we say that p' is a **reduction** of p if p' is obtained from p by substituting the factor $x_{ij}x_{jk}$ of each monomial of p divisible by $x_{ij}x_{jk}$ with $x_{ik}x_{ij} + x_{jk}x_{ik} + \beta x_{ik}$, where $1 \leq i < j < k \leq n$. A consequence of a reduction is that p' has two more monomials than p . A **reduced form** of a monomial M in $\mathcal{S}(\beta)$ is defined to be the final polynomial p_ℓ in a sequence $M = p_0, p_1, \dots, p_\ell$, where each polynomial is obtained from the previous polynomial via a reduction, and no reductions are possible in p_ℓ . Reduced forms are not unique in general.

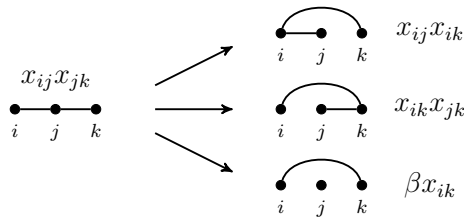


Figure 2.10: A graphical representation of a reduction.

Given a multigraph G in vertex set $[n]$, we can associate to it the following monomial in the subdivision algebra:

$$M(G) = \prod_{(a,b) \in E(G)} x_{ab}.$$

¹A non-commutative version was also studied by Mészáros in [44] called the quasi-classical Yang–Baxter algebra.

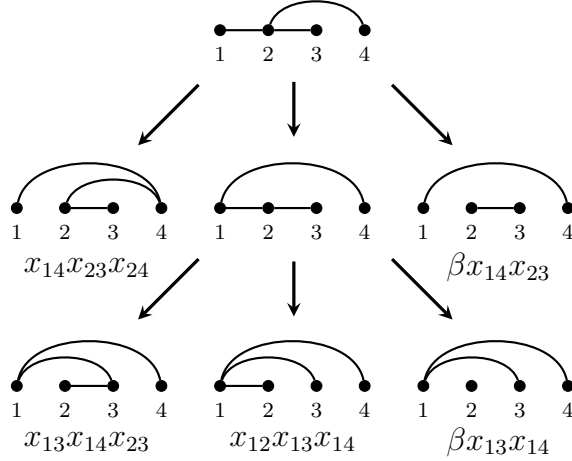


Figure 2.11: A reduction tree corresponding to the reductions in Example 2.4.2.

An application of the relation $x_{ij}x_{jk} = x_{ik}x_{ij} + x_{jk}x_{ik} + \beta x_{ik}$ in Definition 2.4.1 then results in monomials corresponding to the following three new graphs.

$$\begin{aligned}
 G_1 &:= (G \setminus \{(i, j)\}) \cup \{(i, k)\}, \\
 G_2 &:= (G \setminus \{(j, k)\}) \cup \{(i, k)\}, \text{ and} \\
 G_3 &:= (G \setminus \{(i, j), (j, k)\}) \cup \{(i, k)\}.
 \end{aligned}
 \tag{2.3}$$

We may now speak of a reduction of a graph G at a pair of edges (i, j) and (j, k) as the operation giving rise to the three graphs G_1 , G_2 , and G_3 .

Example 2.4.2. Let $G = ([4], \{(1, 2), (2, 3), (2, 4)\})$. Then $M(G) = x_{12}x_{23}x_{24}$, and a possible sequence of reductions of $M(G)$ is as follows:

$$\begin{aligned}
 p_0 &= \mathbf{x}_{12}x_{23}\mathbf{x}_{24} \\
 p_1 &= \mathbf{x}_{12}x_{14}\mathbf{x}_{23} + x_{14}x_{23}x_{24} + \beta x_{14}x_{23} \\
 p_2 &= x_{12}x_{13}x_{14} + x_{13}x_{14}x_{23} + x_{14}x_{23}x_{24} + \beta x_{13}x_{14} + \beta x_{14}x_{23}
 \end{aligned}$$

The reduction in each step is performed on the pairs in boldface. No reductions are possible in p_2 and hence p_2 is a reduced form of $M(G)$.

A reduction of G can be viewed as a rooted tree, with G as the root with the graphs G_1 , G_2 , and G_3 from (2.3) as leaves. Continuing to perform reductions on the leaves until no more reductions are possible, we obtain a rooted ternary tree called a **reduction tree**. The leaves of the reduction tree with the same number of edges as G are said to be **full-dimensional**. It is important to note here that when a reduction is performed on a leaf at a pair $(i, j), (j, k)$, the same pair is reduced in all other leaves where such a reduction is possible. Sometimes it is convenient to consider **simple reductions**, which are obtained by setting $\beta = 0$ in the reduction relation $x_{ik}x_{ij} + x_{jk}x_{ik} + \beta x_{ik}$. The reduction tree obtained from simple reductions is a binary tree, and its leaves are all full-dimensional.

The sequence of reductions in Example 2.4.2 corresponds with the reduction tree in Figure 2.11, with monomials of the reduced form p_2 of $M(G)$ given by the five

leaves of the tree, three of which are full-dimensional. A reduction tree obtained in this way is not unique in general, and depends on the reduction order. However, the number of leaves in two reduction trees of a graph is always the same, and furthermore, the following lemma holds.

Lemma 2.4.3 ([46, Lemma 1]). *For two reduction trees of a graph G , let r_k^1 and r_k^2 denote the number leaves in the two reduction trees with k edges. Then $r_k^1 = r_k^2$.*

As a consequence, the number of degree k monomials in any reduced form of $M(G)$ is the same.

The following lemma explains how the subdivision algebra encodes subdivisions of acyclic root polytopes.

Lemma 2.4.4 (Reduction Lemma for Acyclic Root Polytopes [44, Lemma 5]). *Let G be a graph, with G_1 , G_2 , and G_3 as given in (2.3). Then $\mathcal{R}_G^+ = \mathcal{R}_{G_1}^+ \cup \mathcal{R}_{G_2}^+$, and $\mathcal{R}_{G_1}^+ \cap \mathcal{R}_{G_2}^+ = \mathcal{R}_{G_3}^+$.*

In other words, a reduction cuts the acyclic root polytope \mathcal{R}_G^+ into two full-dimensional faces encoded by G_1 and G_2 , with G_3 encoding their shared inner face. As each resulting piece is again an acyclic root polytope, we can iterate these reductions until we obtain a triangulation. The full dimensional leaves of a reduction tree then correspond with the facets of the triangulation, while the remaining leaves give the inner faces of the triangulation.

Example 2.4.5. The reduced form $x_{12}x_{13} + x_{13}x_{23} + \beta x_{13}$ of $M(P_3) = x_{12}x_{23}$ encodes the subdivision of $\mathcal{R}_{P_3}^+ = \mathcal{R}_2^+$ in Figure 2.12.

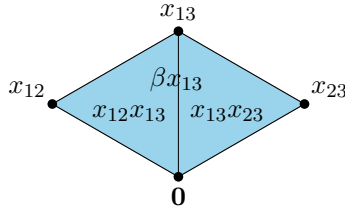


Figure 2.12: The subdivision of \mathcal{R}_2^+ encoded by $x_{12}x_{13} + x_{13}x_{23} + \beta x_{13}$.

Having now seen how reductions of monomials in the subdivision algebra encode subdivisions of acyclic root polytopes, we shift our attention to flow polytopes. The following notion will be useful.

Definition 2.4.6. Let G be a digraph on $[n]$ with all edges oriented from smaller to larger vertices. Define the **fully augmented graph** \tilde{G} to be the connected graph with vertex set $V(\tilde{G}) := [n] \cup \{s, t\}$, where $s < 1 < \dots < n < t$, and edge set $E(\tilde{G}) := E(G) \cup \{(s, i), (i, t) \mid i \in V(G)\}$. The **partial augmentation** of G , denoted \hat{G} , is obtained from the full augmentation \tilde{G} by removing edges (s, i) where i has out-degree one, and any edges (j, t) where j has in-degree one.

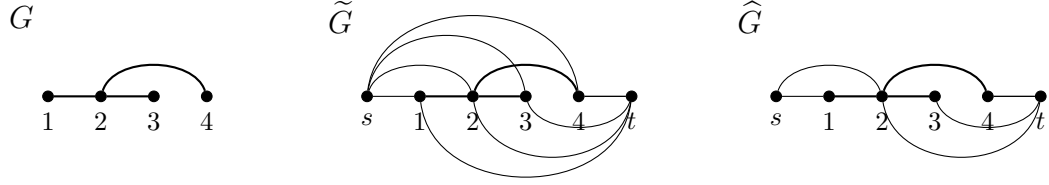


Figure 2.13: A graph G (left) with its full augmentation (center) and partial augmentation (right).

The results in the remainder of this section hold for both fully and partially augmented graphs (see Remark 2.4.10), but we will state them for fully augmented graphs. Letting G_1 , G_2 , and G_3 be as in (2.3), then the following lemma is the flow polytopal version of Lemma 2.4.4.

Lemma 2.4.7 (Reduction Lemma for Flow Polytopes [46, Lemma 2.2], [52, Proposition 2.3]). *Let G be a digraph with G_1 , G_2 , and G_3 as given in (2.3). Then there exists interior disjoint polytopes \mathcal{P}_1 and \mathcal{P}_2 such that $\mathcal{F}_{\tilde{G}} = \mathcal{P}_1 \cup \mathcal{P}_2$, with $\mathcal{P}_1 \equiv \mathcal{F}_{\tilde{G}_1}$, $\mathcal{P}_2 \equiv \mathcal{F}_{\tilde{G}_2}$, and $\mathcal{P}_1 \cap \mathcal{P}_2 \equiv \mathcal{F}_{\tilde{G}_3}$.*

Note in particular that in the above lemma a flow polytope subdivides into flow polytopes only up to an integral equivalence. This differs from Lemma 2.4.4, where an acyclic root polytope subdivides into acyclic root polytopes. Let $e_1 = (i, j)$, $e_2 = (j, k)$, and $e_3 = (i, k)$ be the edges in the construction of G_1 , G_2 and G_3 from (2.3). The polytopes \mathcal{P}_1 and \mathcal{P}_2 are then the polytopes obtained by cutting $\mathcal{F}_{\tilde{G}}$ with the hyperplane $x_{e_1} = x_{e_2}$. We can naturally interpret the flow in the edge e_3 of G_1 , G_2 , and G_3 as the shared flow in e_1 and e_2 of G . This gives rise to the integral equivalences in the reduction lemma above, which is visualized in Figure 2.14.

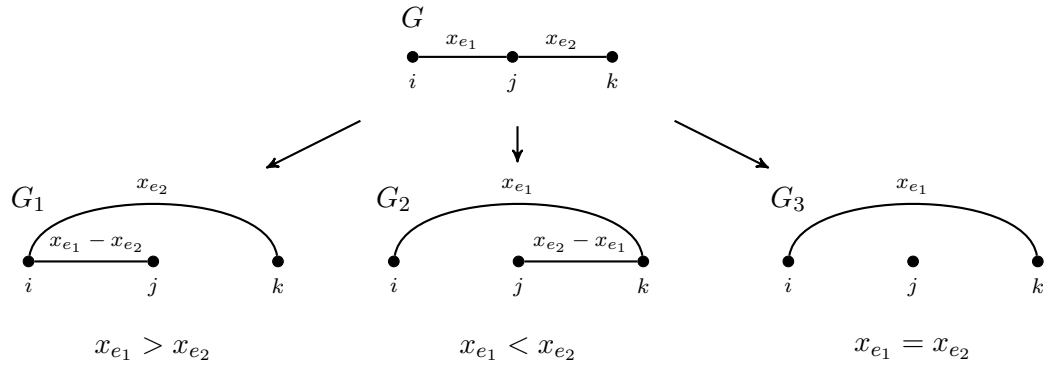


Figure 2.14: A visualization of the integral equivalences in Lemma 2.4.7.

As in the case of acyclic root polytopes, the reduction lemma for flow polytopes can be iterated to obtain a triangulation of the flow polytope $\mathcal{F}_{\tilde{G}}$, which is encapsulated in the following proposition.

Proposition 2.4.8 ([46, Theorem 3]). *The leaves of a reduction tree of G encode a regular flag triangulation of $\mathcal{F}_{\tilde{G}}$. Each leaf with $|E(G)| - k$ edges encodes a codimension k inner face of the triangulation.*

Example 2.4.9. Continuing Example 2.4.2 with $G = ([4], \{(1, 2), (2, 3), (2, 4)\})$, the leaves of the reduction tree in Figure 2.11 encode a triangulation of $\mathcal{F}_{\tilde{G}}$ consisting of three full dimensional simplices and two inner simplices of codimension one. Let H be the graph associated with $\beta x_{13}x_{14}$. The flow polytope $\mathcal{F}_{\tilde{H}}$ is then integrally equivalent to a codimension one simplex of the triangulation, but it is not the simplex itself. From the reduction tree it is possible to recover the vertices of $\mathcal{F}_{\tilde{G}}$ whose convex hull is the simplex associated with $\mathcal{F}_{\tilde{H}}$. To that end, we label the edge $e_3 = (i, k)$ in a reduction with the formal sum of edges $e_1 + e_2$. The edges in a leaf of the reduction tree of G can then be labeled with formal sums of edges in G . For example, in the graph H , the edge $(1, 4)$ was obtained from a reduction of the pair $\{(1, 2), (2, 4)\}$, so we have $e_{(1,4)} = e_{(1,2)} + e_{(2,4)}$. Similarly, since $(1, 3)$ in H was obtained from a reduction of the pair $\{(1, 2), (2, 3)\}$, we have $e_{(1,3)} = e_{(1,2)} + e_{(2,3)}$. A route in \tilde{H} is then expressible as a formal sum of all edges used in the route. The route $(s, 1), (1, 4), (4, t)$ in \tilde{H} is expressed as the formal sum $e_{(s,1)} + e_{(1,2)} + e_{(2,4)} + e_{(4,t)}$, from which we can read the corresponding route $(s, 1), (1, 2), (2, 4), (4, t)$ in \tilde{G} . In this way, we can recover all routes in \tilde{G} corresponding to the routes in \tilde{H} . See Figure 2.15 for an example.

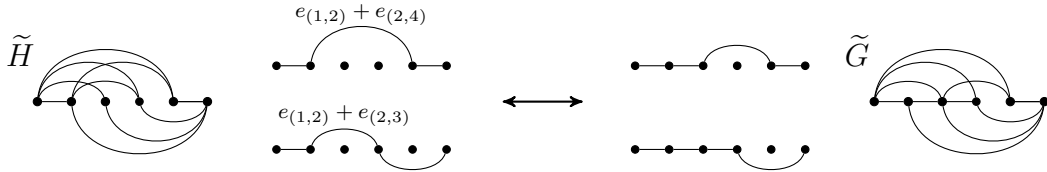


Figure 2.15: The correspondence between the routes not shared by \tilde{H} and \tilde{G} .

Remark 2.4.10. Lemma 2.4.7 also holds if we replace \tilde{G} , \tilde{G}_1 , \tilde{G}_2 , and \tilde{G}_3 with \hat{G} , \hat{G}_1 , \hat{G}_2 , and \hat{G}_3 respectively. This is because the removed edges from the full augmentation \tilde{G} appear only in routes of \tilde{G} which are contained (as vertices) in all inner faces of the triangulation. Thus removing such edges from \tilde{G} amounts to removing cone points of the triangulation. For the same reason Proposition 2.4.8 also holds when replacing \tilde{G} with \hat{G} .

2.5 The ν -associahedron and ν -Tamari lattice

The associahedron is a well-known simple polytope with fascinating connections to many areas of mathematics beyond combinatorics, including homotopy theory [67], real moduli spaces [29], and the theory of scattering amplitudes in quantum field theory [5]. The associahedron first appears in the work of Dov Tamari in the 1950's and independently in the work of Jim Stasheff in the early 1960's. However, it was not realized as a convex polytope until 1980's by Mark Haiman (unpublished) and

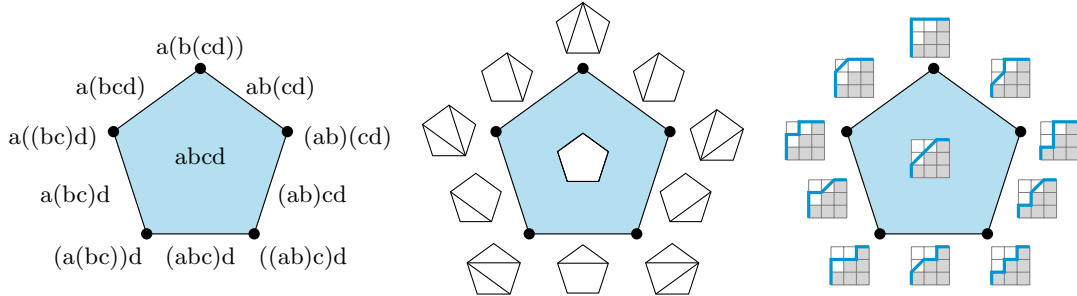


Figure 2.16: The faces of \mathcal{A}_2 correspond with parenthesizations of a word on $n + 2$ letter, subdivisions of an $(n + 3)$ -gon, and little Schröder paths above the path $(NE)^{n+1}$.

independently by Carl Lee [43]. Subsequently, several other realizations have been found and a good overview of various realizations is given by Ceballos, Santos, and Ziegler [18]. The associahedron has also been generalized in various ways, including rational associahedra [7], graph associahedra [14], poset associahedra [34], and ν -associahedra [16], the last of which are of interest in our story.

Before introducing the ν -associahedron, we take a brief look at the classical associahedron. Let D_n denote the partial order on the subdivisions of a regular $(n + 3)$ -gon, ordered by coarsenings. As an abstract polytope, the associahedron can be defined as follows.

Definition 2.5.1. The n -dimensional associahedron \mathcal{A}_n is the (abstract) polytope whose face lattice is given by the lattice $L_n := D_n \cup \{\hat{0}\}$.

The vertices of the associahedron \mathcal{A}_n correspond with the triangulations of the regular $(n+3)$ -gon, which are enumerated by the Catalan number $\text{Cat}(n+1)$. In this way the associahedron can be considered as the secondary polytope of the regular $(n + 3)$ -gon. The faces of \mathcal{A}_n are also in bijection with the set of parenthesizations of a word on $n + 2$ letters, where two vertices are adjacent if their corresponding parenthesizations differ by an application of the associativity law. It is from this characterization that the associahedron gets its name. Another well-known set of combinatorial objects associated with faces of \mathcal{A}_n is the set of Schröder paths from the point $(0, 0)$ to the point $(n + 1, n + 1)$. We will discuss this description in terms of Schröder paths in greater detail in Chapter 3. Figure 2.16 gives an example of \mathcal{A}_2 with its faces labeled using the three mentioned sets of combinatorial objects.

2.5.1 The ν -associahedron

A recent generalization of the associahedron was given by Ceballos, Padrol, and Sarmiento [16] which they call the ν -associahedron. To define it, we first need combinatorial objects known as (I, \bar{J}) -forests. Let $I \subseteq [n]$, $\bar{J} \subseteq [n]$, and let \prec denote the total order $1 \prec \bar{1} \prec 2 \prec \bar{2} \prec \dots \prec n \prec \bar{n}$ on $[n] \sqcup [n]$. Denote by $\prec_{I, \bar{J}}$ the order induced on $I \sqcup \bar{J}$ by \prec . The pair (I, \bar{J}) is said to be **valid** if $\min(I \sqcup \bar{J}) \in I$ and

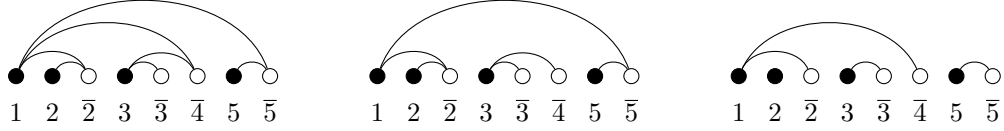


Figure 2.17: Three (I, \bar{J}) -forests. The two left-most graphs are also covering (I, \bar{J}) -forests, while the left-most graph is the only (I, \bar{J}) -tree.

$\max(I \sqcup \bar{J}) \in \bar{J}$. All pairs (I, \bar{J}) are assumed to be valid unless otherwise stated. A pair (i, \bar{j}) is called an **arc** if $i \in I$ and $\bar{j} \in \bar{J}$.

Definition 2.5.2. For a valid pair (I, \bar{J}) , an (I, \bar{J}) -**forest** is a subgraph of the complete bipartite graph $K_{|I|, |\bar{J}|}$ that is

1. **Increasing:** each arc (i, \bar{j}) satisfies $i \prec \bar{j}$ (i.e. $i \leq j$); and
2. **Non-crossing:** no two arcs (i, \bar{j}) and (i', \bar{j}') satisfy $i \prec i' \prec \bar{j} \prec \bar{j}'$.

An (I, \bar{J}) -**tree** is a maximal (I, \bar{J}) -forest. The (I, \bar{J}) -forests which contain the arc $(1, \bar{n})$ and have no isolated nodes are known as **covering (I, \bar{J}) -forests**.

As an example, let $I = \{1, 2, 3, 5\}$ and $\bar{J} = \{\bar{2}, \bar{3}, \bar{4}, \bar{5}\}$. A covering (I, \bar{J}) -forest in this case must contain the arcs $(1, \bar{5})$, $(2, \bar{2})$, $(3, \bar{3})$, and $(5, \bar{5})$. Figure 2.17 shows an example of the three types of (I, \bar{J}) -forests in this case.

To a valid pair (I, \bar{J}) we can associate a lattice path ν . First, we obtain a path $\bar{\nu}(I, \bar{J})$ by reading the steps in the set $\{E_i \mid i \in I\} \cup \{N_j \mid \bar{j} \in \bar{J}\}$ according to the order induced by $\prec_{I, \bar{J}}$. Then removing the initial E step and terminal N step gives a path $\nu(I, \bar{J})$. For example, choosing the pair (I, \bar{J}) as in Figure 2.17, we have $\bar{\nu}(I, \bar{J}) = E_1 E_2 N_2 E_3 N_3 N_4 E_5 N_5$, and $\nu(I, \bar{J}) = E N E N N E$. On the other hand, choosing $I' = \{3, 6, 8, 10\}$ and $\bar{J}' = \{6, 8, 9, 15\}$, we obtain that $\bar{\nu}(I', \bar{J}') = E_3 E_6 N_6 E_8 N_8 N_9 E_{10} N_{15}$ and $\nu(I', \bar{J}') = E N E N N E$. Note in particular that $\nu(I', \bar{J}') = \nu(I, \bar{J})$, and hence different (I, \bar{J}) -pairs can give rise to the same path ν . From the class of (I, \bar{J}) -pairs giving rise to the same path, we select as a unique representative the **canonical (I, \bar{J}) -pair**, which is the pair with minimal labeling according to \prec . For example, the (I, \bar{J}) -pair with $I = \{1, 2, 3, 5\}$ and $\bar{J} = \{\bar{2}, \bar{3}, \bar{4}, \bar{5}\}$ is the minimal pair giving rise to $\nu = E N E N N E$. Decreasing any value in I or \bar{J} gives a different path. As a result, we obtain a natural bijection between lattice paths and the equivalence classes of valid (I, \bar{J}) -pairs giving rise to the paths. When the pair (I, \bar{J}) is the canonical representative, or otherwise clear from context, we write $\bar{\nu} := \bar{\nu}(I, \bar{J})$ and $\nu := \nu(I, \bar{J})$ for brevity. We will also speak of the (I, \bar{J}) -pair **induced by ν** as the minimal (I, \bar{J}) -pair giving rise to ν .

The ν -associahedron can be defined combinatorially as follows.

Definition 2.5.3. For a lattice path $\nu(I, \bar{J})$ the ν -**associahedron** \mathcal{A}_ν is the (abstract) polytopal complex, whose face poset is the poset of covering (I, \bar{J}) -forests ordered by reverse inclusion on arcs.

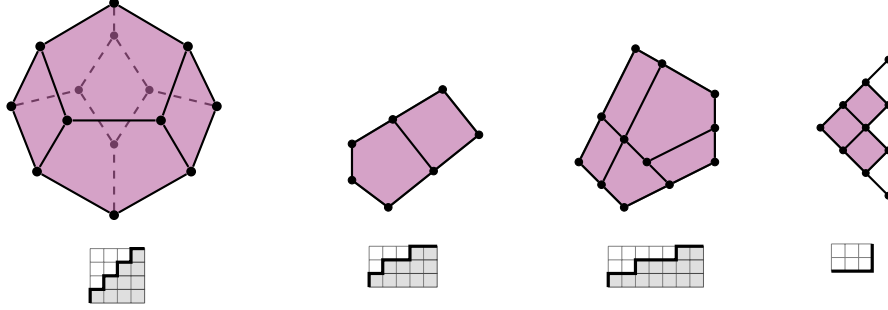


Figure 2.18: Various paths ν and their corresponding ν -associahedra.

Definition 2.5.4. The ν -**Tamari complex** is the flag simplicial complex on (I, \bar{J}) -forests induced by ν whose minimal non-faces are pairs of crossing arcs.

Lemma 2.5.5. *If ν is a lattice path from $(0, 0)$ to (a, b) , the dimension of the ν -Tamari complex is $a + b$.*

Proof. The top-dimensional simplices of the ν -Tamari complex are given by (I, \bar{J}) -trees, which have a total number of $|I| + |\bar{J}| = a + b + 2$ vertices. Hence they contain $a + b + 1$ arcs, and are $a + b$ dimensional. \square

The ν -Tamari complex can be realized by triangulating the polytope

$$\mathcal{U}_{I, \bar{J}} := \{(\mathbf{e}_i, \mathbf{e}_j) \mid i \in I, \bar{j} \in \bar{J}\},$$

with faces of the triangulation given by

$$\Delta_{F_{I, \bar{J}}} := \text{conv}\{(\mathbf{e}_i, \mathbf{e}_j) \mid (i, j) \in F_{I, \bar{J}}\},$$

where $F_{I, \bar{J}}$ denotes an (I, \bar{J}) -forest. The interior faces of the ν -Tamari complex are given by covering (I, \bar{J}) -forests, and ordering them by reverse inclusion gives the face poset of the ν -associahedron. In Chapter 4 we will obtain a related geometric realization of the ν -Tamari complex as a triangulated flow polytope, and thereby also obtain a realization of the ν -associahedron as its dual.

2.5.2 The ν -Tamari lattice

The edges in the 1-skeleton of the ν -associahedron can be directed to obtain the Hasse diagram of a lattice known as the ν -Tamari lattice. The ν -Tamari lattice, denoted $\text{Tam}(\nu)$, was introduced by Préville-Ratelle and Viennot [56] as a lattice of ν -Dyck paths. In addition to this description, we will describe the ν -Tamari lattice using (I, \bar{J}) -trees and ν -trees, both of which are due to Ceballos, Padrol, and Sarmiento [16, 17]. An example of these three combinatorial objects are shown in Figure 2.19, and each description has its advantages.

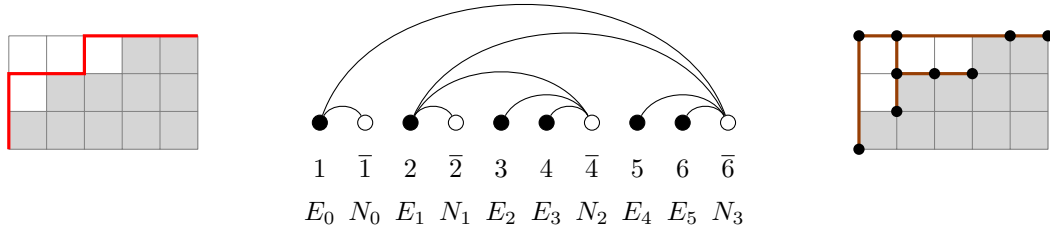


Figure 2.19: Three corresponding ν -Catalan objects, with $\nu = \nu(5, 3)$. A ν -Dyck path (left), an (I, \bar{J}) -tree (center), and a ν -tree (right).

The ν -Dyck path description

A **valley point** of a lattice path is a point p at the end of an E step that is immediately followed by an N step. Let μ be a ν -Dyck path. For any lattice point p on μ , let $\text{horiz}_\nu(p)$ denote the maximum number of E steps that can be taken from p without crossing ν . This is known as the **horizontal distance from p to ν** . For example, $\text{horiz}_\nu(p)$ of the lattice points on the ν -Dyck path in Figure 2.19 are $0, 1, 3, 2, 1, 3, 2, 1, 0$ as it is traversed from $(0, 0)$ to $(5, 3)$. The set of ν -Dyck paths can then be endowed with the structure of a poset with the covering relation \prec_ν defined as follows. If p is a valley point of μ , let q be the first lattice point in μ after p with $\text{horiz}_\nu(p) = \text{horiz}_\nu(q)$, and let $\mu_{[p,q]}$ denote the subpath of μ between p and q . Define a **rotation on μ at p** by switching the east step preceding p with the subpath $\mu_{[p,q]}$. If μ' is the lattice path obtained by rotating μ at p , then $\mu \prec_\nu \mu'$ is a covering relation in $\text{Tam}(\nu)$. Let $<_\nu$ denote the transitive closure of the relation \prec_ν .

Definition 2.5.6 (Préville-Ratelle – Viennot [56]). The ν -Tamari lattice $\text{Tam}(\nu)$ is the lattice of ν -Dyck paths induced by the relation $<_\nu$.

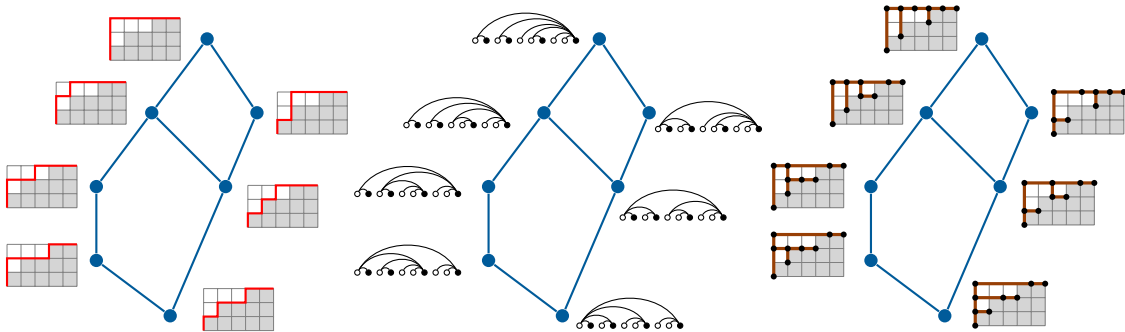


Figure 2.20: The ν -Tamari lattice indexed by ν -Dyck paths (left), (I, \bar{J}) -trees (center), and ν -trees (right) for $\nu = \nu(5, 3)$.

The (I, \bar{J}) -tree description

Given two (I, \bar{J}) -trees T and T' , we say that T' is an **increasing flip** of T if T' is obtained from T by replacing an arc (i, j) with an arc (i', j') , where $i < i'$ and $j < j'$. Define a relation on the set of (I, \bar{J}) -trees by $T \triangleleft_{I, \bar{J}} T'$ whenever T' is obtained from T by an increasing flip. The transitive closure $<_{I, \bar{J}}$ of the relation $T \triangleleft_{I, \bar{J}} T'$ gives a lattice structure on the set of (I, \bar{J}) -trees known as the **increasing flip lattice of (I, \bar{J}) -trees**.

Proposition 2.5.7 ([16, Theorem 3.4]). *The increasing flip lattice on the set of (I, \bar{J}) -trees determined by ν is isomorphic to $\text{Tam}(\nu)$.*

The ν -tree description

Given a lattice path ν from $(0, 0)$ to (a, b) , let \mathcal{P}_ν denote the set of lattice points in the plane which lie weakly above ν inside the rectangle defined by $(0, 0)$ and (a, b) . An (I, \bar{J}) -tree T can be represented as a point configuration in \mathcal{P}_ν . First, we label the E steps in $\bar{\nu}$ with increasing nonnegative integers in the order of their appearance in the path, and similarly we label the N steps with increasing nonnegative integers (see Figure 2.19). We call this indexing the **natural indexing** of $\bar{\nu}$. An arc in T can then be written as (E_x, N_y) , to which we associate the point (x, y) in \mathcal{P}_ν . The collection of points corresponding to the arcs of T in this way is called the **grid representation** of T . These grid representations were studied in detail in [17] under the name ν -trees (see [17, Remark 3.7]). The non-crossing condition for arcs in an (I, \bar{J}) -tree can be translated to ν -trees and a ν -tree can then be defined without reference to an (I, \bar{J}) -tree as follows.

Definition 2.5.8. Two lattice points p and q in \mathcal{P}_ν are **tree-incompatible** if p is southwest or northeast of q , and the smallest rectangle containing p and q contains only lattice points of \mathcal{P}_ν . The points p and q are **tree-compatible** if they are not tree-incompatible². A **ν -tree** is a maximal set of tree-compatible points in \mathcal{P}_ν .

It may seem peculiar that a collection of points is called a ‘tree’, but this is justified as we may associate a planar tree embedded in \mathcal{P}_ν to each ν -tree T as follows. Each point except $(0, b)$ in a grid representation has either one point above it in the same column or one point to its left in the same row, but not both [17, Lemma 2.2]. Thus we can connect each point to the point above it or to its left, forming a rooted binary tree with a root at $(0, b)$. Figure 2.19 (right) gives an example of a ν -tree, which is the grid representation of the (I, \bar{J}) -tree in the center.

If a ν -tree has points p, q , and r such that r is the southwest corner of the rectangle determined by p and q (with p northwest of q or vice versa), then replacing r with the lattice point at the northeast corner of the rectangle is called a **(right) rotation**. For example, in Figure 2.19, the only possible rotation in the ν -tree replaces the lattice point $(1, 2)$ with $(2, 3)$. Rotations in a ν -tree are a direct translation of

²This notion is called ν -compatibility in [16]. We use “tree-compatibility” as it contrasts with the path-compatibility notion in Chapter 4.

increasing flips for (I, \overline{J}) -trees. Define a partial order $<_\nu$ on the set of ν -trees given by a covering relation $T <_\nu T'$ if and only if T' is formed from T by a rotation. This partial order is the **rotation lattice of ν -trees** [17, Theorem 2.8]. The rightmost lattice in Figure 2.20 shows the ν -Tamari lattice indexed with ν -trees.

Proposition 2.5.9 ([17, Theorem 3.3]). *The rotation lattice on the set of ν -trees is isomorphic to $\text{Tam}(\nu)$.*

2.6 The ν -cyclohedron

In their geometric study of Tamari lattices, Ceballos, Padrol, and Sarmiento [16] also gave a cyclic counterpart to the ν -associahedron, which generalizes Simeon's type B associahedron [59].

First, the non-crossing condition for (I, \overline{J}) -forests needs to be extended to the cyclic setting. Two arcs (i, j) and (i', j') are said to **cyclically cross** if any of the following conditions hold (up to reversing the roles of the arcs):

- (1) $i < i' < j < j'$,
- (2) $j' < i < i' < j$,
- (3) $j < j' < i < i'$,
- (4) $i' < j < j' < i$,
- (5) $i < j' < i' < j$,
- (6) $j < i < j' < i'$.

These are visualized in Figure 2.21

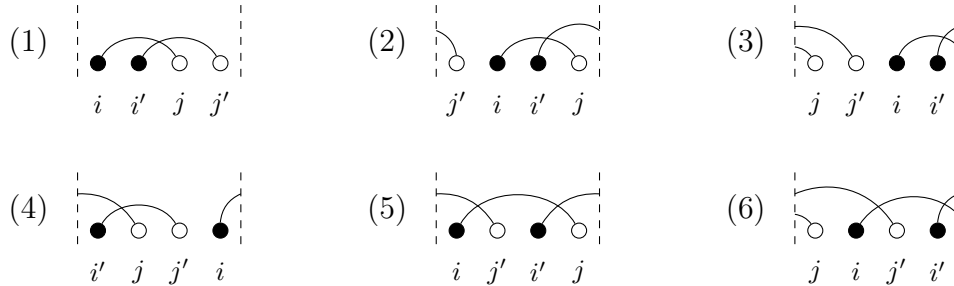


Figure 2.21: The six configurations of cyclically crossing arcs.

Definition 2.6.1. Given a pair (I, \overline{J}) (not necessarily valid), a **cyclic (I, \overline{J}) -forest** is subgraph of $K_{|I|, |\overline{J}|}$ whose arcs are cyclically non-crossing. A **cyclic (I, \overline{J}) -tree** is a maximal cyclic (I, \overline{J}) -forest. A **covering cyclic (I, \overline{J}) -forest** is a cyclic (I, \overline{J}) -forest with no isolated nodes.

We think of cyclic (I, \overline{J}) -forests as being wrapped around a cylinder as suggested in Figure 2.22. The cyclic counterparts to the ν -associahedron and ν -Tamari complex are then defined as follows.

Definition 2.6.2. Let $\nu(I, \overline{J})$ be a lattice path. The ν -cyclohedron is the (abstract) polytopal complex whose face poset is given by covering cyclic (I, \overline{J}) -forests, ordered by reverse inclusion on arcs.

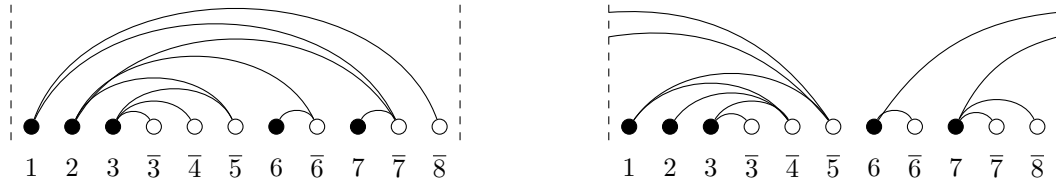


Figure 2.22: Two cyclic (I, J) -trees. The left tree is also an (I, J) -tree.

Definition 2.6.3. The **cyclic ν -Tamari complex** is the flag simplicial complex on cyclic (I, J) -forests whose minimal non-faces are pairs of cyclically crossing arcs.

Two cyclic (I, J) -trees T and T' are related by an **increasing flip** if T' can be obtained from T by replacing an arc $(i, j) \in T$ with an arc (i', j') where $i < i'$. This gives a cover relation $T <_{I, J} T'$ on cyclic (I, J) -trees. The **cyclic ν -Tamari poset** is the transitive closure of the relation $<_{I, J}$ on the set of cyclic (I, J) -trees. The following simple example shows that the cyclic ν -Tamari poset is not a lattice in general.

Example 2.6.4. Let ν be the path ENE . The minimal choices for I and \bar{J} are then $I = \{1, 2, 3\}$ and $\bar{J} = \{\bar{2}, \bar{3}\}$. The Hasse diagram of the cyclic ν -Tamari poset is shown below in Figure 2.23.

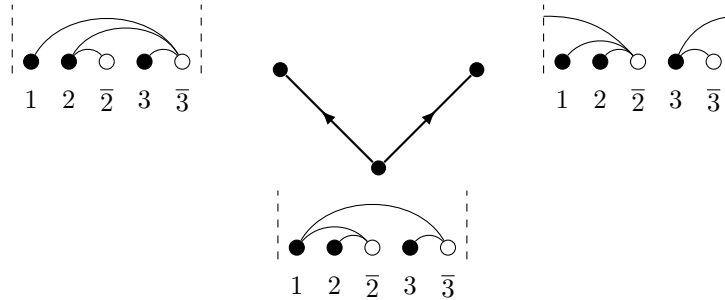


Figure 2.23: A cyclic ν -Tamari poset.

Chapter 3 The ν -associahedron and Schröder combinatorics

The ν -associahedron was introduced by Ceballos, Padrol, and Sarmiento [16] in their study of the geometry of ν -Tamari lattices, where it was defined in terms of covering (I, \bar{J}) -forests. In this chapter we study the ν -associahedron using ν -Schröder paths and ν -Schröder trees, giving alternative combinatorial descriptions to the ν -associahedron. Using these alternate descriptions, we obtain insight into its geometry and topology. Before studying this perspective, however, we consider the combinatorics of the two alternative ν -Schröder objects.

3.1 ν -Schröder objects

In this section, we study two useful sets of ν -Schröder objects. The first is the set of ν -Schröder paths, which generalize the classical Schröder paths. After extending some classical results for Schröder paths to the ν -setting, we introduce the set of ν -Schröder trees, which generalize the ν -trees studied by Ceballos, Padrol, and Sarmiento in [17].

3.1.1 ν -Schröder paths

The set of ν -Schröder paths are a generalization of ν -Dyck paths. In addition to the terminology for ν -Dyck from Chapter 2, we define the following paths and new terminology.

Definition 3.1.1. Let ν be a lattice path from $(0, 0)$ to (a, b) .

1. A **high peak** is a peak point occurring strictly above the path ν .
2. The **ν -diagonal** is the set of squares immediately below the peaks of ν .
3. A **(small) ν -Schröder path** is a lattice path from $(0, 0)$ to (a, b) using north $N := (0, 1)$, east $E := (1, 0)$, or **diagonal** $D := (1, 1)$ steps, which stays weakly above the path ν . We denote the set of (small) ν -Schröder paths by SP_ν and its cardinality by sch_ν .
4. Let μ denote the path obtained from ν by replacing each of its peaks with a D step. A **large ν -Schröder path** is path from $(0, 0)$ to (a, b) using N , E , and D steps, which stays weakly above the path μ . We denote the set of large Schröder paths by LSP_ν and its cardinality by Sch_ν .

Figure 3.1 provides some examples of both small and large ν -Schröder paths. The region below ν is shaded in gray, with the ν -diagonal in a darker gray. In the rightmost path, the point $(0, 2)$ is a high peak, while $(3, 4)$ is a peak point which is not a high peak.

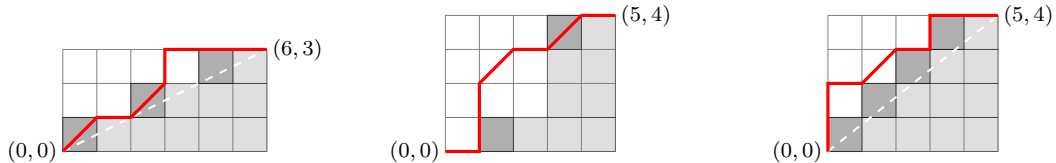


Figure 3.1: From left to right: a large $\nu(6,3)$ -Schröder path, a large ν -Schröder path, and a rational $(4,5)$ -Schröder path.

Remark 3.1.2. We point out two special cases; the classical case and the rational case. Classical Schröder paths to a point (n,n) are obtained by choosing ν to be the staircase path $(NE)^n$. For any pair of nonnegative integers (a,b) , the line segment from $(0,0)$ to (a,b) determines a unique lowest lattice path that stays weakly above it. That is, the path $\nu = \nu(a,b)$ with valleys at the lattice points $\{(k, \lceil kb/a \rceil) \mid \lceil kb/a \rceil \neq \lceil (k+1)b/a \rceil, 1 \leq k \leq a-1\}$. As mentioned in Chapter 1, when a and b are coprime, the set of $\nu(a,b)$ -Dyck paths is the set of rational (a,b) -Dyck paths defined by Armstrong, Rhoades and Williams [7]. Similarly, a rational (a,b) -Schröder path is a $\nu(a,b)$ -Schröder path, where a and b are coprime. The lattice path on the right in Figure 3.1 is an example of a rational $(4,5)$ -Schröder path where $\nu(4,5)$ is determined by the white dotted line segment from $(0,0)$ to $(5,4)$. We point out that the lattice path ν on the left in Figure 3.1 is also determined by the line segment from $(0,0)$ to (a,b) , but we do not consider this to be a rational case as $a = 3$ and $b = 6$ are not coprime.

Furthermore, in the case $a = n + 1$ and $b = n$ for some positive integer n , we have that $\nu(n, n + 1) = (NE)^n E$, and the set of ν -Schröder paths is equivalent to the set of classical Schröder paths.

Aguiar and Moreira [1, Proposition 3.1] showed that the set of classical large Schröder paths can be partitioned into two halves where one half consists of paths that do not contain D steps on the diagonal, and the other half consists of paths that contain at least one D step on the diagonal. Gessel [36] showed that the same result holds in the more general rational (a,b) -case. We further generalize Gessel's argument to the setting of ν -Schröder paths.

Theorem 3.1.3. *Let ν be a lattice path. Then $\text{Sch}_\nu = 2 \cdot \text{sch}_\nu$ if and only if ν begins with an N step and ends with an E step.*

Proof. Suppose ν begins with N and ends with E . Note that the set $\text{LSP}_\nu \setminus \text{SP}_\nu$ contains the ν -Schröder paths with at least one D step on the ν -diagonal. Define a map $f : \text{SP}_\nu \rightarrow \text{LSP}_\nu \setminus \text{SP}_\nu$ as follows: A path $\mu \in \text{SP}_\nu$ can be partitioned as $N\mu_1 E\mu_2$, where E is the first E step on the ν -diagonal. The existence of such an E step is guaranteed by the fact that ν ends in an E step, so there is a ν -diagonal square in the top row. Let $f(\mu)$ be the path $\mu_1 D\mu_2$. We claim that f is a bijection.

To see that $f(\mu) \in \text{LSP}_\nu \setminus \text{SP}_\nu$, note that f shifts the steps in μ_1 down by one unit, while the steps in μ_2 remain fixed. Thus the D step of $f(\mu)$ which is between μ_1 and μ_2 occurs on the ν -diagonal, since it replaced the E step of μ which preceded μ_2 .

A step in $N\mu_1$ can only intersect a horizontal run in ν at the leftmost lattice point of the horizontal run, since otherwise the first E step of the horizontal run is an E step of μ on the ν -diagonal. Therefore, only N steps and D steps which intersect only the leftmost lattice points of horizontal runs can occur in $N\mu_1$, both of which remain weakly above ν after shifting down by one unit. Thus $f(\mu) \in \text{SP}_\nu$, and so f is well-defined.

The inverse map $f^{-1} : \text{LSP}_\nu \setminus \text{SP}_\nu \rightarrow \text{SP}_\nu$ is defined as follows: For $\pi \in \text{LSP}_\nu \setminus \text{SP}_\nu$, partition π into $\pi_1 D \pi_2$ where D is the last D step on the ν -diagonal. Then f^{-1} is given by $\pi_1 D \pi_2 \mapsto N \pi_1 E \pi_2$, with $f(f^{-1}(\pi)) = \pi$ and $f^{-1}(f(\mu)) = \mu$. Hence f is a bijection, and $|\text{SP}_\nu| = 2 \cdot |\text{LSP}_\nu \setminus \text{SP}_\nu|$.

Conversely, suppose ν does not begin with an N step. In this case the map $f^{-1} : \text{LSP}_\nu \setminus \text{SP}_\nu \rightarrow \text{SP}_\nu$ is injective, but for any path $\rho \in \text{SP}_\nu$ that begins with a D (or E) step there is no path $\sigma \in \text{LSP}_\nu \setminus \text{SP}_\nu$ such that $f^{-1}(\rho) = \sigma$. Hence $|\text{LSP}_\nu \setminus \text{SP}_\nu| < |\text{SP}_\nu|$ and so $2 |\text{SP}_\nu| \neq |\text{LSP}_\nu \setminus \text{SP}_\nu|$. The case when ν does not end with an E step can be argued similarly. \square

A ν -Dyck path is completely determined by its high peaks. It is also completely determined by its valleys (see Figure 3.2). Using this fact, we obtain the next result, which is a direct generalization of the arguments in Deutsch [28] and Gessel [36] to the ν -setting.

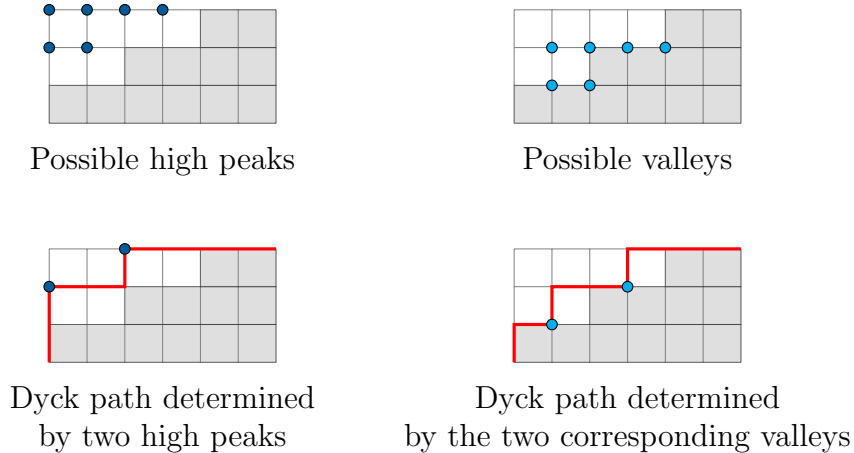


Figure 3.2: High peaks and valley points determine ν -Dyck paths.

Lemma 3.1.4. *Let ν be a lattice path that begins with an N step and ends with an E step. The set of ν -Dyck paths with i high peaks is in bijection with the set of ν -Dyck paths with $i + 1$ peaks.*

Proof. Since ν is a lattice path that begins with a north step and ends with an east step, then each ν -Dyck path with $i + 1$ peaks is determined by its i valleys, and

it suffices to show that there is a bijection between the set of ν -Dyck paths with i high peaks and the set of ν -Dyck paths with i valleys. A bijection is given by mapping a ν -Dyck path with high peaks at the lattice points $(p_1, q_1), \dots, (p_i, q_i)$ to the ν -Dyck path with valleys at the lattice points $(p_1 + 1, q_1 - 1), \dots, (p_i + 1, q_i - 1)$, and mapping the unique ν -Dyck path with no valleys to the unique ν -Dyck path with no high peaks (which is ν itself). This map is well-defined because high peaks are strictly above the path ν . The inverse map sends a ν -Dyck path with i valleys at the lattice points $(p_1, q_1), \dots, (p_i, q_i)$ to the ν -Dyck path with i high peaks at $(p_1 - 1, q_1 + 1), \dots, (p_i - 1, q_i + 1)$, so the map is a bijection. \square

Definition 3.1.5. The i -th ν -Narayana number $\text{Nar}_\nu(i)$ is the number of ν -Dyck paths with exactly i valleys. The ν -Narayana polynomial is

$$N_\nu(x) = \sum_{i \geq 0} \text{Nar}_\nu(i) x^i.$$

This generalization of the Narayana numbers was introduced by Ceballos, Padrol and Sarmiento [16] as the h -vector of the ν -Tamari complex. The rational (a, b) case also appears in the work of Armstrong, Rhoades and Williams [7] as the h -vector of their rational associahedron. Bonin, Shapiro and Simion [13] considered the Narayana polynomial for the dual associahedron.

Proposition 3.1.6. Let $\text{sch}_\nu(i)$ denote the number of ν -Schröder paths with i D steps. Then

$$N_\nu(x + 1) = \sum_{i \geq 0} \text{sch}_\nu(i) x^i.$$

Proof. Note that $\text{sch}_\nu = \text{sch}_{N\nu E}$, that is, appending an N step to the beginning of ν and an E step to the end of ν does not change the number of ν -Schröder paths. Hence we can assume without loss of generality that ν begins with an N step and ends with an E step. By Lemma 3.1.4, $\text{Nar}_\nu(i)$ is also the number of ν -Dyck paths with exactly i high peaks. The result then follows from the computation

$$\sum_{j \geq 0} \text{Nar}_\nu(j) (x + 1)^j = \sum_{i \geq 0} \sum_{j \geq 0} \text{Nar}_\nu(j) \binom{j}{i} x^i = \sum_{i \geq 0} \text{sch}_\nu(i) x^i,$$

where the last equality follows from the observation that for each ν -Dyck path with j high peaks there are exactly $\binom{j}{i}$ ways to choose which i of the high peaks to replace with a D step. \square

Corollary 3.1.7. The number of ν -Schröder paths is given by specializing $N_\nu(x)$ at $x = 2$.

Proof. The claim follows by noting that $\text{sch}_\nu = \sum_{i \geq 0} \text{sch}_\nu(i) = N_\nu(2)$. An alternative way to see this is to note that $\text{Nar}_\nu(i)$ is the number ν -Dyck paths with i high peaks. For each of the high peaks, there are two choices; keep the peak or replace it with a D step. Thus the total number of ν -Schröder paths is

$$\text{sch}_\nu = \sum_{i \geq 0} \text{Nar}_\nu(i) 2^i = N_\nu(2).$$

□

Corollary 3.1.8. *Let $\text{sch}_\nu(i)$ denote the number of ν -Schröder paths with i D steps. Then*

$$\sum_{i \geq 0} (-1)^i \text{sch}_\nu(i) = 1.$$

Proof. This follows from the fact that $\sum_{i \geq 0} (-1)^i \text{sch}_\nu(i) = N_\nu(0)$, and there is a unique ν -Dyck path with no valleys. □

Remark 3.1.9. Corollary 3.1.8 can be obtained topologically from the results in Section 3.2 since $\sum_{i \geq 0} (-1)^i \text{sch}_\nu(i)$ is the Euler characteristic of the ν -associahedron, which we show to be contractible in Theorem 3.2.10.

Remark 3.1.10. Theorem 3.1.3 can be deduced from Corollary 3.1.7 since $\text{Nar}_\nu(i)$ is the number ν -Dyck paths with $i + 1$ peaks if and only if ν begins with a N -step and ends with an E -step, in which case

$$\text{Sch}_\nu = \sum_{i \geq 0} \#(\nu\text{-Dyck paths with } i + 1 \text{ peaks}) \cdot 2^{i+1} = 2 \sum_{i \geq 0} \text{Nar}_\nu(i) 2^i = 2 \cdot \text{sch}_\nu.$$

We end this section with some enumerative results for the rational (a, b) -Schröder paths, but we first recall some results on rational (a, b) -Dyck paths.

For coprime positive integers a and b , the **rational (a, b) -Catalan number** $\text{Cat}(a, b)$ is the number of (a, b) -Dyck paths, and the **rational (a, b) -Narayana number** $\text{Nar}(a, b, i)$ is the number of (a, b) -Dyck paths with i peaks. Armstrong, Rhoades, and Williams [7] showed that

$$\text{Cat}(a, b) = \frac{1}{a+b} \binom{a+b}{a} = \frac{1}{a} \binom{a+b-1}{b} = \frac{1}{b} \binom{a+b-1}{a},$$

and for $i = 0, \dots, a$,

$$\text{Nar}(a, b, i) = \frac{1}{a} \binom{a}{i} \binom{b-1}{b-i}.$$

Next, we enumerate both large and small (a, b) -Schröder paths with respect to the number of D steps. For coprime positive integers a, b , and $i = 0, \dots, a$, let $\text{sch}(a, b, i)$ denote the number of (small) (a, b) -Schröder paths with i D steps and let $\text{Sch}(a, b, i)$ denote the number of large (a, b) -Schröder paths with i D steps.

The proof of the following result closely mirrors the one given by Song [60, Theorem 2.1], who studied Schröder paths from $(0, 0)$ to (kn, n) , which is equivalent to the rational case when $b = n$ and $a = kn + 1$.

Proposition 3.1.11. *For coprime positive integers a, b , and $i = 0, \dots, b$,*

$$\text{Sch}(a, b, i) = \frac{1}{a} \binom{a}{i} \binom{a+b-1-i}{b-i} = \frac{1}{b} \binom{b}{i} \binom{a+b-1-i}{a-i}.$$

Proof. The crucial observation is that the set of large (a, b) -Schröder paths with i D steps can be generated by taking the set of (a, b) -Dyck paths with at least i peaks, and replacing i of the peaks with diagonal steps. Each large (a, b) -Schröder path is obtained in a unique way in this construction, thus

$$\begin{aligned} \text{Sch}(a, b, i) &= \sum_{p \geq i} \binom{p}{i} \text{Nar}(a, b, p) = \sum_{p \geq i} \binom{p}{i} \frac{1}{a} \binom{a}{p} \binom{b-1}{b-p} \\ &= \frac{1}{a} \binom{a}{i} \sum_{p \geq i} \binom{a-i}{p-i} \binom{b-1}{b-p} = \frac{1}{a} \binom{a}{i} \binom{a+b-1-i}{b-i}. \\ &= \frac{1}{b} \binom{b}{i} \binom{a+b-1-i}{a-i}. \end{aligned}$$

□

Following directly from the bijection f constructed in Theorem 3.1.3, we have the next result which relates $\text{Sch}(a, b, i)$ and $\text{sch}(a, b, i)$.

Corollary 3.1.12. *For coprime positive integers a, b , and $i = 0, \dots, a$,*

$$\text{Sch}(a, b, i) = \text{sch}(a, b, i) + \text{sch}(a, b, i-1),$$

with the understanding that $\text{sch}(a, b, -1) = 0$.

From this corollary, we can deduce an explicit formula for the numbers $\text{sch}(a, b, i)$.

Proposition 3.1.13. *For coprime positive integers a, b , and $i = 0, \dots, a-1$,*

$$\text{sch}(a, b, i) = \frac{1}{a} \binom{b-1}{i} \binom{a+b-1-i}{b} = \frac{1}{b} \binom{a-1}{i} \binom{a+b-1-i}{a}.$$

Proof. Induct on i . By definition, $\text{sch}(a, b, 0) = \text{Sch}(a, b, 0) = \text{Cat}(a, b)$, and one can check via a direct computation that $\text{Sch}(a, b, i) - \text{sch}(a, b, i-1) = \text{sch}(a, b, i)$. □

3.1.2 ν -Schröder trees

In this section we introduce ν -Schröder trees, which generalize ν -trees. Let ν be a lattice path from $(0, 0)$ to (a, b) and let \mathcal{P}_ν denote the region of the plane which lies weakly above ν inside the rectangle defined by $(0, 0)$ and (a, b) . In Figure 3.3, \mathcal{P}_ν is represented by the unshaded region in the rectangular grid. Recall from Definition 2.5.8, that two lattice points p and q in \mathcal{P}_ν are **tree-incompatible** if and only if p is southwest or northeast of q , and the smallest rectangle containing p and q is contained in \mathcal{P}_ν . We say that p and q are **tree-compatible** if they are not tree-incompatible.

Definition 3.1.14. A ν -Schröder tree is a set of tree-compatible points in \mathcal{P}_ν including the point $(0, b)$, such that each row and each column contains at least one point. The point $(0, b)$ in a ν -Schröder tree is the **root**, and the other points will be called **nodes**. Let ST_ν denote the set of ν -Schröder trees.

A ν -tree is a maximal collection of tree-compatible points, and note that it is a binary trees. The ν -Schröder trees thus generalize ν -trees just as Schröder trees generalize binary trees in the classical sense.

As in the case of ν -trees, we may associate a planar tree embedded in \mathcal{P}_ν to each ν -Schröder tree T as follows. If a non-root node p of T in \mathcal{P}_ν has a node above it in the same column or a node to the left of it in the same row, we connect them by an edge. Note that the tree-compatibility of the nodes guarantees that it does not have both. However, it could have neither, in which case we consider the smallest rectangular box containing p and exactly one other node q of T . The node q must be the northwest corner of such a box. The root guarantees the existence of such a box, and uniqueness follows from the fact that the northwest corners of two such hypothetical boxes would be tree-incompatible. We then connect p and q by an edge. The resulting tree is guaranteed to be non-crossing, as otherwise the parent nodes of the two crossing edges would be tree-incompatible.

Example 3.1.15. Letting $\nu = \nu(3, 5)$, Figure 3.3 provides two examples of ν -Schröder trees. The region \mathcal{P}_ν is the unshaded region weakly above ν . The root is the node at $(0, 3)$. Note that although the node $(2, 3)$ is northeast of the node at $(0, 1)$ in the left tree, they are tree-compatible since the rectangle determined by them is not contained in \mathcal{P}_ν . No more nodes can be added to the left tree in Figure 3.3 without introducing a pair of tree-incompatible nodes, hence it is a ν -tree.

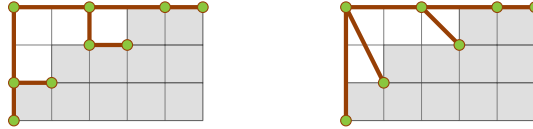


Figure 3.3: A ν -tree (left) and a ν -Schröder tree (right), where $\nu = \nu(3, 5)$.

Definition 3.1.16. Let p , q and r be nodes in a ν -Schröder tree S such that either p is the first node above q and r is the first node to the right of q , or p is the first node to the left of q and r is the first node below q . We define a **contraction of S at node q** as the ν -Schröder tree resulting from removing the node q from S . When p is above q we call it a **right contraction**, when q is above r we call it a **left contraction**. Define a **rotation at q** by removing the point q and placing it in the other corner of the box determined by p and r . If p is above q , we call it a **right rotation**, and if q is above r , we call it a **left rotation**. There is a third contraction possible, namely when r is southeast of a non-leaf node p , with neither corner of the box determined by p and r containing a node of S . If removing the node p yields a ν -Schröder tree, the removal of p will be called a **diagonal contraction**.

Figures 3.4 and 3.5 give diagrammatic illustrations of these definitions.

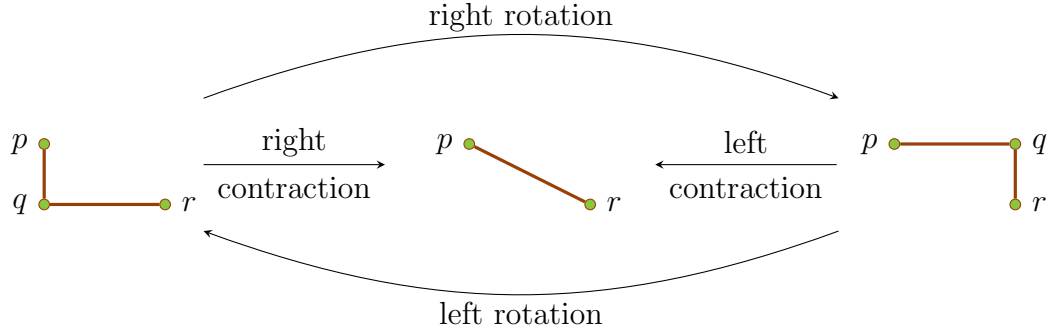


Figure 3.4: A right and left contraction as intermediate steps in a right and left rotation, respectively.

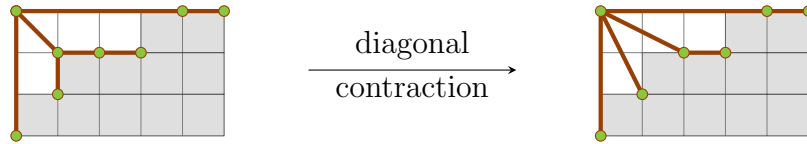


Figure 3.5: A diagonal contraction at the node (1,2).

Remark 3.1.17. The term contraction comes from noticing that removing the node q is equivalent to contracting the edge between q and its neighbor closest to the root. The tree on the right in Figure 3.3 is formed from the tree on the left by contracting at the points $(0, 1)$ and $(2, 2)$. Performing a contraction on a ν -tree T can be thought of as an intermediate step in a left or right rotation of ν -trees as defined in [17]. See Figure 3.4.

Proposition 3.1.18. *The set of ν -Schröder trees is the set of trees obtained from contracting ν -trees.*

Proof. Since contraction always leaves at least one node in every row and column, performing a sequence of contractions on a ν -tree results in a ν -Schröder tree. Conversely, given a ν -Schröder tree T , it is contained in a maximal set of tree-compatible nodes, that is, a ν -tree T' . Contracting T' at the nodes not appearing in T in any order yields T . \square

Remark 3.1.19. Since the set of ν -trees determine a set of binary trees with labels *left* and *right* [17, Lemma 2.4], we can define the set of ν -Schröder trees as the set of labeled trees resulting from contracting internal edges in the corresponding set of binary trees. When contracting at a node p labeled *left* or *right*, assign the label *middle* to all children with a different label than p . If p has label *middle*, assign the label *middle* to all of its children. Relabel the left and right children E and N respectively. In a contraction at q , each child of q receives the label D .

Next, we show that the leaves of a ν -Schröder tree determine the path ν , and vice versa. As a result, the path ν can be read from any ν -Schröder tree.

Proposition 3.1.20. *A node in a ν -Schröder tree is a leaf if and only if it is the starting point of a vertical run or an end point of a horizontal run in ν .*

Proof. If a node in a ν -Schröder tree T occurs at the starting point of a vertical run of ν or at the end point of a horizontal run, then it must be a leaf as it cannot have any nodes to its south, east or southeast.

Conversely let p be a leaf in T . Suppose toward a contradiction that p is not the starting point of a vertical run or the end point of a horizontal run in ν . Then there is a lattice point $q \in \mathcal{P}_\nu$ that is an end point of a horizontal run or beginning point of a vertical run such that q is to the south, east, or southeast of p . Note that q must be in T , as T is maximal and q is tree-compatible with every point in \mathcal{P}_ν . The point q cannot be directly south or east of p , since by definition there would be an edge in T from q to p , contradicting the assumption that p is a leaf. If q is southeast of p , then the points p and q determine a smallest rectangular box B in \mathcal{P}_ν containing both p and q . Since q is in T , there is a path from q to the root of T . Consider the last node s on the path from q to the root such that s is contained in B . Since p is a leaf, we have that s is not south or east of p , and $s \neq p$. Let $t \in T$ be the next node in the path from s towards the root. Then t is either north, west, or northwest of s . If t is north, west, or northwest of p , then s and t forms a box in \mathcal{P}_ν that contains p , implying that there is an edge in T from p to s , contradicting the assumption that p is a leaf. Thus, t must be northeast or southwest of p . However in both cases this means that the nodes t and p in T are tree-incompatible, so t cannot exist. It follows that there is no path from q to the root, which is a contradiction. \square

Since a lattice path is determined by its initial point, terminal point, and valley points, and the previous proposition showed that the leaves of a ν -Schröder tree are precisely these points of ν , then we have the following corollary.

Corollary 3.1.21. *The path ν is determined by a ν -Schröder tree.* \square

Remark 3.1.22. When $\nu = (NE)^n$ we recover the classical Schröder trees, that is, trees with $n + 1$ leaves where each non-leaf node has at least two children.

3.1.3 The posets of ν -Schröder paths and trees

In this section we construct partial orders on the sets of ν -Schröder paths and trees, and then show that the posets are isomorphic. We begin by constructing a bijection between the two ν -Schröder objects.

The bijection $L : \mathbf{ST}_\nu \rightarrow \mathbf{SP}_\nu$ we give here between ν -Schröder trees and ν -Schröder paths is a generalization of the bijection between ν -trees and ν -Dyck paths given by Ceballos, Padrol and Sarmiento [17, Theorem 3.3]. Given a ν -Schröder tree T , we assign labels N , E and D to its non-root nodes as follows: if its parent node

is in the same column then label it N , if its parent node is in the same row then label it E , and if its parent node is in neither then label it D .

First define a **right-flushing map** \mathbf{R} , which takes a ν -Schröder path μ and maps it to a ν -Schröder tree $T = \mathbf{R}(\mu)$ by right-flushing the lattice points of μ as follows. Begin by labeling the points in μ in the order they appear on the path, as it is traversed from the origin to (a, b) . Starting from the bottom row in \mathcal{P}_ν and proceeding upward, place the points in the same row of \mathcal{P}_ν from right to left as far right as possible, while avoiding x -coordinates forbidden by previously right-flushed rows. The x -coordinate of an initial point of an E or D step in μ that has been right-flushed is said to be **forbidden**. We claim that the lattice points obtained by right-flushing all the lattice points in μ are the nodes of a ν -Schröder tree T . See the top of Figure 3.6 for an example of the right-flushing map \mathbf{R} .

We first check that \mathbf{R} is well-defined. It is not immediately clear that right-flushing is always possible on a row, that is, that there is always an x -coordinate available in a row for the placement of a node. To verify that placing a node is always possible, suppose that we are right-flushing a point p in the ν -Schröder path μ . Let \bar{p} denote the node to which p is right-flushed. We need the number of lattice points in the row in \mathcal{P}_ν on which \bar{p} lies to be greater than the number of forbidden x -coordinates before \bar{p} , which we denote by $\text{forb}_\nu(\bar{p})$. Note that $\text{forb}_\nu(\bar{p})$ is equal to the number of E and D steps before p . Let $\text{horiz}_\nu(p)$ denote the maximal number of east steps that can be placed starting at p before crossing ν (while remaining in the smallest rectangle containing ν). For example, in Figure 3.6, $\text{horiz}_\nu(4) = 2$ and $\text{horiz}_\nu(9) = 3$. The difference between the number of lattice points in the row with p and the number of E and D steps before p is equal to $\text{horiz}_\nu(p) + 1$, and since this quantity is greater than or equal to one, there is a free column for the placement of \bar{p} .

Next, we verify that $T = \mathbf{R}(\mu)$ is in fact a ν -Schröder tree. The construction guarantees the tree-compatibility of the nodes, so it remains to verify the existence of the root, and that every row and column has a node. It is clear that every row has a node, as there is a lattice point of μ in every row. The total number of forbidden x -coordinates is the number of E and D steps in μ , which is a , thus when flushing the last point of μ , we must have a forbidden x -coordinates, or in other words, nodes in a columns. Note that the first column cannot be forbidden by any previous node, as such a forbidding node would correspond to a E or D step crossing ν . Thus the last node must be placed in $(0, b)$, and so we have a node in each column, and a root.

Now that \mathbf{R} is well-defined, we define its inverse known as the **left-flushing map** \mathbf{L} , which left-flushes the nodes in a ν -Schröder tree T to form a ν -Schröder path $\mu = \mathbf{L}(T)$ as follows. First order the nodes in T from bottom to top and right to left. Starting from the bottom row in \mathcal{P}_ν and proceeding upward, place the nodes from left to right in the same row as far left as possible, while avoiding x -coordinates forbidden by previously left-flushed rows. The forbidden x -coordinates of a row are the x -coordinates of lattice points corresponding to nodes labeled E or D in T . We claim that the resulting collection of lattice points is a ν -Schröder path μ . Note that by construction μ is the same path as the one obtained by reading the labels

in a post-order traversal of T . See the bottom of Figure 3.6 for an example of the left-flushing map L .

To verify that L is well-defined, we first check that left-flushing a node \bar{p} in a ν -tree is always possible, that is, that there is always an available lattice point of \mathcal{P}_ν in the row of \bar{p} in which to place p . We need more lattice points of \mathcal{P}_ν on the row of \bar{p} than $\text{forb}_\nu(\bar{p})$. Let $\text{hroot}_\nu(\bar{p})$ denote the number of nodes labeled E or D in the unique path from \bar{p} to the root. For example, in Figure 3.6 if \bar{p} is the node labeled N at $(5, 3)$, then $\text{hroot}_\nu(\bar{p}) = 3$. The difference between the number of lattice points of \mathcal{P}_ν on the row of \bar{p} and $\text{forb}_\nu(\bar{p})$ is $\text{hroot}_\nu(\bar{p}) + 1$. Since this quantity is greater than or equal to one, there is an available x -coordinate in the row of \bar{p} in which to place p .

It remains to check that $\mu = L(T)$ is a ν -Schröder path. It is clear from the construction that μ is a lattice path with N , E and D steps. For any $\bar{p} \in T$ the quantity $\text{hroot}_\nu(\bar{p})$ is one less than the difference between the number of lattice points of \mathcal{P}_ν on the row of \bar{p} and the number of E and D nodes read before \bar{p} , which is precisely $\text{horiz}_\nu(p)$. Thus we have $\text{hroot}_\nu(\bar{p}) = \text{horiz}_\nu(p) \geq 0$ for any p , that is, μ lies weakly above ν .

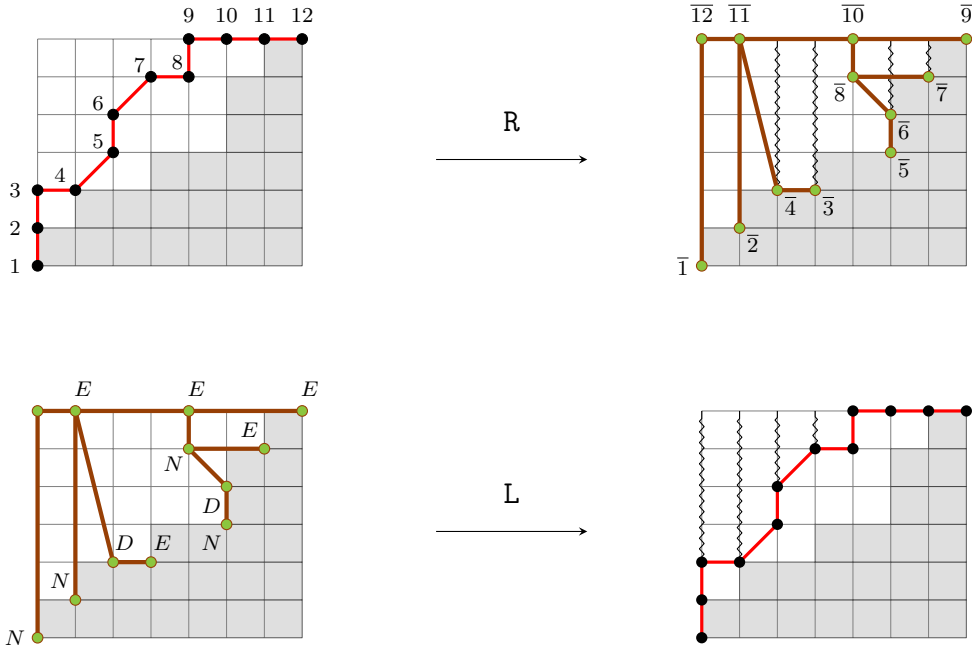


Figure 3.6: The right-flushing map R (top) and the left-flushing map L (bottom). The action of L is equivalent to reading the labels of the ν -Schröder tree in post-order traversal starting at the root and going counter-clockwise. The zigzag lines indicate the forbidden x -coordinates.

Theorem 3.1.23. *The map $L : \text{ST}_\nu \rightarrow \text{SP}_\nu$ is a bijection between the set of ν -Schröder trees and the set of ν -Schröder paths. \square*

Proof. We need only check that the right and left flushing maps R and L are inverses of one another. Let μ be a ν -Schröder path. The x -coordinate of a point p in μ is

determined by the number of E and D steps before p , which is precisely $\text{forb}_\nu(\bar{p})$. Therefore the x -coordinate of the point to which \bar{p} is sent under L is the same as that of p , and since R and L do not alter the y -coordinates, \bar{p} is sent to p . Hence $L(R(\mu)) = \mu$. Consider a node \bar{q} in an ν -Schröder tree T . If there is a lattice point to the east of \bar{q} not containing a node, then that column must have a northmost node \bar{r} southeast of \bar{q} . The label on \bar{r} cannot be N as then its column would have a node tree-incompatible with \bar{q} . Thus any lattice point east of \bar{q} is occupied by a node or is forbidden. In other words, the nodes in T are as far right as possible. Therefore, if the point q in $L(T)$ is the point to which the node \bar{q} is left flushed under L , then it then must taken back to \bar{q} under the right flushing map. Hence $R(L(T)) = T$. \square

Definition 3.1.24. Define a covering relation \triangleleft on the set of ν -Schröder trees by $T \triangleleft T'$ if and only if T' is a contraction of T . We call the poset induced by this cover relation the **poset of ν -Schröder trees**.

To define a poset on ν -Schröder paths, we translate contractions of ν -Schröder trees to ν -Schröder paths. The right, left and diagonal contractions are considered separately, as they correspond to different contraction moves on ν -Schröder paths.

First we consider a right contraction of a ν -Schröder tree T at a node \bar{q} with parent node \bar{p} above \bar{q} and with a child node \bar{r} to the right of \bar{q} . The labels of the nodes \bar{q} and \bar{r} are N and E respectively. Contracting at \bar{q} removes the node \bar{q} and the label on the node \bar{r} becomes D . This corresponds to replacing an E step and a N step in $L(T)$ with a D step. In the counterclockwise post-order traversal of T , the E and N steps are consecutive, and so correspond to a valley in $L(T)$. Thus a right contraction in T corresponds to replacing a valley in $L(T)$ with a D step.

Next, consider a left contraction in T at a node \bar{q} with parent node \bar{p} to the left of \bar{q} and with a child node \bar{r} below \bar{q} . As in the case above, contracting at \bar{q} replaces an E step and N step with a D step at \bar{r} . However, this time the N and E steps are not necessarily consecutive in $L(T)$, as \bar{q} may have other children which are read before \bar{q} in the post-order traversal of T . The node \bar{r} is the previous node in the post order traversal of T such that $\text{hroot}_\nu(\bar{r}) = \text{hroot}_\nu(\bar{q})$. Recall from Section 3.1.3 that $\text{hroot}_\nu(\bar{x}) = \text{horiz}_\nu(x)$. Therefore, r is the previous lattice point on $L(T)$ such that r is the initial point of an N step and $\text{horiz}_\nu(r) = \text{horiz}_\nu(q)$. Left contraction deletes this pair of E and N steps, and places a D step at r . See Figure 3.7 for an example.

Lastly, consider a diagonal contraction in T at a node \bar{r} with parent node \bar{p} . Note that \bar{r} must have a left child \bar{s} and a right child \bar{t} , as otherwise contracting at \bar{r} would not yield a ν -Schröder tree (either the row or column of \bar{r} would not contain a node). The labels of the nodes \bar{r} , \bar{s} , and \bar{t} are D , N , and E respectively. Contracting at \bar{r} changes the labels of both \bar{s} and \bar{t} to D . In the post-order traversal of the tree, this contraction corresponds to replacing the label N at \bar{s} with D , replacing the label E at \bar{t} with D , and removing the point \bar{r} labeled D . Note that \bar{s} is the first point before \bar{t} in the post-order traversal satisfying $\text{hroot}_\nu(\bar{s}) = \text{hroot}_\nu(\bar{r}) = \text{hroot}_\nu(\bar{t}) - 1$. Therefore, s is the previous point on $L(T)$ such that $\text{horiz}_\nu(s) = \text{horiz}_\nu(r) = \text{horiz}_\nu(t) - 1$. Diagonal contraction thus deletes the step E

with end point r and the step N with initial point s , and places a D step at s . See Figure 3.8 for an example.

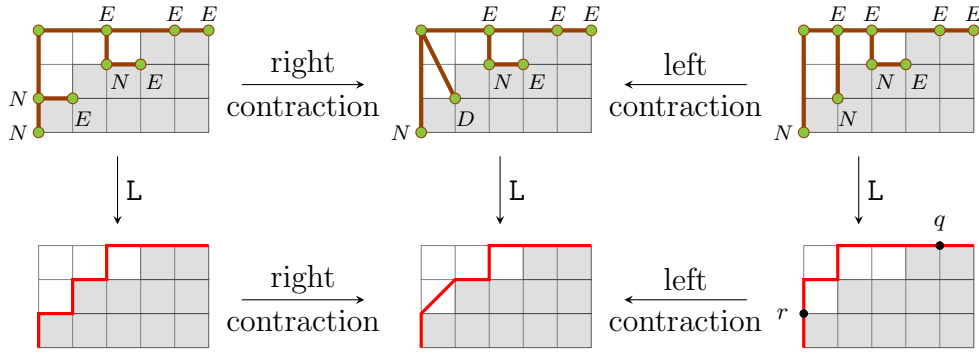


Figure 3.7: A right and left contraction of a pair of $(3, 5)$ -Schröder trees, and the corresponding contractions in the associated $(3, 5)$ -Schröder paths.

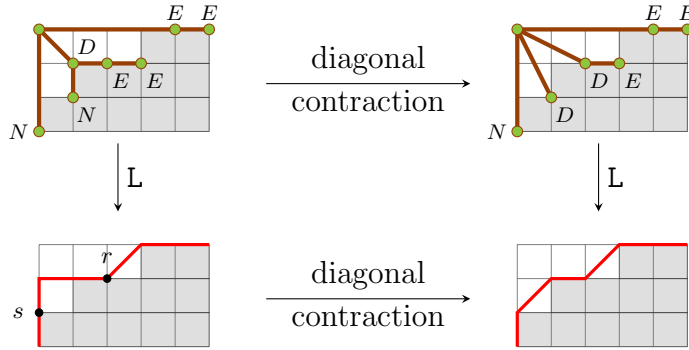


Figure 3.8: A diagonal contraction of a $(3, 5)$ -Schröder tree and the corresponding diagonal contraction in a $(3, 5)$ -Schröder path.

The set of ν -Schröder paths then form a poset with the cover relation inherited from the poset of ν -Schröder trees.

Definition 3.1.25. The **(contraction) poset of ν -Schröder paths** is the set of ν -Schröder paths with cover relation $\mu \prec \lambda$ if and only if λ is formed from μ by a contraction. The three contraction moves are the following:

1. **Right Contraction:** Replace a consecutive EN pair with D .
2. **Left Contraction:** Delete an E step with initial point q , along with the preceding N step with initial point r satisfying $\text{horiz}_\nu(r) = \text{horiz}_\nu(q)$. Shift the subpath between the deleted steps one unit to the right, placing a D step at r .
3. **Diagonal Contraction:** Delete an E step ending at a point r , which is the initial point of a D step, along with the preceding N step with initial point s satisfying $\text{horiz}_\nu(s) = \text{horiz}_\nu(r)$. Shift the subpath between the deleted steps one unit to the right, placing a D step at s .

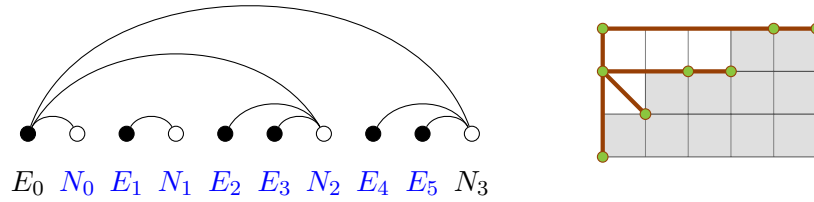


Figure 3.9: On the left is a covering (I, \bar{J}) -forest F . The associated path ν can be read from the labels below the covering (I, \bar{J}) -forest (ignoring the steps E_0 and N_3). On the right is the ν -Schröder tree that corresponds to F under the bijection of Proposition 3.2.1.

See Figure 3.11 for an example of the poset of ν -Schröder paths for the rational $\nu = \nu(3, 5)$. By the bijection in Theorem 3.1.23 and the translation between contractions of ν -Schröder trees and contractions of ν -Schröder paths above, the next theorem now follows.

Theorem 3.1.26. *The poset of ν -Schröder trees is isomorphic to the poset of ν -Schröder paths.* \square

3.2 The face poset of the ν -associahedron

Having constructed the posets of ν -Schröder trees and ν -Schröder paths and shown that they are isomorphic, we proceed to show that they are both isomorphic to the face poset of the ν -associahedron.

We begin by first relating the covering (I, \bar{J}) -forests determined by ν to ν -Schröder trees. Recall from Section 2.5.2 that ν -trees are grid representations of (I, \bar{J}) -trees. We extend the notion of grid representations to covering (I, \bar{J}) -forests. As in Section 2.5.2, we use the natural indexing of $\bar{\nu}$, indexing E steps in $\bar{\nu}$ with increasing nonnegative integers in the order of their appearance in the path, and similarly indexing the N steps with increasing nonnegative integers in the order of appearance in $\bar{\nu}$. Then an arc (E_x, N_y) in a covering (I, \bar{J}) -forest naturally corresponds with the lattice point (x, y) . As in the case with (I, \bar{J}) -trees, we call the collection of lattice points corresponding to the arcs of a covering (I, \bar{J}) -forest F the **grid representation** of F . Thus ν -Schröder paths are grid representations of covering (I, \bar{J}) -forests. See Figure 3.9 for an illustration of this correspondence.

Proposition 3.2.1. *Covering (I, \bar{J}) -forests are in bijection with ν -Schröder trees.*

Proof. Given a covering (I, \bar{J}) -forest F , the arcs of F can be identified with the labels at their end points, that is, pairs of the form (E_i, N_j) . For each such arc, insert a node at the coordinate (i, j) of the grid from $(0, 0)$ to $(|I| - 1, |\bar{J}| - 1)$, and call the resulting configuration of nodes in the grid T . The fact that F has no isolated nodes guarantees that each row and column of the grid contains a node

of T . The increasing condition guarantees that the nodes are in \mathcal{P}_ν , and the non-crossing condition guarantees that the nodes in T are tree-compatible. Thus T is a ν -Schröder tree. This construction is readily invertible. \square

Corollary 3.2.2. *Covering (I, \bar{J}) -forests are in bijection with ν -Schröder paths.*

Recall that the ν -associahedron \mathcal{A}_ν is the polytopal complex whose face poset is given by the poset of covering (I, \bar{J}) -forests. By the following theorem, we can now describe \mathcal{A}_ν in terms of our ν -Schröder objects.

Theorem 3.2.3. *The following posets are isomorphic:*

1. *The face poset of the ν -associahedron.*
2. *The poset of ν -Schröder trees.*
3. *The poset of ν -Schröder paths.*

Proof. Posets 1 and 2 are seen to be isomorphic since the cover relation in the poset of covering (I, \bar{J}) -forests is equivalent to contracting the corresponding node in the ν -Schröder tree. The isomorphism between posets 2 and 3 was shown in Theorem 3.1.26. \square

As an immediate consequence we have the following corollary.

Corollary 3.2.4. *The number of k -dimensional faces of the ν -associahedron is the number of ν -Schröder paths with k D steps. In particular, $\text{sch}_\nu(k)$ enumerates the k -faces of \mathcal{A}_ν . \square*

Combining Corollaries 3.1.8 and 3.2.4 gives the following.

Corollary 3.2.5. *The Euler characteristic of the ν -associahedron is one.*

A lattice is **Eulerian** if every nontrivial interval has an equal number of elements in the even ranks versus the odd ranks. Face lattices of convex polytopes are well known to be Eulerian (see for example [64, p.272]).

Theorem 3.2.6. *Let \hat{P} denote the poset P with an adjoined minimal element $\hat{0}$ and maximal element $\hat{1}$. If P_ν is the poset of ν -Schröder paths or ν -Schröder trees, then \hat{P}_ν is a lattice. Furthermore, every interval $[x, y]$ in $\hat{P}_\nu \setminus \{\hat{1}\}$ is an Eulerian lattice.*

Proof. Since \mathcal{A}_ν is a polytopal complex, $P_\nu \cup \{\hat{0}\}$ is a meet semilattice, with the meet of two faces being their (possibly empty) intersection. Since $z \wedge_{\hat{P}} \{\hat{1}\} = z$, \hat{P}_ν is a meet semilattice. By [64, Proposition 3.3.1], it follows that \hat{P}_ν is a lattice.

Let $x, y \in \hat{P}$. If z and w are two upper bounds in \hat{P} for x and y then the join $x \vee_{\hat{P}} y$ is the unique face at the intersection of w and z . If there is no face containing x and y as subfaces in \mathcal{A}_ν , then $x \vee_{\hat{P}} y = \hat{1}$. Every interval $[\hat{0}, y] \in \hat{P} \setminus \{\hat{1}\}$ corresponds to a convex polytope in a geometric realization of \mathcal{A}_ν , and hence is Eulerian. Therefore every subinterval $[x, y] \subseteq [\hat{0}, y]$ in $\hat{P} \setminus \{\hat{1}\}$ is an Eulerian lattice. \square

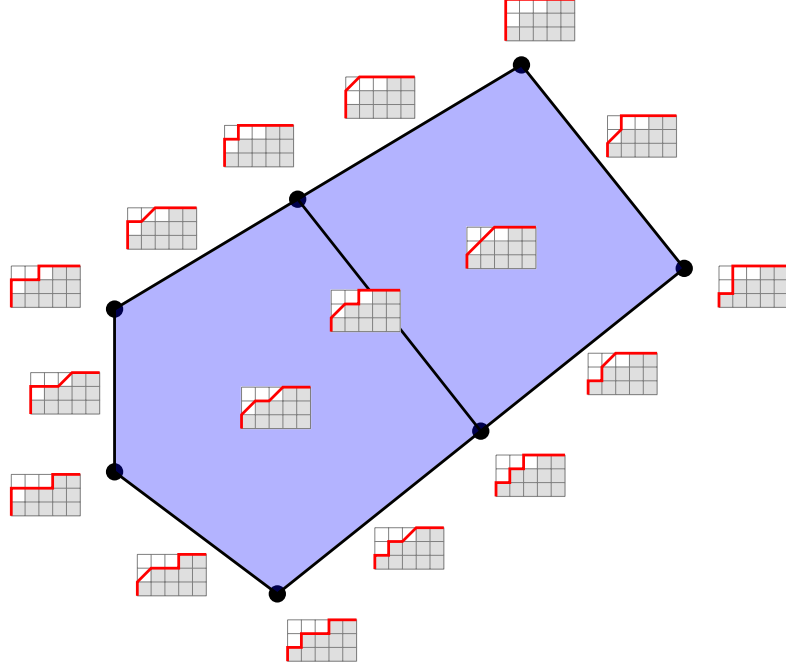


Figure 3.10: A ν -associahedron with its faces indexed by ν -Schröder paths.

Let ν be a lattice path with n steps. Préville-Ratelle and Viennot [56, Theorem 3] showed that the ν -Tamari lattice is isomorphic to an interval in the classical $(NE)^{n+1}$ Tamari lattice. Extending this isomorphism gives that the ν -associahedron is isomorphic to a connected subcomplex of the boundary complex of the n -associahedron. As a result, we have the following corollary.

Corollary 3.2.7. *If $\nu = (EN)^{n+1}$, then $P_\nu \cup \{\hat{0}\}$ is isomorphic to the face lattice of the n -associahedron. For general ν , \hat{P}_ν is isomorphic to a sublattice of the face lattice of the m -associahedron, where m is the number of steps in ν .*

Since the classical Tamari lattice can be partitioned into disjoint intervals of ν -Tamari lattices [56, Theorem 3], another consequence is that

$$\bigcup_{\substack{\nu \text{ path of} \\ \text{length } n}} \hat{P}_\nu \cong F$$

where F is a sublattice of the face lattice of the n -associahedron.

3.2.1 Contractibility of the ν -associahedron

Having shown that the Euler characteristic of the ν -associahedron is one, it is natural to ask whether \mathcal{A}_ν is contractible. We apply discrete Morse theory to the contraction poset of ν -Schröder paths to show that \mathcal{A}_ν is in fact contractible. This contractibility property of \mathcal{A}_ν is a special case of a result on the contractibility of the dual polytopal

complex of a triangulated polytope, which Francisco Santos generously shared with us.

Definition 3.2.8. Given a poset P , a **partial matching** in P is a matching in the underlying graph of the Hasse diagram of P . That is, a subset $M \subseteq P \times P$, such that

- $(a, b) \in M$ implies $a \prec b$;
- each element $a \in P$ belongs to at most one element of M .

When $(a, b) \in M$, we write $a = d(b)$ and $b = u(a)$. A partial matching is **acyclic** if there does not exist a cycle

$$b_1 \succ d(b_1) \prec b_2 \succ d(b_2) \prec \cdots \prec b_n \succ d(b_n) \prec b_1$$

where $n \geq 2$ and the $b_i \in P$ are distinct. Any elements of P not in an element of M are called **critical** elements.

The main theorem of discrete Morse theory for complexes is the following.

Theorem 3.2.9 ([42, Theorem 11.13]). *Let \mathcal{C} be a polytopal complex with face poset F . Let M be an acyclic matching on F , and let c_i denote the number of critical elements in F corresponding to i -dimensional faces of \mathcal{C} . Then \mathcal{C} is homotopy equivalent to a CW complex of \mathcal{C} consisting of c_i faces of dimension i .*

For more on discrete Morse theory, see [42].

Theorem 3.2.10. *The ν -associahedron \mathcal{A}_ν is contractible.*

Proof. Let \mathcal{A}_ν be the ν -associahedron with face poset P_ν . By Theorems 3.2.3 and 3.2.9, it suffices to find an acyclic matching on P_ν with a single critical element corresponding to a vertex in \mathcal{A}_ν .

Let M be the set of edges (π, σ) where π is formed from σ by replacing with EN the first D step not preceded by any valley. We claim that M is the desired acyclic partial matching. See Figure 3.11 for an example.

First we check that M is in fact a partial matching. If $(\pi, \sigma) \in M$, then σ is formed by a contraction of π , so $\pi \prec \sigma$ in P_ν . Next we show that a path π cannot be in more than one element of M . Note that there cannot be a pair of elements (τ, π) and (π, σ) in M because all D steps in $\pi = d(\sigma)$ are preceded by the added valley and so $\tau = d(\pi)$ cannot exist. Also, there cannot be two pairs (τ, π) and (τ', π) in M where $\tau \neq \tau'$ since $d(\pi)$ is unique by construction. It remains to check that there are no two pairs (π, σ) and (π, ρ) in M with $\sigma \neq \rho$. Suppose the contrary, then σ and ρ can be partitioned into $\sigma = \sigma_1 D_\sigma \sigma_2$ and $\rho = \rho_1 D_\rho \rho_2$, where the D_σ and D_ρ steps are the first D steps not preceded by a valley in the respective paths σ and ρ . If σ_1 and ρ_1 have the same number of steps, then it follows from $\pi = \sigma_1 EN \sigma_2 = \rho_1 EN \rho_2$ that $\sigma_1 = \rho_1$. However, we cannot have $\sigma_1 = \rho_1$, because then we would also have $\sigma_2 = \rho_2$, from which it would follow that $\sigma = \sigma_1 D_\sigma \sigma_2 = \rho_1 D_\rho \rho_2 = \rho$. Thus either σ_1

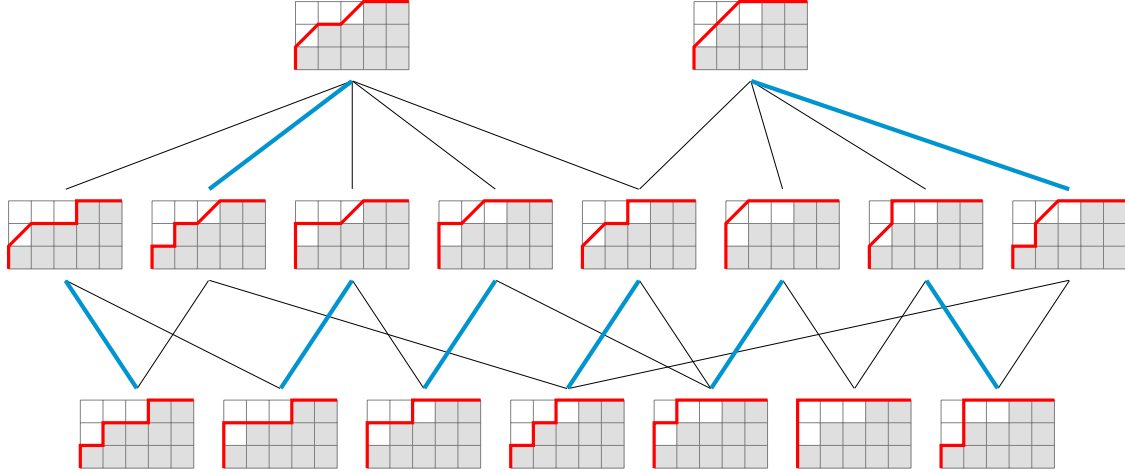


Figure 3.11: The contraction poset of $(3, 5)$ -Schröder paths, which is the face poset of the $\nu(3, 5)$ -associahedron of Figure 3.10. The bolded edges denote the acyclic partial matching M described in the proof of Theorem 3.2.10. The path N^3E^5 is the unique critical element in this matching.

has fewer steps than ρ_1 or vice versa. If σ_1 has fewer steps, then π can be partitioned as $\pi = \pi_1 EN \pi_2 EN \rho_2$, where $\pi_1 EN \pi_2 = \rho_1$. However, this means $\rho = \pi_1 EN \pi_2 D_\rho \rho_2$ has a valley before D_ρ , which contradicts the fact that (π, ρ) is in M . Similarly ρ_1 cannot have fewer steps. We conclude that M is a partial matching.

Next, we check that M is acyclic. Suppose to the contrary that there exists a cycle

$$\pi_1 \succ d(\pi_1) \prec \pi_2 \succ d(\pi_2) \prec \cdots \prec \pi_n \succ d(\pi_n) \prec \pi_1$$

with $n \geq 2$. Note that any pair $(d(\pi_i), \pi_i)$ satisfies $\text{area}(d(\pi_i)) = \text{area}(\pi_i) - 1/2$, where $\text{area}(\pi)$ denotes the area between π and ν . Every pair $d(\pi_i) \prec \pi_j$ in the cycle is related by a contraction of $d(\pi_i)$, and each contraction move either decreases the area of the path, or adds exactly half a unit of area. Since $\text{area}(\pi_1)$ at the beginning and the end of the cycle must be equal, each contraction between $d(\pi_i)$ and π_j must increase the area by exactly one half, and must therefore be a right contraction. The first valley in $d(\pi_1)$ is the one added to π_1 . Since π_2 must have a D step not preceded by a valley, it must be a result of a right contraction at the first EN pair in $d(\pi_1)$, which means $\pi_1 = \pi_2$. Therefore $n < 2$, giving the desired contradiction, and so M is acyclic.

Finally, we check that the only critical element in P_ν is the path $N^b E^a$. Any other path π will have either a first D step not preceded by a valley, or not. If it does, then $(d(\pi), \pi) \in M$. If it does not have such a D step, then it must have a first valley. Letting σ be the path π but with the first valley replaced with a D step gives an element $(\pi, \sigma) \in M$. \square

Remark 3.2.11. The acyclic matching M is more difficult to describe in the setting of ν -Schröder trees or of (I, \bar{J}) -trees, thus highlighting a benefit of the ν -Schröder

path perspective. The utility of paths is the clear linear order on the steps, making it easy to check if valleys occur before a D step.

In [16], Ceballos, Padrol, and Sarmiento show that the ν -associahedron appears as a dual polytopal complex of a triangulation of the polytope $\mathcal{U}_{I,\bar{J}} = \text{conv}\{(\mathbf{e}_i, \mathbf{e}_j) \mid i \in I, j \in \bar{J}, i < j\}$. In Chapter 4 we will obtain it as the dual polytopal complex of a triangulated flow polytope. In either case, the following result by Santos then gives an alternative proof of the contractibility of the ν -associahedron.

Proposition 3.2.12 (Santos [58]). *The dual polytopal complex of a triangulated polytope is contractible.*

Proof. Let \mathcal{B} be the barycentric subdivision of the triangulation. That is, the triangulation obtained by putting a vertex at the barycenter of every simplex of every dimension and taking as simplices the vertex sets that correspond to flags in the original triangulation. Topologically, the dual polytopal complex of the original triangulation is homeomorphic to the subcomplex of \mathcal{B} consisting of faces fully contained in the interior of the polytope. Now, \mathcal{B} consists of three types of faces, namely faces F_i contained entirely in the interior, faces F_b contained entirely on the boundary, and intermediate faces F_m with vertices in the interior and boundary. Every face of \mathcal{B} can be expressed as the join $F = F_i * F_b$ of (possibly empty) faces, where F_i is an interior face and F_b is a boundary face. In the intermediate case when neither F_b nor F_i is empty, $F \setminus F_b$ is a half-open simplex that deformation retracts to F_i . Simultaneously performing such deformations on the intermediate faces gives a deformation retract from the topological interior of the polytope (an open ball) to the barycentric subdivision of the dual polytopal complex. Hence, the dual polytopal complex is homotopically equivalent to an open ball, and thereby contractible. \square

Chapter 4 The family of ν -caracol flow polytopes

In this chapter, we study a family of flow polytopes which we call ν -caracol flow polytopes, whose normalized volumes are given by ν -Catalan numbers. After constructing these flow polytopes and studying their basic properties, we consider two particular DKK triangulations arising from two different framings. The triangulations we obtain have connections to two lattices on ν -Catalan objects that appear recurrently in the literature:

1. The ν -Tamari lattice $\text{Tam}(\nu)$ introduced by Préville-Ratelle and Viennot [56].
2. The principal order ideal $I(\nu)$ determined by ν in Young's lattice Y .

We study these triangulations in Sections 4.2.1 and 4.2.2. In Section 4.3.2, we show that the ν -caracol flow polytope is integrally equivalent to a subpolytope $\mathcal{U}_{I,\bar{J}}$ of a product of two simplices studied by Ceballos, Padrol, and Sarmiento [16]. They were curious to know if the subdivision algebra can be used to obtain subdivisions of $\mathcal{U}_{I,\bar{J}}$, which we show is possible through the connection to flow polytopes. We also provide an alternative way to answer the question via acyclic root polytopes.

4.1 The ν -caracol flow polytope

The ν -caracol flow polytope is obtained from a graph which we call the ν -caracol graph, which is defined using the lattice path ν as follows.

Definition 4.1.1. Let a and b be nonnegative integers, and let ν be a lattice path from $(0, 0)$ to (a, b) with w valleys. We can write $\nu = \prod_{i=0}^{w+1} N^{b_i} E^{a_{i+1}}$, and we set $a_0 = b_{w+1} = 1$. The ν -**caracol graph** $\text{car}(\nu)$ is the path graph on vertex set $[w+2]$ with added vertices s and t , together with a_i copies of $(s, i+1)$ and b_i copies of $(i+1, t)$ for $0 \leq i \leq w$. We direct all edges from the smaller vertex to the larger vertex, with the convention that $s = 0$ and $t = w+3$.

An example of a ν -caracol graph is given in Figure 4.1. Note that there are $a+1$ and $b+1$ edges incident to the source and sink respectively, along with $w+1$ edges in the path on vertices $[w+2]$. Thus the total number of edges in $\text{car}(\nu)$ is $a+b+w+3$. Recall from Chapter 2 that the (intrinsic) dimension of a flow polytope is given by $\dim \mathcal{F}_G = |E(G)| - |V(G)| + 1$, so we conclude that $\dim \mathcal{F}_{\text{car}(\nu)} = (a+b+w+3) - (w+4) + 1 = a+b$.

The flow polytope on the graph $\text{car}(\nu)$ in the special case when $\nu = (NE)^n$ has previously been studied by Mészáros [48] and by Benedetti et al. [12]. The graph was dubbed the caracol graph by the latter, as it resembles a snail shell in the planar drawing, with “caracol” being the word for snail in Spanish.

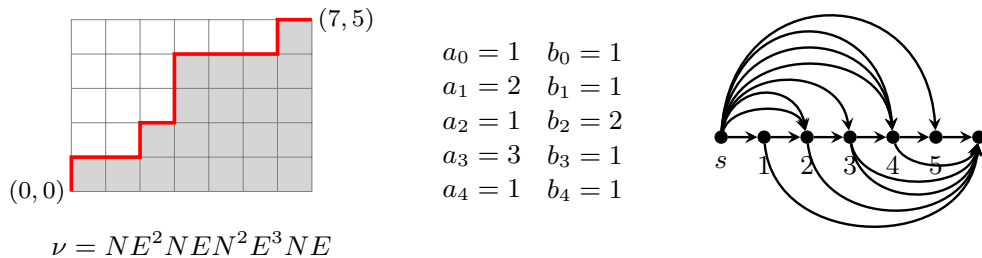


Figure 4.1: A lattice path and its associated ν -caracol graph.

4.1.1 The volume of $\mathcal{F}_{\text{car}(\nu)}$

Mészáros and Morales [49] have previously considered a closely-related variant of the flow polytope $\mathcal{F}_{\text{car}(\nu)}$, denoted as $\mathcal{F}_{\Pi_b^*(\nu)}$ in their work. When ν has no initial N steps, the underlying graph $\Pi_b^*(\nu)$ can be obtained from $\text{car}(\nu)$ by contracting all inner edges which are idle, and a simple transformation reveals that the flow polytopes $\mathcal{F}_{\text{car}(\nu)}$ and $\mathcal{F}_{\Pi_b^*(\nu)}$ are integrally equivalent. They observed that the normalized volume of $\mathcal{F}_{\Pi_b^*(\nu)}$ is the number of lattice points in the Pitman–Stanley polytope $\text{PS}_b(\nu) = \{\mathbf{y} \in \mathbb{R}_{\geq 0}^b \mid \sum_{i=1}^k y_i \leq \sum_{i=1}^k \nu_i\}$, which is equal to the number of ν -Dyck paths.

We obtain a proof of this result by giving a combinatorial interpretation to the vector partitions enumerated by the Kostant partition function in the Lidskii volume formula. This method was first considered in [12] and further developed in [69].

For flow polytopes of ν -caracol graphs with unitary net flow, the Kostant partition function $K_{\text{car}(\nu)}(\mathbf{v}_{\text{in}})$ has a simple combinatorial interpretation which we now describe. This generalizes the construction for the case $\nu = NE^{k-1}NE^k \dots NE^k$ considered in [69, Section 2.4].

Definition 4.1.2. Let ν be a lattice path from $(0, 0)$ to (a, b) and let ℓ be the number of initial N steps in ν . Let ν_i denote the number of E steps at height $\ell + i - 1$ for $1 \leq i \leq b - \ell + 1$. An **in-degree gravity diagram** for the flow polytope $\mathcal{F}_{\text{car}(\nu)}$ consists of a collection of dots and line segments with the following properties:

- (i) The dots are arranged in columns indexed by the simple roots $\alpha_3, \dots, \alpha_{b+2}$, with $\nu_1 + \dots + \nu_{j-2}$ dots in the column indexed by α_j , and all dots are drawn justified upwards.
- (ii) Horizontal line segments may be drawn between dots in consecutive columns so that each dot is incident to at most one line segment. A trivial line segment is a singleton dot. All non-trivial line segments must contain a dot in the column indexed by α_{b+2} (that is, all line segments are justified to the right). Longer line segments appear above shorter line segments.

We denote the set of all in-degree gravity diagrams by $\mathcal{G}_{\text{car}(\nu)}(\mathbf{v}_{\text{in}})$. See Figure 4.2 for an example of an in-degree gravity diagram.

The proof of the following Lemma is analogous to the one in [12, Theorem 3.1] for out-degree gravity diagrams. See also [69].

Lemma 4.1.3. *There is a bijection between the set of vector partitions of \mathbf{v}_{in} with respect to $\Phi_{\text{car}(\nu)}^+$ and the set of in-degree gravity diagrams for the flow polytope $\mathcal{F}_{\text{car}(\nu)}$. Consequently, $K_{\text{car}(\nu)}(\mathbf{v}_{\text{in}}) = |\mathcal{G}_{\text{car}(\nu)}(\mathbf{v}_{\text{in}})|$.*

Example 4.1.4. Let $\nu = NE^2NENNE^3NE$. A vector partition of $\mathbf{v}_{\text{in}} = 2\alpha_3 + 3\alpha_4 + 3\alpha_5 + 6\alpha_6 + 7\alpha_7$ with respect to the positive roots in $\Phi_{\text{car}(\nu)}^+$ is

$$\mathbf{v}_{\text{in}} = \alpha_{(3,8)} + \alpha_{(5,8)} + 2\alpha_{(6,8)} + \alpha_3 + 2\alpha_4 + \alpha_5 + 2\alpha_6 + 3\alpha_7.$$

This vector partition is represented by the gravity diagram on the left of Figure 4.2.

The connection between in-degree gravity diagrams and ν -Dyck paths is given by the following.

Lemma 4.1.5. *There is a bijection between the set $\mathcal{G}_{\text{car}(\nu)}(\mathbf{v}_{\text{in}})$ of in-degree gravity diagrams for the flow polytope $\mathcal{F}_{\text{car}(\nu)}$ and the set \mathcal{D}_ν of ν -Dyck paths.*

Proof. In an in-degree gravity diagram for $\text{car}(\nu)$, the column indexed by α_k has $\nu_1 + \dots + \nu_k$ dots, for $k = 3, \dots, b+2$. This is precisely the number of squares in the row between the lines $x = 0$, $y = k - 1$, $y = k$, and above ν .

Therefore, given an in-degree gravity diagram $\Gamma \in \mathcal{G}_{\text{car}(\nu)}(\mathbf{v}_{\text{in}})$, we may rotate it 90 degrees counterclockwise and embed the array of dots into the squares of \mathbb{Z}^2 so that the dots in the column indexed by α_{b+2} lie in the row of squares just above the line $y = b$, and the dots in the first row of Γ lie in the column of squares just right of the line $x = 0$. By the previous observation, we see that the dots of Γ occupy every square in \mathbb{Z}^2 between the lines $x = 0$, $x = a$ and $y = b + 1$, and which lie above the path ν . See Figure 4.2 for an illustration.

Line segments of the rotated embedded gravity diagram Γ are now vertical, and they extend down from just above the top row of the rectangular grid. The lengths of these vertical line segments are weakly decreasing from left to right, so the line segments of Γ define a unique ν -Dyck path that separates the dots in Γ which are incident to a line segment in Γ , from the dots which are not incident to any (proper) line segment in Γ . This construction defines a map $\Xi : \mathcal{G}_{\text{car}(\nu)}(\mathbf{v}_{\text{in}}) \rightarrow \mathcal{D}_\nu$.

Conversely, any ν -Dyck path defines an in-degree gravity diagram Γ for $\mathcal{F}_{\text{car}(\nu)}$, where every dot of Γ that occupies a square that is above the ν -Dyck path is incident to a line segment of Γ , and every dot of Γ that occupies a square that is below the ν -Dyck path is not incident to any (proper) line segment of Γ . Therefore, Ξ is a bijection. \square

Theorem 4.1.6 ([49, Corollary 6.17]). *The volume of $\mathcal{F}_{\text{car}(\nu)}$ is the ν -Catalan number $\text{Cat}(\nu)$.*

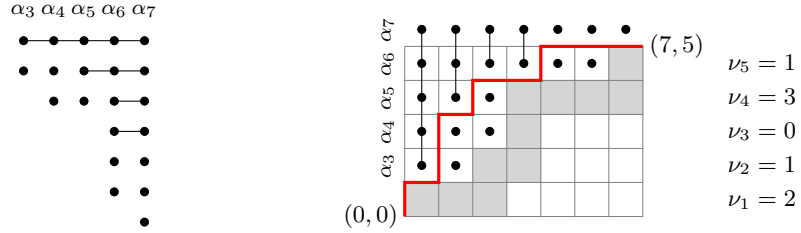


Figure 4.2: A gravity diagram (left) representing a vector partition of \mathbf{v}_{in} associated with $\text{car}(\nu)$ for $\nu = NE^2NENNE^3NE$. The bijection Ξ from Theorem 4.1.6 sends the gravity diagram to the ν -Dyck path via a 90 degree rotation (right).

Proof. Combining Proposition 2.3.8 and Lemmas 4.1.3 and 4.1.5, the normalized volume of $\mathcal{F}_{\text{car}(\nu)}$ is

$$\text{vol } \mathcal{F}_{\text{car}(\nu)} = K_{\text{car}(\nu)}(\mathbf{v}_{\text{in}}) = |\mathcal{G}_{\text{car}(\nu)}(\mathbf{v}_{\text{in}})| = |\mathcal{D}_\nu| = \text{Cat}(\nu).$$

□

In the next section, we construct two regular unimodular triangulations for the flow polytope $\mathcal{F}_{\text{car}(\nu)}$ with combinatorially interesting dual graph structures, giving two more proofs that the normalized volume of $\mathcal{F}_{\text{car}(\nu)}$ is the number of ν -Dyck paths.

4.2 Framed triangulations of $\mathcal{F}_{\text{car}(\nu)}$

We introduce two particular framed triangulations of $\mathcal{F}_{\text{car}(\nu)}$, which we call the planar-framed triangulation and the length-framed triangulation. In order to describe these framings we define the length of an edge (i, j) to be $|j - i|$, and assign labels to the edges in $\text{car}(\nu)$ incident to the source and sink as follows. We label the edges incident to s with integers $0, 1, \dots, a$ in any fixed order such that longer edges have larger labels than shorter edges. We then label the edges incident to t with integers $0, 1, \dots, b$ in any fixed order such that longer edges have smaller labels than shorter edges. See Figure 4.3 for an example of such a labeling.

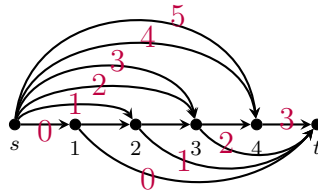


Figure 4.3: The edge labeling for source and sink edges in $\text{car}(\nu(5, 3))$.

Definition 4.2.1. The **length framing** \prec_{length} of $\text{car}(\nu)$ is the framing obtained by ordering both the incoming and outgoing edges at each inner vertex from longest to shortest. To break ties between multiedges of the same length, we consider the edge with the larger label to be longer.

Definition 4.2.2. The **planar framing** \prec_{planar} of $\text{car}(\nu)$ is the framing obtained by ordering the incoming edges at each inner vertex from longest to shortest, while ordering their outgoing edges from shortest to longest. We break ties between multiedges of the same length by considering edges with larger labels to be longer.

We point out that the study of length-framed and planar-framed triangulations of flow polytopes on the ν -caracol graphs can be extended systematically to all graphs. Particularly for graphs which are symmetric with respect to the vertical axis, our viewpoint suggests that these two framings are in a sense dual to one another, so perhaps we should not be surprised to find that both framings lead to combinatorially interesting triangulations of $\mathcal{F}_{\text{car}(\nu)}$.

To describe the combinatorial structure of the length-framed and planar-framed triangulations of $\text{car}(\nu)$ we use three different ν -Catalan families of objects, as each highlights the combinatorics in crucial and distinct ways. These are (I, \bar{J}) -trees, ν -Dyck paths, and ν -trees which were discussed in Section 2.5.2. The role that they play in the combinatorics of the triangulations is summarized in Table 4.1 below.

Table 4.1: ν -Catalan objects and their role in the combinatorial structure of the two framed triangulations.

Triangulation	Vertices	Facets	Adjacency	Dual graph
Length-framed	Arcs of (I, \bar{J}) -trees	(I, \bar{J}) -trees	Two (I, \bar{J}) -trees that differ by one arc	Hasse diag. of $\text{Tam}(\nu)$
	Lattice points above ν	ν -trees	Two ν -trees that differ by a rotation	
	(not obtained directly)	ν -Dyck paths	Two ν -Dyck paths that differ by a rotation	
Planar-framed	Lattice points above ν	ν -Dyck paths	Two ν -Dyck paths that differ by a pair EN to NE	Hasse diag. of $I(\nu)$

4.2.1 The length-framed triangulation

The goal of this section is to show that the flow polytope $\mathcal{F}_{\text{car}(\nu)}$ has a regular unimodular triangulation whose dual graph structure is given by the Hasse diagram of the ν -Tamari lattice. The triangulation in question arises from the length-framing (Definition 4.2.1). We show that this length-framed triangulation is combinatorially equivalent to the ν -Tamari complex (Definition 2.5.4).

Recall from Section 2.3 that the vertices of $\mathcal{F}_{\text{car}(\nu)}$ are determined by routes (unitary flows) in $\text{car}(\nu)$. These are completely characterized by two edges in $\text{car}(\nu)$:

the initial edge from the source s , and the terminal edge to the sink t . A route in $\text{car}(\nu)$ with initial edge labeled x and terminal edge labeled y will be denoted by $R_{x,y}$. For example, the route $s, 2, 3, t$ in Figure 4.3 is denoted $R_{1,2}$.

Next, we describe a key bijection between the set of routes \mathcal{R}_ν in the ν -caracol graph $\text{car}(\nu)$ and the set \mathcal{A}_ν of possible arcs in an (I, \bar{J}) -tree determined by ν . Recall from Section 2.5.1 that the lattice path ν determines a canonical pair (I, \bar{J}) , where the elements in the sets I and \bar{J} respectively correspond to the E and N steps in the path $\bar{\nu} = E\nu N$. Describing the bijection in terms of the N and E steps is easier than using the elements of I and \bar{J} , so we index the steps in $\bar{\nu}$ according to the natural indexing described in Section 2.5.2. In other words, we index the E steps left to right by $0, 1, \dots, a$, and index the N steps left to right by $0, 1, \dots, b$. Then arcs in an (I, \bar{J}) -trees can then be expressed as pairs of the form (E_x, N_y) .

Define the map $\varphi : \mathcal{R}_\nu \rightarrow \mathcal{A}_\nu$ by $\varphi(R_{x,y}) = (E_x, N_y)$. To see that this is well-defined, suppose the initial and terminal edges of $R_{x,y}$ are (s, i) and (j, t) respectively. Then $i \leq j$, which implies E_x appears before N_y in $\bar{\nu}$, so (E_x, N_y) is a valid arc in \mathcal{A}_ν . Figure 4.4 shows an example of this correspondence between routes and arcs.

Lemma 4.2.3. *The map $\varphi : \mathcal{R}_\nu \rightarrow \mathcal{A}_\nu$ is a bijection.*

Proof. Define the inverse map $\varphi^{-1} : \mathcal{A}_\nu \rightarrow \mathcal{R}_\nu$ by $\varphi^{-1}((E_x, N_y)) = R_{x,y}$. Suppose the edge in $\text{car}(\nu)$ that is incident to the vertex s having the label x is (s, i) , and the edge that is incident to the vertex t having the label y is (j, t) . Since (E_x, N_y) is an arc, this implies $i \leq j$, and $s, i, i+1, \dots, j-1, j, n+1$ is the route $R_{x,y}$ in $\text{car}(\nu)$, so φ^{-1} is well-defined. It is clear that $\varphi \circ \varphi^{-1}$ and $\varphi^{-1} \circ \varphi$ are identity maps. \square

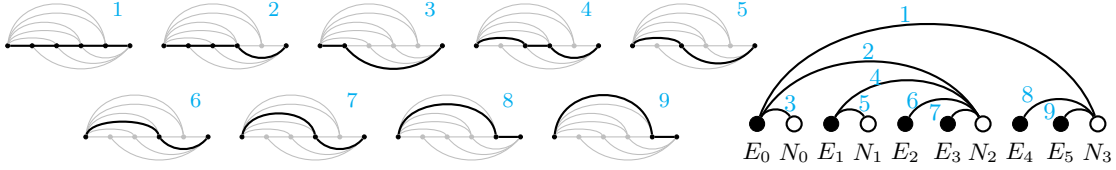


Figure 4.4: A maximal clique of routes (left) representing a top-dimensional simplex in the length-framed triangulation of $\mathcal{F}_{\text{car}(\nu)}$ for $\nu = \nu(5, 3)$. The bijection φ from Lemma 4.2.3 sends each route to the corresponding arc of the (I, \bar{J}) -tree on the right.

Lemma 4.2.4. *Let φ be the bijection in Lemma 4.2.3. Two routes $R_{x,y}$ and $R_{x',y'}$ in the framed graph $(\text{car}(\nu), \prec_{\text{length}})$ are coherent if and only if $\varphi(R_{x,y}) = (E_x, N_y)$ and $\varphi(R_{x',y'}) = (E_{x'}, N_{y'})$ are non-crossing arcs in \mathcal{A}_ν .*

Proof. If $x = x'$, then the routes are coherent and the corresponding arcs (E_x, N_y) and $(E_{x'}, N_{y'})$ are non-crossing. Otherwise assume $x < x'$. If the arcs (E_x, N_y) and $(E_{x'}, N_{y'})$ cross then $y < y'$ necessarily and $E_x, E_{x'}, N_y, N_{y'}$ appear in that order in $\bar{\nu}$. Denote the terminal edge of the route $R_{x,y}$ by (ℓ, t) . Then $x < x'$ and $y < y'$ imply that the routes $R_{x,y}$ and $R_{x',y'}$ are incoherent at the vertex ℓ . Conversely, let

(s, j) and (s, j') respectively denote the initial edges of $R_{x,y}$ and $R_{x',y'}$ so that $j \leq j'$, and suppose these routes are incoherent. They must be incoherent at a maximal vertex ℓ for which (ℓ, t) is the terminal edge of $R_{x,y}$, and $\ell \leq \ell'$ where (ℓ', t) is the terminal edge of $R_{x',y'}$. Moreover, since $R_{x,y}$ and $R_{x',y'}$ coincide at ℓ , then $j' \leq \ell$, and hence $E_x, E_{x'}, N_y, N_{y'}$ appear in that order in $\bar{\nu}$ and the arcs (E_x, N_y) and $(E_{x'}, N_{y'})$ cross. \square

Theorem 4.2.5. *The length-framed triangulation of $\mathcal{F}_{\text{car}(\nu)}$ is a regular unimodular triangulation whose dual graph is the Hasse diagram of the ν -Tamari lattice $\text{Tam}(\nu)$.*

Proof. By Lemma 4.2.4, the bijection φ in Lemma 4.2.3 extends to a bijection Φ from the set of maximal cliques of routes in the length-framed $\text{car}(\nu)$ to the set of (I, \bar{J}) -trees determined by ν . Two facets in a DKK triangulation of a flow polytope are adjacent if and only if they differ by a single vertex, that is, if the corresponding maximal cliques differ by a single route. Under the bijection Φ , two facets are adjacent if and only if their corresponding (I, \bar{J}) -trees differ by a single arc, which is precisely the description of the Hasse diagram of the ν -Tamari lattice. \square

Example 4.2.6. Let $\nu = \nu(5, 3)$. One example of the bijection Φ between cliques of routes of $\text{car}(\nu)$ and (I, \bar{J}) -trees is illustrated in Figure 4.4. The dual graph of the length-framed triangulation of $\mathcal{F}_{\text{car}(\nu)}$ is shown in Figure 4.7.

As a simplicial complex, the length-framed triangulation of $\text{car}(\nu)$ is a flag simplicial complex whose minimal non-faces are pairs of incoherent routes. This is precisely the description of the ν -Tamari complex in Definition 2.5.4, but with arcs replaced with routes. The following result is then a corollary of Theorem 4.2.5.

Corollary 4.2.7. *Let ν be the lattice path from $(0, 0)$ to (a, b) . The length-framed triangulation of $\mathcal{F}_{\text{car}(\nu)}$ is a geometric realization of the ν -Tamari complex of dimension $a + b$ in $\mathbb{R}^{|E(\text{car}(\nu))|}$.*

A second description in terms of ν -trees

Another useful combinatorial object for indexing facets in the length-framed triangulation of $\mathcal{F}_{\text{car}(\nu)}$ is the ν -tree discussed in Section 2.5.2. The vertices of $\mathcal{F}_{\text{car}(\nu)}$ can be associated with the set \mathcal{P}_ν of lattice points lying weakly above ν in the rectangle defined by $(0, 0)$ and (a, b) . We will see that the lattice points in a ν -tree correspond to vertices in a facet of the length-framed triangulation, and that two facets are adjacent if their corresponding ν -trees differ by a rotation.

Let $\gamma : \mathcal{A}_\nu \rightarrow \mathcal{P}_\nu$ be the map from the set of possible arcs in an (I, \bar{J}) -tree determined by ν to the lattice points in \mathcal{P}_ν given by $(E_x, N_y) \mapsto (x, y)$. For any arc (E_x, N_y) , since E_x appears before N_y in $\bar{\nu}$, we have $\gamma(E_x, N_y) = (x, y) \in \mathcal{P}_\nu$, so γ is well-defined. Note that γ takes the arcs of an (I, \bar{J}) -tree to the lattice points in its grid representation. Also, γ^{-1} is well-defined since if $(x, y) \in \mathcal{P}_\nu$, then N_y is preceded by at least x E steps in $\bar{\nu}$, and hence $(E_x, N_y) \in \mathcal{A}$. Thus γ is a bijection, and the next lemma follows.

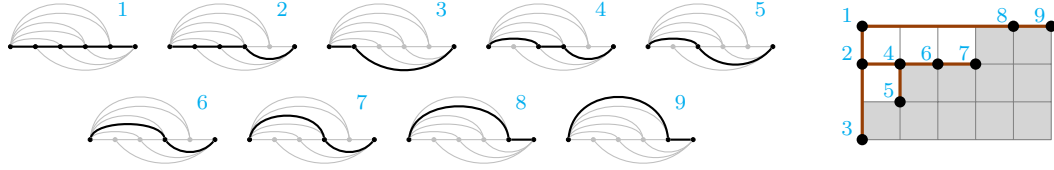
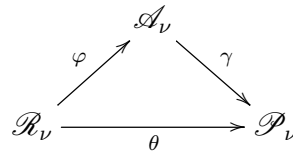


Figure 4.5: A maximal clique of routes in $\text{car}(\nu)$ representing a facet in the length-framed triangulation of $\mathcal{F}_{\text{car}(\nu)}$ with $\nu = \nu(5, 3)$. The bijection θ from Lemma 4.2.8 sends each route to a node in the ν -tree, while Θ_1 sends the maximal clique to the ν -tree.

Lemma 4.2.8. *The map $\theta : \mathcal{R}_\nu \rightarrow \mathcal{P}_\nu$ given by $\theta = \gamma \circ \varphi$ is a bijection. \square*

In summary, we have the following bijections between routes in $\text{car}(\nu)$, possible arcs in an (I, \bar{J}) -trees determined by ν , and lattice points lying weakly above ν .



The bijection θ leads to a characterization of the routes which appear in every facet of the length-framed triangulation of $\mathcal{F}_{\text{car}(\nu)}$. Recall from Lemma 4.2.4 that two routes in \mathcal{R}_ν are coherent if and only if their corresponding arcs in \mathcal{A}_ν are non-crossing. Since the non-crossing condition for arcs in (I, \bar{J}) -trees translates to the tree-compatibility condition of ν -trees, we have that routes in \mathcal{R}_ν are coherent if and only if their corresponding lattice points via θ are tree-compatible. Note that a ν -tree will always contain the root $(0, b)$, the valleys of the lattice path ν , along with each initial point of any initial N steps of ν and each terminal point of any terminal E steps of ν . These points correspond to the routes which are coherent with all other routes in the length-framing, and thus appear in every facet of the length-framed triangulation. In the example in Figure 4.5, the routes which appear in every top-dimensional simplex of the length-framed triangulation of $\mathcal{F}_{\text{car}(\nu)}$ are labeled 1, 3, 5, 7, 8, and 9.

By mapping routes to lattice points, θ extends to a bijection Θ_1 from the set of maximal cliques in the length framing of $\text{car}(\nu)$ to the set of ν -trees. The map Θ_1 takes the maximal clique of routes in Figure 4.5 to the ν -tree on the right. It is now also clear that two adjacent facets in the length-framed triangulation of $\mathcal{F}_{\text{car}(\nu)}$ differ by a single vertex, and the corresponding ν -trees under Θ_1 differ by a single lattice point via a rotation.

4.2.2 The planar-framed triangulation

In this section we show that the flow polytope $\mathcal{F}_{\text{car}(\nu)}$ has a regular unimodular triangulation whose dual graph is the Hasse diagram of a principal order ideal $I(\nu)$ in Young's lattice.

Principal order ideals in Young's lattice

Recall that **Young's lattice** Y is the poset on integer partitions with covering relations $\lambda \prec \lambda'$ if λ is obtained from λ' by removing one corner box of λ' . Recall that a lattice path ν in the rectangular grid defined by $(0, 0)$ to (a, b) defines a partition $\lambda(\nu) = (\lambda_1, \dots, \lambda_b)$ by letting λ_k denote the number of E steps appearing before the $(b - k + 1)$ -th N step in ν . The Young diagram for $\lambda(\nu)$ may be visualized as the region within the rectangle from $(0, 0)$ to (a, b) which lies NW of ν . For example, the path ν in Figure 4.1 defines the partition $\lambda(\nu) = (6, 3, 3, 2, 0)$. An **order ideal** of a poset P is a subset $I \subseteq P$ with the property that if $x \in I$ and $y \leq x$, then $y \in I$. An ideal is said to be **principal** if it has a single maximal element $x \in P$, and such an ideal will be denoted by $I(x)$.

If μ is a ν -Dyck path, then it lies weakly above the path ν and so μ can be identified with a partition $\lambda(\mu)$ that is contained in $\lambda(\nu)$. Thus there is a one-to-one correspondence between the set of ν -Dyck paths with the set of elements in the order ideal $I(\nu) := I(\lambda(\nu))$ in Y . Under this correspondence, in terms of ν -Dyck paths, a path π covers a path μ if and only if π can be obtained from μ by replacing a consecutive NE pair by a EN pair. See the right side of Figure 4.7 for an example of $I(\nu)$ with $\nu = NENE^2NE^2$.

The planar-framed triangulation

We can now study the dual structure of the planar-framed triangulation. The set of routes which are coherent in the planar framing are different than those under the length framing. However, the bijection $\theta : \mathcal{R}_\nu \rightarrow \mathcal{P}_\nu$ in Lemma 4.2.8 given by $R_{x,y} \mapsto (x, y)$ is not dependent on any framing, and still maps the routes in a simplex to a set of lattice points in \mathcal{P}_ν . To translate the coherence of routes in the planar framing to the collections of lattice points in \mathcal{P}_ν , we need the following notion. Two lattice points (x_1, y_1) and (x_2, y_2) with $x_1 < x_2$ are said to be **path-incompatible** if $y_1 > y_2$. Otherwise, any other pair of lattice points are said to be **path-compatible**. Maximal sets of path-compatible lattice points lying above ν determine a unique ν -Dyck path.

Lemma 4.2.9. *Let $\theta : \mathcal{R}_\nu \rightarrow \mathcal{P}_\nu$ be the bijection $R_{x,y} \mapsto (x, y)$. Two routes $R_{x,y}$ and $R_{x',y'}$ in the framed graph $(\text{car}(\nu), \prec_{\text{planar}})$ are coherent if and only if (x, y) and (x', y') are path-compatible.*

Proof. A result of Mészáros, Morales and Striker [51, Lemma 6.5] states that two routes in a planar framing of a G are coherent if and only if they are non-crossing in a planar drawing of G . Let $R_{x,y}$ and $R_{x',y'}$ be two non-crossing routes in $\text{car}(\nu)$, with $x < x'$. The non-crossing condition guarantees that if $x < x'$, then $y < y'$. Thus (x, y) and (x', y') are path-compatible. Conversely, if (x, y) and (x', y') are path-compatible, then $y < y'$, which guarantees that $R_{x,y}$ and $R_{x',y'}$ are non-crossing. \square

As a consequence, θ maps a maximal clique of coherent routes in $(\text{car}(\nu), \prec_{\text{planar}})$ to a maximal set of path-compatible points in \mathcal{P}_ν , which is a ν -Dyck path. Thus θ extends to a bijection Θ_2 from maximal cliques of routes in $(\text{car}(\nu), \prec_{\text{planar}})$ to the

set of ν -Dyck paths. We observe that a ν -Dyck path always contains the lattice points of any initial N steps and terminal E steps of ν . Hence, under θ , these points correspond to the routes that are coherent with all other routes, and thus appear in every facet of the planar-framed triangulation. For example, the routes in Figure 4.6 appearing in every facet of the planar-framed triangulation of $\mathcal{F}_{\text{car}(\nu)}$ are labeled 1, 2, 7, 8, and 9.

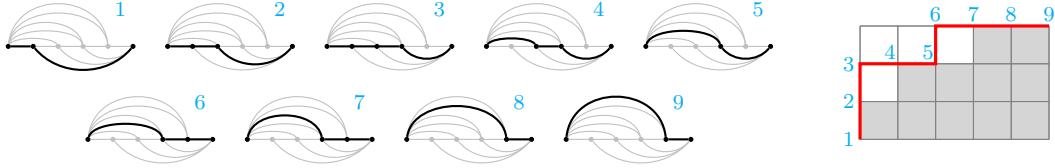


Figure 4.6: A maximal clique of routes in $\text{car}(\nu)$ corresponding to a facet in the planar-framed triangulation of $\mathcal{F}_{\text{car}(\nu)}$ for $\nu = \nu(5, 3)$. The map θ from Lemma 4.2.8 sends each route (left) to a lattice point on the ν -Dyck path (right), while Θ_2 sends the maximal clique to the ν -Dyck path.

Theorem 4.2.10. *The planar-framed triangulation of $\mathcal{F}_{\text{car}(\nu)}$ is a regular and unimodular triangulation whose dual graph is the Hasse diagram of the principal order ideal $I(\nu)$ in Young’s lattice Y .*

Proof. Under the bijection Θ_2 , two top-dimensional simplices are adjacent if and only if their corresponding ν -Dyck paths π_1 and π_2 differ by a single lattice point. Let $(x_1, y_1) \in \pi_1$ and $(x_2, y_2) \in \pi_2$ be the lattice points which are not contained in both paths. Assume without loss of generality that $x_1 < x_2$. Since these lattice points are not path-compatible, we must have $y_1 > y_2$. Thus (x_1, y_1) is in the top left corner of the single square determined by (x_1, y_1) and (x_2, y_2) , while (x_2, y_2) is in the bottom left. In other words, π_1 and π_2 differ by a transposition of a consecutive NE pair, which is precisely the description of the covering relation in the principal order ideal $I(\nu)$. \square

The graph on the right in Figure 4.7 is an example of the dual graph of the planar-framed triangulation of $\mathcal{F}_{\text{car}(\nu)}$, where $\nu = \nu(5, 3)$.

In summary, we’ve now seen the map $\theta : \mathcal{R}_\nu \rightarrow \mathcal{P}_\nu$ extend to a bijection between facets in triangulations and combinatorial objects in two ways. In the length-framed case, θ extended to the bijection Θ_1 between maximal cliques and ν -trees, while in the planar-framed case θ extended to a bijection Θ_2 between maximal cliques and ν -Dyck paths.

4.2.3 Comparing the length-framed and planar-framed triangulations

A special case when the dual graph of the length-framed and planar-framed triangulations of $\mathcal{F}_{\text{car}(\nu)}$ are the same is given by the following proposition.

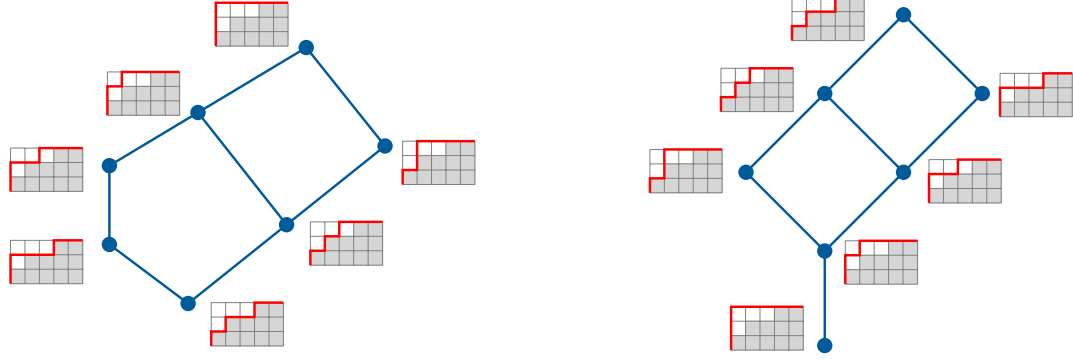


Figure 4.7: The ν -Tamari lattice (left) and the Hasse diagram of the order ideal $I(\nu) \subseteq Y$ (right) for $\nu = \nu(5, 3)$. These are the dual graphs of the length-framed and planar-framed triangulations of $\mathcal{F}_{\text{car}(\nu)}$.

Proposition 4.2.11. *When $\nu = E^a N^b$, so that the set of ν -Dyck paths is the set of all lattice paths from $(0, 0)$ to (a, b) , the length-framed triangulation and the planar-framed triangulation of $\mathcal{F}_{\text{car}(\nu)}$ have the same dual graph. Furthermore, $\text{Tam}(\nu)$ is isomorphic to $I(\nu)$.*

Proof. We use the ν -Dyck path description (see Section 2.5.2) of the ν -Tamari lattice $\text{Tam}(\nu)$ in this proof. Let μ be a ν -Dyck path. For any valley point p of μ , the next lattice point q in μ with $\text{horiz}_\nu(p) = \text{horiz}_\nu(q)$ is the next lattice point after p . This is because the horizontal distance of any of the lattice points in a run of consecutive N steps is the same when $\nu = E^a N^b$. Performing a rotation on μ at the valley point p to obtain the ν -Dyck path μ' is then the same as exchanging the EN pair centered at p with an NE pair in μ . Thus $\mu <_\nu \mu'$ is a covering relation in the lattice $\text{Tam}(\nu)$ if and only if it is a covering relation in the dual order ideal $I(\nu)^*$. Therefore, $\text{Tam}(\nu) = I(\nu)^*$. Lastly, the lattice $I(\nu)$ is self-dual since $\nu = E^a N^b$. Therefore, $\text{Tam}(\nu)$ and $I(\nu)$ are isomorphic. \square

This special case when $\nu = E^a N^b$ will be encountered again in Chapter 5, where we will see that $\mathcal{F}_{\text{car}(\nu)}$ is integrally equivalent to the product of two simplices $\Delta_a \times \Delta_b$. The triangulations induced on $\Delta_a \times \Delta_b$ via this integral equivalence by the length-framed and planar-framed triangulations are both examples of “staircase triangulations” of $\Delta_a \times \Delta_b$. Staircase triangulations will be discussed in more detail in Chapter 5.

4.2.4 The h^* -vector of the ν -caracol flow polytope

Recall that the h^* -vector of a lattice polytope can be computed from any of its unimodular triangulations. Therefore, to obtain h^* -vector of $\mathcal{F}_{\text{car}(\nu)}$, we can compute the h -vector of the planar-framed triangulation of $\mathcal{F}_{\text{car}(\nu)}$.

We begin by recalling some relevant definitions from [71]. Given a simplicial complex, a **shelling** is an ordering F_1, \dots, F_s of its facets such that for every $i < j$ there is some $k < j$ such that the intersection $F_i \cap F_j \subseteq F_k \cap F_j$, and $F_k \cap F_j$ is a facet of F_j . A simplicial complex is said to be **shellable** if it admits a shelling.

The h -vectors of shellable simplicial complexes have nonnegative entries which can be computed combinatorially from the shelling order as follows. For a fixed shelling order F_1, \dots, F_s define the restriction R_j of the facet F_j as the set $R_j := \{v \in F_j : v \text{ is a vertex in } F_j \text{ and } F_j \setminus v \subseteq F_i \text{ for some } 1 \leq i < j\}$. Then the i -th entry of the h -vector is given by $h_i = |\{j : |R_j| = i, 1 \leq j \leq s\}|$.

Lemma 4.2.12. *Let \mathcal{C} be the planar-framed triangulation of $\mathcal{F}_{\text{car}(\nu)}$ interpreted as a simplicial complex. Any linear extension of $I(\nu)$ gives a shelling order of \mathcal{C} .*

Proof. By Theorem 4.2.10 we can give the dual graph of \mathcal{C} the structure of $I(\nu)$, identifying each facet in \mathcal{C} with the associated ν -Dyck path in $I(\nu)$. For a linear extension L of $I(\nu)$, we can order the facets F_1, \dots, F_s of \mathcal{C} according to L . Let π_i and π_j be two ν -Dyck paths in L , with $i < j$. Let π_{s_1} be the minimal ν -Dyck path that covers both π_i and π_j , i.e. $\pi_{s_1} = \pi_i \vee \pi_j$ in $I(\nu)$. Now π_{s_1} contains the lattice points in $\pi_i \cap \pi_j$, and so $F_i \cap F_j \subseteq F_{s_1}$. It is clear that there exists a sequence of ν -Dyck paths $\pi_{s_1}, \pi_{s_2}, \dots, \pi_j$ such that each path contains the lattice points $\pi_i \cap \pi_j$, and each path is formed from the previous path by replacing a consecutive NE pair with EN . Given such a sequence of paths, let π_k be the second to last path in the sequence. Replacing a consecutive NE pair with EN in π_k yield π_j . Now $k < j$, and $F_i \cap F_j$ is contained in every facet F_{s_ℓ} for $1 \leq \ell \leq k$. In particular, $F_i \cap F_j \subseteq F_k \cap F_j$. Furthermore, π_k and π_j differ by a single lattice point, hence we obtain that $F_k \cap F_j$ is a facet of F_j . \square

Let ν be a lattice path from $(0, 0)$ to (a, b) . Recall from Definition 3.1.5 that the ν -Narayana number $\text{Nar}_\nu(i)$ is the number of ν -Dyck paths with i valleys. The ν -Narayana polynomial is $N_\nu(x) = \sum_{i \geq 0} \text{Nar}_\nu(i)x^i$. The following now extends a result of Mészáros [48, Theorem 4.4] for the classical case when $\nu = (NE)^n$ to general ν .

Theorem 4.2.13. *The h^* -polynomial of $\mathcal{F}_{\text{car}(\nu)}$ is the ν -Narayana polynomial.*

Proof. As previously mentioned, it will suffice to find the h -vector of the planar-framed triangulation of $\mathcal{F}_{\text{car}(\nu)}$, which can be computed from a shelling order of the planar-framed triangulation of $\mathcal{F}_{\text{car}(\nu)}$. We fix a linear extension of $I(\nu)$, which by Lemma 6.1 a gives a shelling order F_1, \dots, F_s . For a facet F_i , $|R_i|$ is the number of facets incident to F_i appearing before F_i in the shelling order. Since the shelling order is given by a linear extension of $I(\nu)$, $|R_i|$ is the number of elements covered by F_i in $I(\nu)$. By the cover relation in $I(\nu)$, F_i covers exactly as many elements as its corresponding ν -Dyck path has valleys. The i -th entry of the h -vector can now be computed as follows

$$\begin{aligned} h_i &= |\{j : |R_j| = i, 1 \leq j \leq s\}| \\ &= |\{\text{paths in } I(\nu) \text{ that cover exactly } i \text{ paths}\}| \\ &= |\{\nu\text{-Dyck paths with exactly } i \text{ valleys}\}| \\ &= \text{Nar}_\nu(i). \end{aligned} \quad \square$$

Example 4.2.14. Let $\nu = NENE^2NE^2$. The dual graph of the planar-framed triangulation of $\mathcal{F}_{\text{car}(\nu)}$ is then the Hasse diagram of $I(\nu)$ as shown on the right in Figure 4.7. The number of ν -Dyck paths with 0, 1, and 2 valleys are respectively 1, 4, and 2. Thus the ν -Narayana polynomial is $\text{Nar}_\nu(x) = 1 + 4x + 2x^2$.

A different proof of Theorem 4.2.13 can be obtained by computing the h -vector of the length-framed triangulation of $\mathcal{F}_{\text{car}(\nu)}$, which by Corollary 4.2.7 is combinatorially equivalent to the ν -Tamari complex with the pair (I, \bar{J}) associated to ν . In [16, Lemma 4.5] a shelling order on facets of this complex was used to show that the h -vector of the (I, \bar{J}) -Tamari complex is given by the ν -Narayana numbers. Since any lattice unimodular triangulation can be used to calculate the h^* -vector of $\mathcal{F}_{\text{car}(\nu)}$, Theorem 4.2.13 provides a new proof that the h -vector of the ν -Tamari complex is given by the ν -Narayana numbers.

4.2.5 A connection with order polytopes

Let G be a planar graph with a unique source and sink. A result of Mészáros, Morales and Striker [51, Theorem 3.11] states that for such a graph G , the flow polytope \mathcal{F}_G is integrally equivalent to the order polytope $\mathcal{O}(P_G)$, where P_G is a poset induced by the bounded faces of the planar embedding of G .

In this section, we explain how our results for flow polytopes on the caracol graphs $\text{car}(\nu)$ lead to analogous results for a certain class of order polytopes $\mathcal{O}(Q_\nu)$. We give a brief background of known results relating order polytopes and flow polytopes following the exposition of [51], and explain their implications when applied to $\text{car}(\nu)$.

Let (P, \leq_P) be a finite poset with elements $\{p_1, \dots, p_d\}$. The **order polytope** of P is the set of points

$$\mathcal{O}(P) = \{(x_{p_1}, \dots, x_{p_d}) \in [0, 1]^d \mid x_{p_i} \leq x_{p_j} \text{ if } p_i \leq_P p_j\}.$$

Given a linear extension $\sigma : P \rightarrow [d]$ of the poset P , i.e. an order preserving bijection with $[d]$ endowed with its natural order, define the simplex

$$\Delta_\sigma = \{(x_{p_1}, \dots, x_{p_d}) \in [0, 1]^d \mid x_{\sigma^{-1}(1)} \leq \dots \leq x_{\sigma^{-1}(d)}\}.$$

The **canonical triangulation** of $\mathcal{O}(P)$, first defined by Stanley [62], is the set of top-dimensional simplices

$$\{\Delta_\sigma \mid \sigma \text{ is a linear extension of } P\}.$$

Thus the normalized volume of $\mathcal{O}(P)$ is the number of linear extensions of P .

For a planar graph G with a fixed embedding in the plane, the **truncated dual graph** G^* of G is the dual graph whose vertices correspond to the bounded faces of G . Viewing G^* as embedded on the plane also, then the orientation on the edges of G induces an orientation on the edges of G^* . The graph G^* then induces the Hasse diagram of a poset that is denoted by P_G . We demonstrate this in the case of $\text{car}(\nu)$.

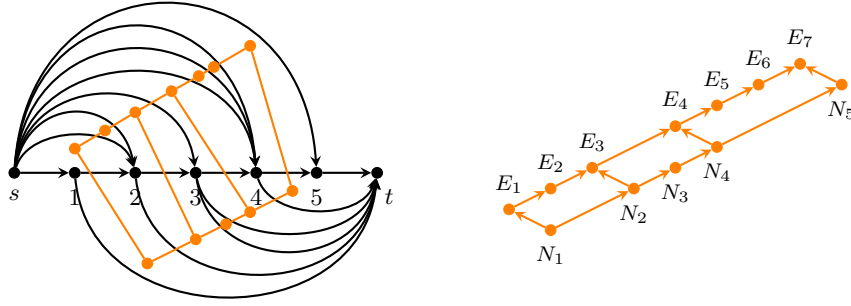


Figure 4.8: A graph $\text{car}(\nu)$ and its truncated dual $\text{car}(\nu)^*$ in orange (left), and the induced Hasse diagram of the poset $Q_\nu = P_{\text{car}(\nu)}$ (right).

For a lattice path ν from $(0, 0)$ to (a, b) , we fix the embedding of $\text{car}(\nu)$ onto the plane so that the vertices of $\text{car}(\nu)$ are in increasing order on the x -axis, and edges incident to the source s and sink t are respectively drawn above and below the x -axis. Then the poset $P_{\text{car}(\nu)}$ has $a+b$ elements corresponding to the bounded faces of the embedded $\text{car}(\nu)$, and is constructed as follows. Using the edge labeling for $\text{car}(\nu)$ described in Section 4.1 and shown in Figure 4.3, we label the vertices in the truncated dual graph $\text{car}(\nu)^*$ in the following manner. Each vertex in a bounded region above the x -axis is labeled E_k where k is the label of the longest bounding edge of the region, and each bounded region below the x -axis is labeled N_k where k is the label of the shortest labeled bounding edge of the region. If two vertices p and q are adjacent in $\text{car}(\nu)^*$, then the regions associated with them share a directed edge (i, j) of $\text{car}(\nu)$. We direct the edge (p, q) in $\text{car}(\nu)^*$ toward the vertex corresponding to the region to the left of the edge (i, j) . Figure 4.8 gives an example.

Note that we recover ν from $P_{\text{car}(\nu)}$ by taking the linear extension of $P_{\text{car}(\nu)}$ where E steps are read before N steps whenever possible. With this observation, it means that we can define a class of posets Q_ν (equal to $P_{\text{car}(\nu)}$) indexed by lattice paths ν without any reference to flow polytopes. The Hasse diagram of the poset Q_ν can be constructed from ν by forming an increasing chain of the E steps and an increasing chain of the N steps, and then connecting the chains at each NE pair forming a peak of ν (directed toward the E step).

It was first observed by Postnikov (also see Mészáros, Morales and Striker [51, Theorem 1.3]) that the canonical triangulation of $\mathcal{O}(P_G)$ is the same as the planar-framed DKK triangulation of \mathcal{F}_G up to an integral equivalence. Combined with Theorems 4.2.5 and 4.2.10, we have the following two corollaries.

Corollary 4.2.15. *The canonical triangulation of the order polytope $\mathcal{O}(Q_\nu)$ has dual graph which is the Hasse diagram of the principal order ideal $I(\nu)$ in Young's lattice.*

Corollary 4.2.16. *The order polytope $\mathcal{O}(Q_\nu)$ has a regular unimodular triangulation whose dual graph is the ν -Tamari lattice $\text{Tam}(\nu)$.*

Corollary 4.2.17. *The number of linear extensions of the poset Q_ν is $\text{Cat}(\nu)$.*

For a poset P , let $J(P)$ denote the lattice of order ideals of P ordered by inclusion. From [62, Section 5], the maximal chains of $J(P)$ are in bijection with the facets in the canonical triangulation of $\mathcal{O}(P)$. This gives another perspective on the direct relationship between facets in the planar-framed triangulation of $\mathcal{F}_{\text{car}(\nu)}$, maximal cliques in the flow polytope $\mathcal{F}_{\text{car}(\nu)}$, ν -Dyck paths, maximal chains in $J(Q_\nu)$, and facets in the canonical triangulation of $\mathcal{O}(Q_\nu)$. In this case, the Hasse diagram of $J(Q_\nu)$ can be obtained by taking the lattice on the points \mathcal{P}_ν which lie above ν , and rotating it counterclockwise by 45 degrees.

Having obtained results for order polytopes via methods for flow polytopes, we now end this section with a result for flow polytopes via methods for order polytopes. Stanley [62, Section 1] gave a full description of the faces of an order polytope $\mathcal{O}(P)$ via partitions of the poset $\widehat{P} := P \cup \{\widehat{0}, \widehat{1}\}$ into connected blocks satisfying a compatibility criterion. Translating these results to our setting, we can describe the face lattice of $\mathcal{F}_{\text{car}(\nu)}$ using the following notion of valid subwords of $\widehat{\nu} := N\nu E$.

Definition 4.2.18. Let $\widehat{\nu} := N\nu E$, with its letters indexed by their position in the word. A subword σ of $\widehat{\nu}$ is **valid** if it satisfies the following conditions.

1. If σ contains an E step and an N step of $\widehat{\nu}$, then it contains a peak of $\widehat{\nu}$.
2. If σ contains E_i and E_j with $i < j$, then σ contains all E_k with $i < k < j$.
3. If σ contains N_i and N_j with $i < j$, then σ contains all N_k with $i < k < j$.
4. If σ contains N_i and E_j with $i < j$, then σ contains all steps X_k of $\widehat{\nu}$ with $i < k < j$.

In particular, $\widehat{\nu}$ itself is a valid subword, as are each of the letters in $\widehat{\nu}$. The word $\widehat{\nu}$ can now be partitioned into valid subwords. As an example, consider the word $\widehat{\nu} = N_1 N_2 E_3 E_4 N_5 E_6 N_7 N_8 E_9$, which can be partitioned into the valid subwords $\sigma_1 = N_1 N_2 E_3 N_5$, $\sigma_2 = E_4$, and $\sigma_3 = E_6 N_7 N_8 E_9$. The following is a direct consequence of [62, Theorem 1.2] when translated to our setting (connectedness corresponds with conditions 1, 2, and 3 in Definition 4.2.18, while compatibility corresponds with condition 4).

Proposition 4.2.19. *The face lattice of $\mathcal{F}_{\text{car}(\nu)}$ is the poset of partitions of $\widehat{\nu}$ into valid subwords, ordered by reverse inclusion of the partitions. The face lattice is ranked by the number of valid subwords in the partition.*

The empty face of $\mathcal{F}_{\text{car}(\nu)}$ corresponds to $\widehat{\nu}$ itself and the top dimensional face is the partition into $a + b + 2$ subwords, each consisting of a single step of $\widehat{\nu}$. We have the following corollary.

Corollary 4.2.20. *Let $\text{peak}(\nu)$ denote the number of consecutive NE pairs in a lattice path ν from $(0, 0)$ to (a, b) . The number of facets of $\mathcal{F}_{\text{car}(\nu)}$ is then $a + b + \text{peak}(\widehat{\nu})$.*

Proof. The facets of $\mathcal{F}_{\text{car}(\nu)}$ correspond with the partitions of $\widehat{\nu}$ into $a + b + 1$ valid subwords. In such a partition, exactly one subword contains two letters. From the conditions of a valid subword, we see that such a subword is either a peak, or consists of two E steps, or two N steps. As there are exactly a valid subwords with two E steps and b valid subwords with two N steps, the result follows. \square

4.3 The polytope $\mathcal{U}_{I, \bar{J}}$

Having seen in Corollary 4.2.7 that the length-framed triangulation of $\mathcal{F}_{\text{car}(\nu)}$ gives a geometric realization of the ν -Tamari complex, we wish to know how it relates to other known realizations. Recall from Chapter 2 that for any valid pair (I, \bar{J}) , Ceballos, Padrol, and Sarmiento [16] gave a realization of the $\nu(I, \bar{J})$ -Tamari complex by triangulating the polytope

$$\mathcal{U}_{I, \bar{J}} := \{(\mathbf{e}_i, \mathbf{e}_j) \mid i \in I, \bar{j} \in \bar{J}\}.$$

The faces of the triangulation were given by

$$\Delta_{F_{I, \bar{J}}} := \text{conv}\{(\mathbf{e}_i, \mathbf{e}_j) \mid (i, j) \in F_{I, \bar{J}}\},$$

where $F_{I, \bar{J}}$ is a (I, \bar{J}) -forest.

Having two different polytopes, each with a triangulation giving rise to the ν -Tamari complex, it is natural to consider the connection between them. In this section we determine that the polytopes $\mathcal{U}_{I, \bar{J}}$ and $\mathcal{F}_{\text{car}(\nu)}$ are in fact integrally equivalent. As a consequence, we obtain that $\mathcal{U}_{I, \bar{J}}$ can be subdivided using the subdivision algebra, answering a question of Ceballos, Padrol, and Sarmiento. We further show how $\mathcal{U}_{I, \bar{J}}$ can be projected onto an acyclic root polytope, which answers the same question from the perspective of acyclic root polytopes.

4.3.1 The graph $G(I, \bar{J})$

In order to relate the polytopes $\mathcal{F}_{\text{car}(\nu)}$ and $\mathcal{U}_{I, \bar{J}}$, we construct a flow polytope over a graph $G(I, \bar{J})$ which is integrally equivalent to both. The graph $G(I, \bar{J})$ will also allow us to make explicit the connection between $\mathcal{U}_{I, \bar{J}}$ and acyclic root polytopes.

Crucial to our construction is the following relabeling of certain elements in \bar{J} . Define the map $\text{prec} : \bar{J} \rightarrow [n]$ as follows. If with respect to the order $\prec_{I, \bar{J}}$, the element $\bar{j} \in \bar{J}$ is not immediately preceded by an element in I , then $\text{prec}(\bar{j}) = j$. Otherwise, $\text{prec}(\bar{j})$ is defined to be this immediately preceding element that is in I .

Let $A(I, \bar{J})$ be the graph with vertex set $I \cup \bar{J}$ and edge set $\{(i, \bar{j}) \mid i \prec_{I, \bar{J}} \bar{j}, i \in I, \bar{j} \in \bar{J}\}$. If each $\bar{j} \in \bar{J}$ is identified with $\text{prec}(\bar{j})$, then the identification partitions $I \cup \bar{J}$ into blocks of size one or two. Define $\text{prec}(A(I, \bar{J}))$ to be the quotient graph of $A(I, \bar{J})$ under this partition of its vertices. We may identify its vertex set with $I \cup \text{prec}(\bar{J})$, and its edge set is $\{(i, \text{prec}(\bar{j})) \mid i < \text{prec}(\bar{j}), i \in I, \bar{j} \in \bar{J}\}$.

Definition 4.3.1. Let G be a simple graph on a linearly ordered vertex set whose edges are ordered from the smaller to the larger vertex. Define the **minimal graph**

$\min(G)$ to be the graph obtained from G by removing every edge (i, j) such that there is a directed path i, i_1, \dots, i_k, j in G with $k \geq 1$.

As an example, the graph $G(I, \bar{J})$ in Figure 4.9 is the minimal graph of the graph $\text{prec}(A(I, \bar{J}))$. In fact, it is easy to verify that for any valid (I, \bar{J}) -pair, $G(I, \bar{J}) = \min \text{prec}(A(I, \bar{J}))$.

We note that $G(I, \bar{J})$ can be thought of as a directed graph, with edges directed from the smaller to the larger vertex. Also, the head of each edge is in I , while the tail of each edge is in $\text{prec}(\bar{J})$.

Recall that given a graph G on $[n]$, the fully augmented graph \tilde{G} is the connected graph \tilde{G} with vertex set $\tilde{V}(G) = [n] \cup \{s, t\}$, where $s < 1 < \dots < n < t$, and edge set $\tilde{E}(G) \cup \{(s, i), (i, t) \mid i \in V(G)\}$. Also, recall that the partially augmented graph \hat{G} is obtained by removing from \tilde{G} the set of edges of the form (s, i) or (j, t) where i is a sink of G or j is a source of G .

Example 4.3.2. Consider the valid pair $I = \{1, 2, 3, 5, 9\}, \bar{J} = \{\bar{2}, \bar{7}, \bar{8}, \bar{9}\}$. Then $1 < 2 < \bar{2} < 3 < 5 < \bar{7} < \bar{8} < 9 < \bar{9}$ with respect to the order $<_{I, \bar{J}}$, so $\text{prec}(\bar{J}) = \{2, 5, 8, 9\}$. The graphs $A(I, \bar{J})$ and $\text{prec}(A(I, \bar{J}))$ are shown on the right of Figure 4.9. The minimal graph $G(I, \bar{J})$ has vertex set $I \cup \text{prec}(\bar{J}) = \{1, 2, 3, 5, 8, 9\}$. The partially augmented graph $\hat{G}(I, \bar{J})$ has vertex set $V(G(I, \bar{J})) \cup \{s, t\}$ and edge set $E(G(I, \bar{J})) \cup \{(s, i) \mid i \in I\} \cup \{(\text{prec}(\bar{j}), t) \mid \bar{j} \in \bar{J}\}$. These are shown on the left of Figure 4.9.

Remark 4.3.3. Looking ahead, the four graphs displayed in Figure 4.9 are central to the four polytopes of Theorem 4.3.8 in the sense that the polytopes $\mathcal{S}(G)$ and $\mathcal{F}_{\hat{G}}$ can respectively be seen as the convex hulls of (sub)paths of the graphs $G = G(I, \bar{J})$ and \hat{G} , while $\mathcal{U}_{I, \bar{J}}$ and the acyclic root polytope \mathcal{R}_G^+ can be seen as the convex hulls of edges of the graphs $A = A(I, \bar{J})$ and $\text{prec}(A)$. Perhaps this viewpoint illuminates why these four polytopes have the ‘same’ subdivision algebra.

Lemma 4.3.4. *For any two vertices v and w of $G(I, \bar{J})$ with $v < w$ there exists at most one directed path from v to w .*

Proof. Suppose there are two distinct paths P and Q from v to w . We can assume without loss of generality that v is the first point at which P and Q differ. Then the first edges (v, p_1) and (v, q_1) of P and Q are different, and we may assume that $p_1 < q_1$. Now, the path P is of the form $v, p_1, \dots, p_k, \dots, w$ where p_k is the largest vertex in P which is smaller than q_1 . Since (v, q_1) and (p_k, p_{k+1}) are edges in $G(I, \bar{J})$, then $p_k \in I$ and $q_1 \in \text{prec}(\bar{J})$. Since $p_k < q_1$, by definition, the edge (p_k, q_1) is in $\text{prec}(A(I, \bar{J}))$, and furthermore there is a path P' in $G(I, \bar{J})$ from p_k to q_1 . However, the concatenation of the paths v, p_1, \dots, p_k and P' is then a path from v to q_1 , and by the definition of $G(I, \bar{J})$, the edge (v, q_1) cannot be in $G(I, \bar{J})$, which is a contradiction. \square

We have just shown that as a directed graph, $G(I, \bar{J}) = \min \text{prec}(A(I, \bar{J}))$ is acyclic. However, in general, it is possible to start with a graph and obtain a

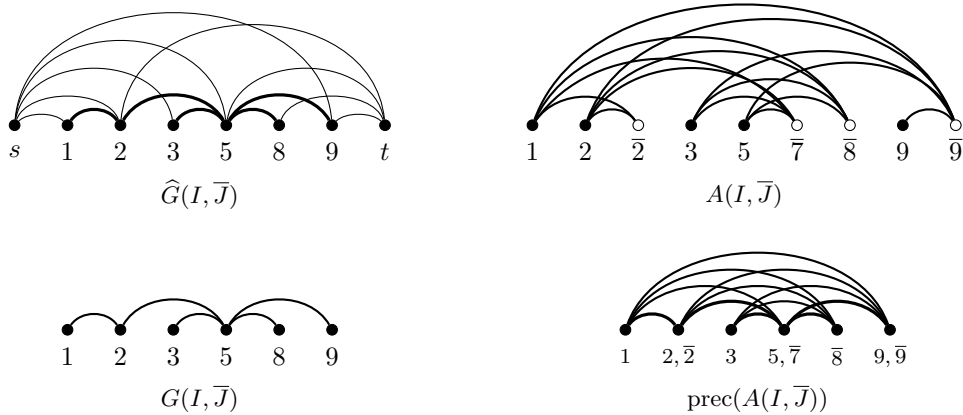


Figure 4.9: Various graphs associated to the valid pair $I = \{1, 2, 3, 5, 9\}$ and $\bar{J} = \{\bar{2}, \bar{7}, \bar{8}, \bar{9}\}$. The graph $A(I, \bar{J})$ (top right), its quotient graph $\text{prec}(A(I, \bar{J}))$ (bottom right), its minimal graph $G(I, \bar{J})$ (bottom left), and the partially augmented graph $\widehat{G}(I, \bar{J})$ (top left). See Remark 4.3.3 for an explanation of the roles played by these graphs in Theorem 4.3.8.

minimal graph that contains cycles (as an undirected graph). For example, let H be the graph on the vertex set $[4]$ with directed edges $(1, 3)$, $(1, 4)$, $(2, 3)$, and $(2, 4)$. Then $\min(H) = H$ is not acyclic, as an undirected graph. This example illustrates why under the uniform projection map of Ceballos et al. [16, Section 1.4], certain $\mathcal{U}_{I, \bar{J}}$ do not project to acyclic root polytopes. See Example 4.3.5.

Example 4.3.5. Let $I = \{1, 2\}$ and $\bar{J} = \{\bar{3}, \bar{4}\}$ so that $\mathcal{U}_{I, \bar{J}} = \text{conv}\{(\mathbf{e}_1, \mathbf{e}_3), (\mathbf{e}_1, \mathbf{e}_4), (\mathbf{e}_2, \mathbf{e}_3), (\mathbf{e}_2, \mathbf{e}_4)\}$. The map of Ceballos et al. which projects $\mathbb{R}^8 \rightarrow \mathbb{R}^4$ along the subspace spanned by $\{(\mathbf{e}_i, \mathbf{e}_i) \mid i = 1, \dots, 4\}$ sends $\mathcal{U}_{I, \bar{J}}$ to the polytope $\mathcal{Q} = \text{conv}\{\mathbf{e}_1 - \mathbf{e}_3, \mathbf{e}_1 - \mathbf{e}_4, \mathbf{e}_2 - \mathbf{e}_3, \mathbf{e}_2 - \mathbf{e}_4\}$. This is not an acyclic root polytope for the simple reason that it does not contain the origin. Aside from that, \mathcal{Q} also cannot be described as the convex hull of points $\overline{\Phi}_G^+ = \Phi_{A_{n-1}}^+ \cap \text{cone}(G)$ where G is acyclic. If such a G exists, it must contain the edges $(1, 3)$, $(2, 3)$, $(2, 4)$ because they correspond to positive roots which cannot be expressed as positive linear combinations of other lower roots lying in \mathcal{Q} . If these edges are in G , then the acyclic G cannot contain the edge $(1, 4)$. However, the vertex $\mathbf{e}_1 - \mathbf{e}_4 \notin \text{cone}(G)$ for this G .

For the class of graphs $\text{prec}(A(I, \bar{J}))$, Lemma 4.3.6 shows that if we forget the orientation on the edges of $G(I, \bar{J}) = \min \text{prec}(A(I, \bar{J}))$, then $G(I, \bar{J})$ remains acyclic.

Lemma 4.3.6. *The graph $G(I, \bar{J})$ is acyclic as an non-oriented graph.*

Proof. Suppose there is a cycle in $G(I, \bar{J})$. Let v and w be the smallest and largest vertices in the cycle respectively. We can partition the cycle into two sequences of edges, each beginning at v and ending at w . By Lemma 4.3.4 we know that these sequences cannot both form directed paths from v to w . Thus at least one of the sequences is of the form $v, v_1, v_2, \dots, v_\ell, w$ where $v_k > v_{k+1}$ for some k . We choose k

so that v_k is the smallest vertex for which $v_{k+1} < v_k$. The edge (v_{k+1}, v_k) is an edge in $G(I, \bar{J})$ with $v_{k+1} < v_k$, so $v_{k+1} \in I$ and $v_k = \text{prec}(\bar{j})$ for some $\bar{j} \in \bar{J}$. Now any u_i in \bar{J} satisfying $v_{k+1} < u_i < v_k$ must satisfy $u_i = \text{prec}(u_i)$, as otherwise (v_{k+1}, v_k) can be written as a linear combination of (v_{k+1}, u_i) and (u_i, v_k) . It follows that the vertices u_1, \dots, u_ℓ satisfying $v_{k+1} < u_1 < \dots < u_\ell < v_k$ are all in I or are all in \bar{J} with $\text{prec}(u_i) = u_i$ for each i . We therefore also obtain that $v_{k-1} < v_{k+1} < v_k < v_{k+2}$. In the case that $u_i \in I$ for each i , we have that $u_\ell \neq v_k = \text{prec}(j)$, and hence $v_k \in I$. Now (v_k, v_{k+2}) is either an edge in $G(I, \bar{J})$ or a nonnegative linear combination of edges in $G(I, \bar{J})$. In either case, we can write (v_{k+1}, v_{k+2}) as a nonnegative linear combination of edges in $G(I, \bar{J})$ which is a contradiction. We similarly obtain a contradiction if all u_i are in \bar{J} and satisfy $\text{prec}(u_i) = u_i$. \square

4.3.2 A subdivision algebra for $\mathcal{U}_{I, \bar{J}}$

In this section we make explicit the relationships between four polytopes. These are the polytope $\mathcal{U}_{I, \bar{J}}$, the flow polytope $\mathcal{F}_{\widehat{G}(I, \bar{J})}$, the acyclic root polytope $\mathcal{R}_{G(I, \bar{J})}^+$, and a polytope $\mathcal{S}(G(I, \bar{J}))$ which generalizes a polytope of Mészáros from [48]. We begin with the construction of these polytopes using the graphs of Section 4.3.1. The reader may find it helpful to refer often to Figure 4.9.

For a valid pair $(I, \bar{J}) \in [n] \times [\bar{n}]$, suppose the graph $G(I, \bar{J})$ has m edges, so that the partially augmented graph \widehat{G} has $\widehat{m} = m + |I| + |\bar{J}|$ edges. For brevity we will generally suppress notation in this section, and simply write $G := G(I, \bar{J})$. Let $\{\mathbf{e}_{(i,j)} \mid (i,j) \in E(G)\}$ be the orthonormal basis for \mathbb{R}^m and let $\{\mathbf{e}_{(i,j)} \mid (i,j) \in E(\widehat{G})\}$ be the orthonormal basis for $\mathbb{R}^{\widehat{m}}$. Recall that the flow polytope $\mathcal{F}_{\widehat{G}}$ can be defined in terms of its routes, i.e.

$$\mathcal{F}_{\widehat{G}} = \text{conv}\{\text{routes } (s, \dots, t) \text{ in } \widehat{G}\} \subseteq \mathbb{R}^{\widehat{m}}.$$

Next, we show that $\mathcal{F}_{\widehat{G}}$ is integrally equivalent to a ν -caracol flow polytope.

Lemma 4.3.7. *For any valid pair (I, \bar{J}) and $\nu = \nu(I, \bar{J})$, the flow polytopes $\mathcal{F}_{\widehat{G}(I, \bar{J})}$ and $\mathcal{F}_{\text{car}(\nu)}$ are integrally equivalent.*

Proof. Recall from Lemma 2.3.6 that if e is an idle edge, then $\mathcal{F}_G \equiv \mathcal{F}_{G/e}$. Therefore, it suffices to show that we can contract idle edges in $\widehat{G}(I, \bar{J})$ and $\text{car}(\nu)$ to obtain the same graph. Let w be the number of valleys in $\bar{\nu}$. We can then write $\bar{\nu} = \prod_{i=1}^w E^{a_i} N^{b_i}$. If P_w denotes the path graph of $[w]$, let H be the graph obtained from $P_w \cup \{s, t\}$ by adding a_i copies of the edge (s, i) and b_i copies of the edge (i, t) for each $i \in [w]$. Contracting all idle inner edges of $\widehat{G}(I, \bar{J})$ and $\text{car}(\nu)$ yield H up to a relabeling of the vertices (see Figure 4.10), and so the result follows. \square

Let $\pi_1 : \mathbb{R}^{\widehat{m}} \rightarrow \mathbb{R}^m$ be the projection onto the coordinates associated with the inner edges of \widehat{G} , and define the polytope $\mathcal{S}(G)$ to be the image of $\mathcal{F}_{\widehat{G}}$ under π_1 . Note that since (I, \bar{J}) is a valid pair, we have that $I \cap \text{prec}(\bar{J}) \neq \emptyset$, and moreover every route in \widehat{G} of the form (s, v, t) with $v \in I \cap \text{prec}(\bar{J})$ projects to $\mathbf{0}$ under π_1 .

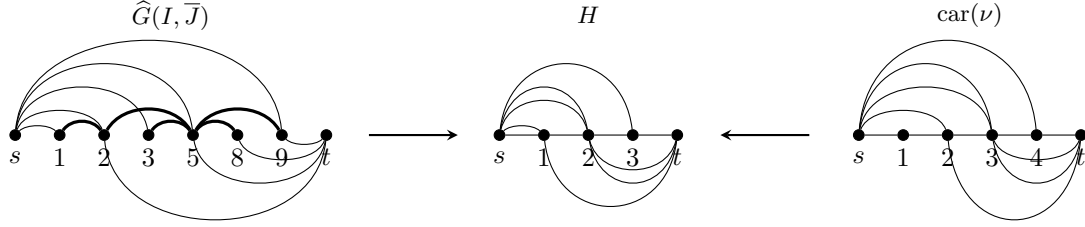


Figure 4.10: Contracting idle edges in $\widehat{G}(I, \bar{J})$ and $\text{car}(\nu)$ gives the graph H up to relabeling of the vertices. Here $I = \{1, 2, 3, 5, 9\}$ and $\bar{J} = \{\bar{2}, \bar{7}, \bar{8}, \bar{9}\}$.

The polytope $\mathcal{S}(G)$ can equivalently be defined as

$$\mathcal{S}(G) = \text{conv}\{\text{paths } (v_1, \dots, v_\ell) \text{ in } G \mid v_1 \in I \text{ and } v_\ell \in \text{prec}(\bar{J})\} \subseteq \mathbb{R}^m,$$

and in this definition we include the empty path in G so that $\mathbf{0} \in \mathcal{S}(G)$.

Recall that $A = A(I, \bar{J})$ is the graph on $I \cup \bar{J}$ with the edge set $\{(i, \bar{j}) \mid i \prec \bar{j}\} \subseteq I \times \bar{J}$. It follows that we can express $\mathcal{U}_{I, \bar{J}}$ as

$$\mathcal{U}_{I, \bar{J}} = \text{conv}\{(\mathbf{e}_i, \mathbf{e}_{\bar{j}}) \mid (i, \bar{j}) \in E(A)\} \subseteq \mathbb{R}^{2n}.$$

The acyclic root polytope \mathcal{R}_G^+ defined in Section 2.2 is

$$\mathcal{R}_G^+ = \text{conv}\{\mathbf{0}, \mathbf{e}_i - \mathbf{e}_j \mid (i, j) \in E(\text{prec}(A))\} \subseteq \mathbb{R}^n,$$

where $\text{prec}(A)$ is the quotient graph of A defined in Section 4.3.1.

We define the map $\pi_2 : \mathbb{R}^{2n} \rightarrow \mathbb{R}^n$ on the standard basis of \mathbb{R}^{2n} as follows. Let $\pi_2((\mathbf{e}_i, \mathbf{0})) = \mathbf{e}_i$ for $i = 1, \dots, n$, and

$$\pi_2((\mathbf{0}, \mathbf{e}_{\bar{j}})) = \begin{cases} -\mathbf{e}_{\text{prec}(\bar{j})}, & \text{if } \bar{j} \in \bar{J}, \\ -\mathbf{e}_j, & \text{if } \bar{j} \notin \bar{J}. \end{cases}$$

Let $\mathbb{A}_{I, \bar{J}}$ denote the affine span $\text{aff}\{(\mathbf{e}_i, \mathbf{e}_{\bar{j}}) \mid (i, \bar{j}) \in E(A)\}$, so that $\mathcal{U}_{I, \bar{J}} \subseteq \mathbb{A}_{I, \bar{J}}$. Now, the restriction $\pi_2 : \mathbb{A}_{I, \bar{J}} \rightarrow \mathbb{R}^n$ gives $\pi_2(\mathbf{e}_i, \mathbf{e}_{\bar{j}}) = \mathbf{e}_i - \mathbf{e}_{\text{prec}(\bar{j})}$ for each $(i, \bar{j}) \in E(A)$, and the image of $\mathcal{U}_{I, \bar{J}}$ under π_2 is \mathcal{R}_G^+ .

Recall $\mathbb{R}^{\widehat{m}} = \text{span}\{\mathbf{e}_e \mid e \in E(\widehat{G})\}$. We define a map $\varphi_1 : \mathbb{R}^{\widehat{m}} \rightarrow \mathbb{R}^{2n}$ by

$$\varphi_1(\mathbf{e}_e) = \begin{cases} (\mathbf{e}_i, \mathbf{0}), & \text{if } e = (s, i), \\ (\mathbf{0}, \mathbf{e}_j), & \text{if } e = (\text{prec}(\bar{j}), t), \\ (\mathbf{0}, \mathbf{0}), & \text{otherwise,} \end{cases}$$

where $\mathbf{0} \in \mathbb{R}^n$, and extend linearly. Now φ_1 maps routes of \widehat{G} to vertices of $\mathcal{U}_{I, \bar{J}}$, and the image of $\mathcal{F}_{\widehat{G}}$ is $\mathcal{U}_{I, \bar{J}}$ under φ_1 .

Let $\varphi_2 : \mathbb{R}^m \rightarrow \mathbb{R}^n$ be the linear map defined by $\varphi_2(\mathbf{e}_{(i,j)}) = \mathbf{e}_i - \mathbf{e}_j$ for $(i, j) \in E(G)$, extended linearly. We can now state our main theorem.

Theorem 4.3.8. *Let $I \subseteq [n]$, $\bar{J} \subseteq [\bar{n}]$ be a valid pair. For the polytope $\mathcal{U}_{I,\bar{J}}$, there exists an acyclic root polytope \mathcal{R}_G^+ and a flow polytope $\mathcal{F}_{\widehat{G}}$ such that the following diagram commutes:*

$$\begin{array}{ccc} \mathcal{F}_{\widehat{G}} & \xrightarrow{\varphi_1} & \mathcal{U}_{I,\bar{J}} \\ \pi_1 \downarrow & & \downarrow \pi_2 \\ \mathcal{S}(G) & \xrightarrow{\varphi_2} & \mathcal{R}_G^+ \end{array}$$

where φ_1 and φ_2 are integral equivalences.

Proof. We first check that φ_1 and φ_2 are integral equivalences. Let x_e denote the coordinate in \mathbb{R}^m associated with the edge e in \widehat{G} . Now φ_1 restricts to the linear map $\varphi_1 : \mathbb{R}^m \rightarrow \mathbb{A}_{I,\bar{J}}$ given by

$$\varphi_1((x_e)_{e \in \widehat{G}}) = \left(\sum_{i \in I} x_{(s,i)} \mathbf{e}_i, \sum_{\bar{j} \in \bar{J}} x_{(\text{prec}(\bar{j}),t)} \mathbf{e}_j \right)$$

where \mathbf{e}_i and \mathbf{e}_j are in \mathbb{R}^n .

If \mathbf{v} is a vertex in $\mathcal{F}_{\widehat{G}}$, then it corresponds to a unique route in G , which by Lemma 4.3.4 is determined by a pair of edges (s, i) and $(\text{prec}(\bar{j}), t)$ with $i \leq \text{prec}(\bar{j})$. Thus $x_{(s,i)} = x_{(\text{prec}(\bar{j}),t)} = 1$ and so $\varphi_1(\mathbf{v}) = (\mathbf{e}_i, \mathbf{e}_j)$, which is a vertex in $\mathcal{U}_{I,\bar{J}}$. In particular, φ_1 is a bijection between the vertices of $\mathcal{F}_{\widehat{G}}$ and $\mathcal{U}_{I,\bar{J}}$, and it extends to a bijection between the polytopes. Furthermore, since φ_1 maps $\mathcal{F}_{\widehat{G}} \subseteq [0, 1]^m$ into $\mathcal{U}_{I,\bar{J}} \subseteq [0, 1]^{2n}$ while preserving its dimension, it also preserves the respective lattices intersected with the affine span of the polytopes. Thus φ_1 is an integral equivalence.

In [47, Theorem 4.4] Mészáros showed that φ_2 is a linear map restricting to a bijection between $\mathcal{S}(G)$ and \mathcal{R}_G^+ , so it remains to check that φ_2 preserves the lattice. Note that the edges of G form an orthonormal basis for $\mathbb{R}^{|E(G)|}$, and so $\dim(\mathcal{S}(G)) = |E(G)|$. Since the dimension of \mathcal{R}_G^+ is the number of edges in its minimal graph, it also has dimension $|E(G)|$. Therefore φ_2 is a dimension preserving linear map between $[0, 1]$ -polytopes, and hence preserves the lattice.

Finally, we check that the diagram commutes. By linearity of the maps, it suffices to check that the square commutes for vertices of $\mathcal{F}_{\widehat{G}}$. Let \mathbf{v} be a vertex of $\mathcal{F}_{\widehat{G}}$, which then corresponds with a route R determined by a pair of edges (s, i) and $(\text{prec}(j), t)$. Now $\pi_2(\varphi_1(\mathbf{v})) = \pi_2((\mathbf{e}_i, \mathbf{e}_j)) = \mathbf{e}_i - \mathbf{e}_{\text{prec}(j)}$. On the other hand, if $(i_0, i_1), (i_1, i_2), \dots, (i_k, i_{k+1})$ is the unique path in $\widehat{G}(I, \bar{J})$ from $i = i_0$ to $\text{prec}(j) = i_{k+1}$, then we have $\varphi_2(\pi_1(\mathbf{v})) = \varphi_2\left(\sum_{\ell=0}^k \mathbf{e}_{(i_\ell, i_{\ell+1})}\right) = \sum_{\ell=0}^k \mathbf{e}_{i_\ell} - \mathbf{e}_{i_{\ell+1}} = \mathbf{e}_i - \mathbf{e}_{\text{prec}(j)}$. \square

Example 4.3.9. Let $I = \{1, 2, 3, 5, 9\}$ and $\bar{J} = \{\bar{2}, \bar{7}, \bar{8}, \bar{9}\}$. The graph $G = G(I, \bar{J})$ shown at the bottom left of Figure 4.9 has $m = 5$ edges, and the partially augmented graph \widehat{G} at the top left of Figure 4.9 has $\widehat{m} = 14$ edges. The flow polytope $\mathcal{F}_{\widehat{G}} \subseteq \mathbb{R}^{14}$ is the convex hull of the 15 routes of \widehat{G} . Under the projection $\pi_1 : \mathbb{R}^{\widehat{m}} \rightarrow \mathbb{R}^m$, the three routes $(s, 2, t)$, $(s, 5, t)$, and $(s, 9, t)$ are mapped to $\mathbf{0}$. We then see that the polytope $\mathcal{S}(G) \subseteq \mathbb{R}^5$ is the convex hull of $\mathbf{0}$ and the points defined by the 12 subpaths

in G from a vertex $i \in I$ to a vertex $k \in \text{prec}(\bar{J}) = \{2, 5, 8, 9\}$. The map φ_2 then takes a subpaths in G to the root determined by the its end points. For example, the path $(2, 5, 8)$ is taken to the root $\mathbf{e}_2 - \mathbf{e}_8 = (\mathbf{e}_2 - \mathbf{e}_5) + (\mathbf{e}_5 - \mathbf{e}_8)$. The convex hull of $\mathbf{0}$ and the roots obtainable in this way is precisely \mathcal{R}_G^+ . The map φ_1 takes the 15 routes in \widehat{G} to the 15 arcs of $A(I, \bar{J})$. For example the route $(s, 2, 5, t)$ is taken to the arc $(2, \bar{7})$ since $5 = \text{prec}(\bar{7})$, while the route $(s, 2, 5, 8, t)$ in $\mathcal{F}_{\widehat{G}}$ is taken to the arc $(2, \bar{8})$. The projection π_2 now takes $(2, \bar{7})$ to the root $\mathbf{e}_2 - \mathbf{e}_5$, and it takes $(2, \bar{8})$ to the root $\mathbf{e}_2 - \mathbf{e}_8$.

Theorem 4.3.8 is the key to obtaining subdivisions of $\mathcal{U}_{I, \bar{J}}$ with the subdivision algebra. Let $M(G) = \prod_{(i,j) \in E(G)} x_{ij}$ be the monomial corresponding to $G = G(I, \bar{J})$. Then reductions of $M(G)$ encode subdivisions of $\mathcal{F}_{\widehat{G}(I, \bar{J})}$, and via the integral equivalence φ_1 they induce subdivisions of $\mathcal{U}_{I, \bar{J}}$, and we have the following corollary.

Corollary 4.3.10. *Reductions of the monomial $M(G(I, \bar{J}))$ in the subdivision algebra encode subdivisions of $\mathcal{U}_{I, \bar{J}}$.*

The above corollary can also be seen using the acyclic root polytope \mathcal{R}_G^+ . Since a reduced form of $M(G)$ encodes a triangulation of \mathcal{R}_G^+ , any such triangulation induces a triangulation of $\mathcal{U}_{I, \bar{J}}$ by adding cone points.

Example 4.3.11. For the $G = G(I, \bar{J})$ in Figure 4.9, $M(G)$ is the monomial $x_{12}x_{25}x_{35}x_{58}x_{59}$. We can perform a sequence of reductions on $M(G)$ with $\beta = 0$ to obtain the following polynomial p .

$$\begin{aligned} & x_{12}x_{15}x_{35}x_{18}x_{19} + x_{12}x_{18}x_{35}x_{38}x_{19} + x_{12}x_{18}x_{38}x_{58}x_{19} + x_{12}x_{19}x_{35}x_{58}x_{39} \\ & + x_{12}x_{19}x_{38}x_{58}x_{39} + x_{12}x_{19}x_{39}x_{58}x_{59} + x_{15}x_{25}x_{35}x_{18}x_{19} + x_{18}x_{25}x_{35}x_{28}x_{19} \\ & + x_{18}x_{28}x_{35}x_{38}x_{19} + x_{18}x_{28}x_{38}x_{58}x_{19} + x_{19}x_{25}x_{35}x_{28}x_{29} + x_{19}x_{28}x_{35}x_{38}x_{29} \\ & + x_{19}x_{28}x_{38}x_{58}x_{29} + x_{19}x_{29}x_{38}x_{58}x_{39} + x_{19}x_{29}x_{35}x_{38}x_{39} + x_{19}x_{29}x_{39}x_{58}x_{59} \end{aligned}$$

Each monomial simultaneously encodes a simplex of a triangulation of $\mathcal{F}_{\widehat{G}(I, \bar{J})}$, $\mathcal{R}_{G(I, \bar{J})}^+$, and $\mathcal{U}_{I, \bar{J}}$. Consider for example the first monomial $M = x_{12}x_{15}x_{35}x_{18}x_{19}$ in p . For the flow polytope $\mathcal{F}_{\widehat{G}(I, \bar{J})}$ it encodes the convex hull of the routes in $\widehat{G}(I, \bar{J})$ determined by the edge pairs $\{(s, i), (j, t) \mid x_{ij} \text{ divides } M\}$ and the exceptional routes. For the acyclic root polytope $\mathcal{R}_{G(I, \bar{J})}^+$ it encodes the simplex $\text{conv}\{\mathbf{0}, \mathbf{e}_i - \mathbf{e}_j \mid x_{ij} \text{ divides } M\}$. Finally, for $\mathcal{U}_{I, \bar{J}}$ it encodes the simplex $\text{conv}\{\mathbf{e}_i, \mathbf{e}_j \mid x_{i, \text{prec}(\bar{j})} \text{ divides } M \text{ or } \text{prec}(\bar{j}) = i\}$. Since $5 = \text{prec}(\bar{7})$, we can replace any 5 appearing as a second subscript in M with 7, giving $x_{12}x_{17}x_{37}x_{18}x_{19}$. With such a shift, the vertices of the simplex can be directly read from the monomial. In this case, the vertices correspond with non-crossing arcs in the (I, \bar{J}) -tree in Figure 4.11. In fact, p encodes the simplices of the (I, \bar{J}) -Tamari complex as we shall see in the next section.

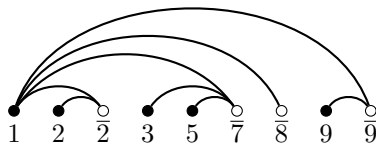


Figure 4.11: The (I, \bar{J}) -tree corresponding to the monomial $x_{12}x_{17}x_{37}x_{18}x_{19}$.

4.3.3 The ν -Tamari complex via the subdivision algebra

Having seen how the subdivision algebra can be used to subdivide $\mathcal{U}_{I, \bar{J}}$, we will conclude this chapter by giving a reduction order for the monomial $M(G(I, \bar{J}))$ which gives rise to the $\nu(I, \bar{J})$ -Tamari complex. Recall that many (I, \bar{J}) -pairs can give rise to the same path ν . For the sake of clarity, we will assume in the remainder of the chapter that (I, \bar{J}) is the canonical (I, \bar{J}) -pair, although the results obtained also hold more generally for any valid (I, \bar{J}) -pair. For a canonical pair (I, \bar{J}) , we have that $\text{prec}(\bar{J}) = J = \{j \mid \bar{j} \in \bar{J}\}$, allowing us to omit the prec function in the exposition.

A graph is said to be **alternating** if none of its vertices have both incoming and outgoing edges. A graph is **non-crossing** if it does not have a pair of edges (i, j) and (i', j') satisfying $i < i' < j < j'$. Let $D_{\bar{\nu}}$ denote the set of all maximal alternating non-crossing graphs on vertex set $I \cup J$ with edges (i, j) with $i \in I$, $j \in J$, and $i < j$. Note that by maximality the graphs in $D_{\bar{\nu}}$ must be trees and therefore have $|I \cup J| - 1$ edges.

Lemma 4.3.12. *The alternating non-crossing graphs in $D_{\bar{\nu}}$ are in bijection with the (I, \bar{J}) -trees determined by $\bar{\nu}$.*

Proof. The bijection is given by mapping each arc (i, j) in an (I, \bar{J}) -tree to the edge (i, j) in a graph, and noting that non-crossing condition is identical for arcs and edges. Although the arcs of the form (i, i) are mapped to empty edges, the map is a bijection as such arcs appear in all (I, \bar{J}) -trees. \square

At a vertex j , the edges (i, j) and (j, k) where $i < j < k$ form a **longest pair** if (i, j) is the longest incoming edge to j and (j, k) is the longest outgoing edge from j .

Lemma 4.3.13. *The reduced forms of $M(G(I, \bar{J}))$ obtained by any reduction order in which longest pairs are reduced first at each vertex are equal.*

Proof. We begin by observing that it suffices to show that the monomials of highest degree encode the graphs in $D_{\bar{\nu}}$, as they determine the remaining terms in the reduced form. This can be seen from the reduction tree, as the simple reductions determine the entire reduction tree.

We first show that a reduction at a longest pair preserves the non-crossing condition. Let G be a non-crossing graph on $I \cup J$ with all edges directed forward. Consider any vertex j with its longest incoming and outgoing edges (i, j) and (j, k) , i.e. there are no edges (i', j) and (j, k') with $i' < i$ and $k < k'$. Since no edge in

G crosses (i, j) or (j, k) , and they are a longest pair, the edge (i, k) does not cross any edge in G . Thus each of the three graphs obtained by a reduction at j are non-crossing.

Let R be a reduced form of $M(G(I, \bar{J}))$ obtained by reducing longest pairs first. Since the graph $G(I, \bar{J})$ is non-crossing by construction, all graphs encoded by the monomials in R are non-crossing. In addition, the graphs obtained from $G(I, \bar{J})$ by reductions do not have multiedges, as $G(I, \bar{J})$ is acyclic as an undirected graph. In $G(I, \bar{J})$, there is an edge for each $i \in I \setminus J$, an edge for each $j \in J \setminus I$, and the edges on the path through vertices in $I \cap J$. Thus the number of edges in $G(I, \bar{J})$ is $|I \cup J| - 1$. Since simple reductions preserve the number of edges, the monomials of highest degree in R encode simple alternating graphs with $|I \cup J| - 1$ edges, and hence must be maximal.

Since the monomials of highest degree in a reduced form of $M(G(I, \bar{J}))$ correspond with the facets of a unimodular triangulation of $\mathcal{F}_{\widehat{G}(I, \bar{J})}$, they are enumerated by its volume, namely, the ν -Catalan number $\text{Cat}(\nu)$. This is also the number of (I, \bar{J}) -trees, and therefore via the bijection in Lemma 4.3.12 the monomials of highest degree in R must comprise the whole set $D_{\bar{J}}$. Since the inner faces of a triangulation are determined by the facets of the triangulation, the reduced form R is determined by its monomials of highest degree. \square

Define the **length reduction order** to be the reduction order obtained by reducing the longest pair $\{(i, j), (j, k)\}$ with minimal j at each reduction step.

Theorem 4.3.14. *The triangulation of $\mathcal{F}_{\widehat{G}(I, \bar{J})}$ obtained by reducing the monomial $M(G(I, \bar{J}))$ in the length reduction order is a geometric realization of the ν -Tamari complex.*

Proof. Let R be the reduced form obtained from reducing $G(I, \bar{J})$ in the length reduction order. Let M be a monomial of highest degree in R and let G_M be the graph with vertex set $V(G) = I \cup \text{prec}(J)$ and edges set $E(G) = \{(i, j) \mid x_{ij} \text{ divides } M\}$. Label each edge (s, i) in \widehat{G}_M with E_i and each edge (j, t) with N_j . As G_M is alternating, a route in \widehat{G}_M has edges (s, i) , (i, j) , and (j, t) , with $i \in I$, $j \in \text{prec}(\bar{J})$, and (i, j) is the empty edge if $i = j$. Let $\mathcal{A}_{I, \bar{J}}$ denote the set of possible arcs on the pair (I, \bar{J}) . Define the map $\Phi : \mathcal{R}_{\widehat{G}(I, \bar{J})} \rightarrow \mathcal{A}_{I, \bar{J}}$ by mapping the route determined by the pair of edges $(E_i, N_{\text{prec}(j)})$ to the arc (i, j) . Now Φ extends to a bijection between simplicial complexes, taking faces of the triangulation to (I, \bar{J}) -forests. Since $\nu(I, \bar{J}) = \nu(I, \text{prec}(\bar{J}))$, the conclusion follows. \square

By Corollary 4.3.10, the following is immediate.

Corollary 4.3.15. *The triangulation of $\mathcal{U}_{I, \bar{J}}$ obtained by reducing $M(G(I, \bar{J}))$ in the length reduction order encodes a geometric realization of the ν -Tamari complex.*

Mészáros showed in [47] that the h -polynomial of a framed triangulation of a flow polytope $\mathcal{F}_{\widehat{G}}$ can be obtained from any reduced form R of $M(G)$ as a polynomial

in β . In particular the h -polynomial is obtained by first substituting $x_{ij} = 1$ for all x_{ij} in R , and then computing $R(\beta - 1)$.

We know from Theorem 4.2.13 that the h -vector of $\mathcal{F}_{\text{car}(\nu)} \equiv \mathcal{F}_{\widehat{G}(I, \bar{J})} \equiv \mathcal{U}_{I, \bar{J}}$ is the ν -Narayana polynomial. Thus $R(x_{ij} = 1, \beta - 1)$ is the ν -Narayana polynomial, and from Proposition 3.1.6 we know that the shifted h -polynomial, i.e. $R(x_{ij} = 1, \beta)$, is the ν -Schröder polynomial.

Chapter 5 A subdivision algebra for $\Delta_a \times \Delta_b$ via flow polytopes

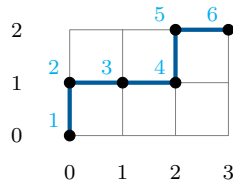
Given a standard a -simplex Δ_a and a standard b -simplex Δ_b , their Cartesian product is the $(a + b)$ -dimensional polytope

$$\Delta_a \times \Delta_b = \text{conv}\{(\mathbf{e}_i, \mathbf{e}_j) \mid \mathbf{e}_i \in \Delta_a \text{ and } \mathbf{e}_j \in \Delta_b\}.$$

The triangulations of $\Delta_a \times \Delta_b$ have been extensively studied. They serve as building blocks in the study of triangulations of more complicated polytopes [39, 53], and play an important role in understanding triangulations more generally [25, 57]. They have also garnered interest from a variety of perspectives, having connections to algebraic geometry (Schubert calculus [3], Segre varieties [22], Gröbner bases [68]), tropical geometry (tropical convexity [30], tropical hyperplane arrangements and oriented matroids [4, 16]), and optimization (dual transportation polytopes [26]).

The vertices of $\Delta_a \times \Delta_b$ are of the form $(\mathbf{e}_i, \mathbf{e}_j)$, where $1 \leq i \leq a + 1$ and $1 \leq j \leq b + 1$. They can be associated with the lattice points in the rectangular region determined by $(0, 0)$ and (a, b) by mapping the vertex $(\mathbf{e}_i, \mathbf{e}_j)$ to the point $(i - 1, j - 1)$. With this identification, we can describe a triangulation of $\Delta_a \times \Delta_b$ known as the **staircase triangulation**, which is given by the following theorem.

Theorem 5.0.1 ([27, Theorem 6.2.13]). *The lattice points in a lattice path from $(0, 0)$ to (a, b) give a full-dimensional simplex in $\Delta_a \times \Delta_b$. Furthermore, the set of all such lattice paths give a triangulation of $\Delta_a \times \Delta_b$. The volume of $\Delta_a \times \Delta_b$ is thus given by $\binom{a+b}{a} = \binom{a+b}{b}$.*



- | | | |
|-----------------------------------|-----------------------------------|-----------------------------------|
| 1. $(\mathbf{e}_1, \mathbf{e}_1)$ | 2. $(\mathbf{e}_1, \mathbf{e}_2)$ | 3. $(\mathbf{e}_2, \mathbf{e}_2)$ |
| 4. $(\mathbf{e}_3, \mathbf{e}_2)$ | 5. $(\mathbf{e}_3, \mathbf{e}_3)$ | 6. $(\mathbf{e}_4, \mathbf{e}_3)$ |

Figure 5.1: A lattice path encoding a simplex in the staircase triangulation of $\Delta_3 \times \Delta_2$. The six vertices of the simplex (right) are given by the six lattice points on the lattice path.

Theorem 5.0.1 does not depend on the identification of the vertex $(\mathbf{e}_i, \mathbf{e}_j)$ with the point $(i - 1, j - 1)$. In fact, given any permutation pair $(\pi_1, \pi_2) \in S_{a+1} \times S_{b+1}$, we can choose to identify $(\mathbf{e}_i, \mathbf{e}_j)$ with the lattice point $(\pi_1(i) - 1, \pi_2(j) - 1)$, thereby obtaining a (possibly) different staircase triangulation. In this way, the permutations give rise to a symmetry class of triangulations, collectively known as the **staircase triangulations of $\Delta_a \times \Delta_b$** . However, not all permutation pairs give unique triangulations. If a permutation pair (π_1, π_2) is obtained from another pair (π'_1, π'_2) by reversing both permutations, then paths given by the identification using

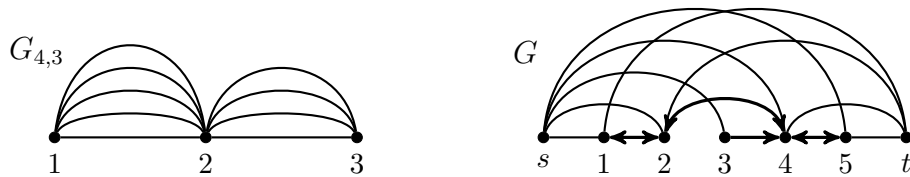


Figure 5.2: The flow polytopes of the above graphs are integrally equivalent. In particular $\mathcal{F}_G \equiv \mathcal{F}_{G_{4,3}} = \Delta_4 \times \Delta_3$.

(π_1, π_2) are a 180° rotation of those using (π'_1, π'_2) . The two staircase triangulations are therefore identical. As such permutation pairs are the only ones giving rise to identical staircase triangulations, $\Delta_a \times \Delta_b$ has exactly $\frac{1}{2}(a+1)!(b+1)!$ staircase triangulations [27, Proposition 6.2.16].

Having studied the subpolytope $\mathcal{U}_{I,\bar{J}} \subseteq \Delta_a \times \Delta_b$ from the perspective of flow polytopes in Chapter 4, we now extend this perspective to $\Delta_a \times \Delta_b$. As a result, we obtain a subdivision of $\Delta_a \times \Delta_b$ into flow polytopes (up to integral equivalence), allowing for an extension of Mészáros' subdivision algebra to $\Delta_a \times \Delta_b$.

The product of simplices $\Delta_a \times \Delta_b$ can be viewed as the flow polytope over the graph $G_{a,b}$ with vertex set $[3]$ and $a+1$ copies of the edge $(1,2)$ and $b+1$ copies of the edge $(2,3)$. For example, the flow polytope over the left graph in Figure 5.2 is $\Delta_4 \times \Delta_3$. At first glance, the flow polytope perspective does not seem to yield anything new in regards to triangulations of $\Delta_a \times \Delta_b$. In particular, any Danilov–Karzanov–Koshevoy triangulation (Theorem 2.3.10) or Stanley–Postnikov triangulation (see [51]) of $\mathcal{F}_{G_{a,b}}$ is a staircase triangulation of $\Delta_a \times \Delta_b$. To obtain more triangulations, we will slightly expand the definition of a flow polytope in Section 5.1 by allowing negative flows and letting the underlying graph G have bidirectional edges. This lets us generate a large class of flow polytopes which are integrally equivalent to $\Delta_a \times \Delta_b$.

5.1 Flow polytopes and negative flows

The traditional definition of a flow polytope given in the introduction does not allow negative flows or bidirectional edges. In this section, we remedy the situation by giving a slightly modified definition. We will see that flow polytopes with the modified definition are integrally equivalent to traditional flow polytopes, which might suggest that the new definition given is unnecessary. However, the extended definition proves to be pivotal for our purposes in the remainder of the chapter.

Let G be a connected directed acyclic graph with vertex set $V(G) = \{1, 2, \dots, n\}$ and edge multiset $E(G)$ with m directed edges. An edge (i, j) with $i < j$ can be of three possible types: a **forward edge** $(i, j, +)$ directed toward j , a **backward edge** $(i, j, -)$ directed toward i , or a **bidirectional edge** (i, j, \pm) . For a vertex j , we divide the edges incident to j into **smaller** and **larger** edges, that is, sets $S(j)$ and $L(j)$, where $S(j)$ denotes the set of edges (i, j) with $i < j$, and let $L(j)$ denote

the set of edges (j, k) with $j < k$. At each vertex $i \in V(G)$ we assign a netflow $a_i \in \mathbb{Z}$ satisfying the balance condition $\sum_{i=1}^n a_i = 0$, and hence $a_n = -\sum_{i=1}^{n-1} a_i$. For $\mathbf{a} = (a_0, \dots, a_n, -\sum_{i=1}^{n-1} a_i) \in \mathbb{Z}^n$, an **a-flow on G** is a tuple $(x_e)_{e \in E} \in \mathbb{R}^m$ satisfying

$$\sum_{e \in L(j)} x_e - \sum_{e \in S(j)} x_e = a_j \quad (5.1)$$

with $x_e \geq 0$ if e is a forward edge, $x_e \leq 0$ if e is a backward edge, and $x_e \in \mathbb{R}$ if e is bidirectional. We think of x_e as the amount of flow in the edge e . If a bidirectional edge has positive flow, we treat it as a forward edge, and if it has negative flow, we treat it as a backward edge.

As in previous chapters, we denote the set of all **a-flows** on G by $\mathcal{F}_G(\mathbf{a})$. Here we also consider only the unit flow case $\mathcal{F}_G(\mathbf{u})$ with $\mathbf{u} = \mathbf{e}_1 - \mathbf{e}_n$, and so we suppress the notation to $\mathcal{F}_G := \mathcal{F}_G(\mathbf{u})$. We prove in Proposition 5.1.1 that \mathcal{F}_G is a convex polytope, which justifies calling \mathcal{F}_G the **flow polytope of G** . When all edges in G are forward edges, G is necessarily acyclic, and in this case our definition of a flow polytope here agrees with Definition 2.3.1. The terminology for flow polytopes from Section 2.3 naturally extends to this slightly more general setting.

Recall that a route in G is a maximal path from the source to the sink, and the set of all routes in G is denoted \mathcal{R}_G . An edge in G which is not in a route cannot have non-zero flow, so we can assume that all edges in G belong to some route in \mathcal{R}_G . Furthermore, since G is acyclic, the source and sink vertex are each incident to at most one edge in a route. We can therefore also assume that all edges incident to the source and sink are forward edges. To each route $R \in \mathcal{R}_G$ we now associate a signed characteristic vector $\mathbf{x}_R = (x_e)_{e \in E(G)}$ as follows. If $e = (i, j) \in R$ with $i < j$, we set $x_e = 1$ if the path traverses e from i to j , and we set $x_e = -1$ if the path traverses e from j to i , and if $e \notin R$, we set $x_e = 0$. We can now give a \mathcal{V} -description of \mathcal{F}_G as the convex hull of routes in G , which also serves to justify the fact that \mathcal{F}_G is a polytope.

Proposition 5.1.1. *The set of all **u-flows** \mathcal{F}_G is a polytope if and only if G is acyclic. Furthermore, when G is acyclic, the vertex description of \mathcal{F}_G is given by*

$$\mathcal{F}_G = \text{conv}\{\mathbf{x}_R \mid R \in \mathcal{R}_G\}.$$

Proof. First, if G is not acyclic, then it has a cycle C . Given any unit flow, one can arbitrarily change the flow in C while preserving the conservation of flow condition (2.1). Thus the set of unit flows is not bounded and hence not a polytope.

If G is acyclic, we show that $\mathcal{F}_G = \text{conv}\{\mathbf{x}_R \mid R \in \mathcal{R}_G\}$ and hence a polytope. We can label the routes in \mathcal{R}_G such that $\mathcal{R}_G = \{R_1, \dots, R_k\}$ for some positive integer k , and we let \mathbf{x}_i denote the signed characteristic vector for R_i . Letting $\mathbf{p} \in \text{conv}\{\mathbf{x}_R \mid R \in \mathcal{R}_G\}$, we can now write $\mathbf{p} = \sum_{i=1}^k \lambda_i \mathbf{x}_i$ where $\lambda_i \in \mathbb{R}_{\geq 0}$ and $\sum_{i=1}^k \lambda_i = 1$. Note that the netflow at vertex 1 is given by the sum $\sum \lambda_i$ where the sum is taken over only the indices of routes using an edge in $L(1)$. However, since every route in \mathcal{R}_G must begin with an edge in $L(1)$, the netflow at vertex 1 is $\sum_{i=1}^k \lambda_i = 1$. Similarly we obtain that the netflow at vertex n is -1 . Furthermore,

since each \mathbf{x}_i adds no netflow at any inner vertex we see that any linear combination $\sum_{i=1}^k \lambda_i \mathbf{x}_i$ also has netflow 0 at each inner vertex. Thus $\mathbf{p} \in \mathcal{F}_G$.

Let \mathbf{q}_1 be a \mathbf{u} -flow in \mathcal{F}_G , and let $q_{1,e}$ denote the coordinate of \mathbf{q}_1 corresponding to the edge e . We construct \mathbf{q}_1 as a linear combination of routes in an iterative fashion. Consider an edge $e_1 \in R_1$ such that $|q_{1,e_1}|$ is minimal, and let $\lambda_1 = |q_{1,e_1}|$. Then $\mathbf{q}_1 - \lambda_1 \mathbf{x}_1$ is a $((1 - \lambda_1)\mathbf{u})$ -flow. Let $\mathbf{q}_2 = \mathbf{q}_1 - \lambda_1 \mathbf{x}_1$ and consider an edge $e_2 \in R_2$ such that $|q_{2,e_2}|$ is minimal and let $\lambda_2 = |q_{2,e_2}|$. We obtain that $\mathbf{q}_1 - \lambda_1 \mathbf{x}_1 - \lambda_2 \mathbf{x}_2$ is a $((1 - \lambda_1 - \lambda_2)\mathbf{u})$ -flow. We continue this process, constructing a $((1 - \sum_{i=1}^j \lambda_i)\mathbf{u})$ -flow \mathbf{q}_j for each $R_j \in \mathcal{R}_G$ by removing the maximal amount of flow from all edges in R_j . At each step the netflow of inner vertices is unaffected, while the netflow at the source decreases by λ_i and the netflow at the sink increases by λ_i . This process can be continued until we obtain that $\mathbf{q}_1 - \sum_{i=1}^k \lambda_i \mathbf{x}_i$ is a $((1 - \sum_{i=1}^k \lambda_i)\mathbf{u})$ -flow. If there remains an edge e in G with non-zero flow in the $((1 - \sum_{i=1}^k \lambda_i)\mathbf{u})$ -flow, then by conservation of flow e is either in a cycle or a route. Since G is acyclic, e must be in a route R_j with non-zero flow in the $((1 - \sum_{i=1}^k \lambda_i)\mathbf{u})$ -flow on G . This contradicts the fact that the largest possible flow in R_j was subtracted at step j . Thus all edges in an $((1 - \sum_{i=1}^k \lambda_i)\mathbf{u})$ -flow on G are zero. It then follows that $\mathbf{q}_1 = \sum_{i=1}^k \lambda_i \mathbf{x}_i$ and $\sum_{i=1}^k \lambda_i = 1$, and therefore $\mathcal{F}_G = \text{conv}\{\mathbf{x}_R \mid R \in \mathcal{R}_G\}$.

It remains to show that every route in \mathcal{R}_G corresponds to a vertex of \mathcal{F}_G . Note that since \mathcal{F}_G is a lattice polytope in $[-1, 1]^m$ not containing the origin, it cannot have interior lattice points. It then suffices to show that no three vectors in $\{\mathbf{x}_R \mid R \in \mathcal{R}_G\}$ are colinear. Let $\mathbf{x}_u = \mu_1 \mathbf{x}_v + \mu_2 \mathbf{x}_w$ for routes R_u, R_v , and R_w , and $\mu_1, \mu_2 \in \mathbb{R}$. We show that the vectors $\mathbf{x}_u, \mathbf{x}_v$ and \mathbf{x}_w cannot be distinct. Let e be the edge in R_u incident to the source. Then $x_{u,e} = 1$ as source edges are forward edges. Now $x_{v,e}$ and $x_{w,e}$ cannot both be zero since $\mu_1 x_{v,e} + \mu_2 x_{w,e} = 1$. If $x_{v,e} = 1$ and $x_{w,e} = 0$, then $\mu_1 = 1$. In this case the equation $\mu_1 x_{v,f} + \mu_2 x_{w,f} = x_{u,f} = 0$ must also be satisfied, where f is the edge of R_w incident to the source. Since $x_{v,f} = 0$, it follows that $\mu_2 = 0$, and thus $\mathbf{x}_u = \mathbf{x}_v$. Similarly if $x_{v,e} = 0$ and $x_{w,e} = 1$, we obtain that $\mathbf{x}_u = \mathbf{x}_w$. If $x_{v,e} = x_{w,e} = 1$, then $\mu_1 + \mu_2 = 1$. Now either $R_v = R_w$, or there exists an edge g in R_v which is not in R_w . In the latter case we obtain that $x_{v,g} = 0$ or $x_{w,g} = 0$. Then either $\mu_1 = 0$ or $\mu_2 = 0$, respectively yielding that $\mathbf{x}_u = \mathbf{x}_w$ or $\mathbf{x}_u = \mathbf{x}_v$. \square

Having now shown that our notion of a flow polytope is well-defined, we proceed by showing that a theory for flow polytopes with negative flows and bidirectional edges is not needed.

Lemma 5.1.2. *Let G be an acyclic digraph. Then \mathcal{F}_G is integrally equivalent to a flow polytope \mathcal{F}_{G^*} , where all edges of G^* are forward edges.*

Proof. First we consider backward edges in G . Since G is acyclic, the vertex labels can be permuted such that G has no backward edges. Changing the orientation of a backward edge e amounts to reflecting the flow polytope about the hyperplane $x_e = 0$, which is an integral equivalence.

Next we show that the operation of contracting a bidirectional edge (i, j, \pm) with $i < j$ is an integral equivalence. If the edge (i, j, \pm) is the k -th edge in a fixed

ordering of the edges of G , the integral equivalence is given by $\varphi : \mathbb{R}^m \rightarrow \mathbb{R}^{m-1}$, where

$$\varphi(x_1, \dots, x_k, \dots, x_m) = (x_1, \dots, \widehat{x}_k, \dots, x_m).$$

Let D denote the set of edges incident to i not including (i, j, \pm) . Define a map $\psi : \mathbb{R}^{m-1} \rightarrow \mathbb{R}^m$ by

$$\psi(x_1, \dots, \widehat{x}_k, \dots, x_m) = (x_1, \dots, x_{k-1}, \left(\sum_{e \in L(i) \cap D} x_e - \sum_{e \in S(i)} x_e \right), x_{k+1}, \dots, x_m).$$

Now restricting φ to \mathcal{F}_G gives a bijection between \mathcal{F}_G and $\mathcal{F}_{G/(i,j,\pm)}$, with its inverse given by restricting ψ to $\mathcal{F}_{G/(i,j,\pm)}$. It is also easy to verify that φ restricts to a bijection between $\mathbb{Z}^m \cap \text{aff}(\mathcal{F}_G)$ and $\mathbb{Z}^{m-1} \cap \text{aff}(G/(i, j, \pm))$. \square

5.2 The flow polytope $\mathcal{F}_{\tilde{G}_B(\nu)}$ and its simplex subdivisions

In this section we construct a flow polytope $\mathcal{F}_{\tilde{G}_B(\nu)}$ arising from a graph determined by a lattice path ν with bidirectional edges. This flow polytope is integrally equivalent to a product of two simplices, and we study a particular subdivision of it which has as its dual a w -simplex, where w is the number of valleys of $\bar{\nu} = E\nu N$.

5.2.1 The flow polytope $\mathcal{F}_{\tilde{G}_B(\nu)}$

Let a and b be nonnegative integers, and let ν be a lattice path from $(0, 0)$ to (a, b) , with steps $E = (1, 0)$ and $N = (0, 1)$. Let (I, \bar{J}) be the canonical pair associated with ν . We label the steps in $\bar{\nu}$ according to this canonical pair (I, \bar{J}) , with E steps indexed by elements of I and N steps indexed by elements of \bar{J} , and ordered according to $\prec_{I, \bar{J}}$. We call this the **canonical indexing** for the path $\bar{\nu}$. For an example, the path $\bar{\nu}$ in Figure 5.3 demonstrates this labeling for $I = \{1, 2, 3, 5, 6\}$ and $\bar{J} = \{\bar{1}, \bar{3}, \bar{4}, \bar{6}\}$. Note that the set of valleys of $\bar{\nu}$ are indexed by elements in $I \cap J$, where $J = \{j \mid \bar{j} \in \bar{J}\}$.

Definition 5.2.1. Let n be the largest index in a canonical indexing of a path $\bar{\nu}$. We define the ν -**graph** $G(\nu)$ to be the graph on vertex set $[n]$ with its edge set defined as follows. A pair (i, j) is an edge of $G(\nu)$ if and only if $E_i \cdots N_j$ is a connected subword of $\bar{\nu}$ and its only valleys are of the form $E_k N_k$ with $k = i$ or $k = j$. All edges in $G(\nu)$ are directed forward. The **bidirectional ν -graph** $G_B(\nu)$ is the graph $G(\nu)$, but with edges (i, j) chosen to be bidirectional whenever E_i and N_j are both steps in valleys.

The graph $G(\nu)$ here is equal to the graph $G(I, \bar{J})$ of Section 4.3.1 for the canonical (I, \bar{J}) -pair associated with ν . Although it is possible to consider valid (I, \bar{J}) -pairs more generally in this chapter, we choose to work only with the canonical pair for the sake of clarity. By construction, the bidirectional edges in $G_B(\nu)$ form a path of length $w - 1$. When $\bar{\nu}$ has only one valley, there are no edges whose end points are in $I \cap J$, in which case $G_B(\nu) = G(\nu)$.

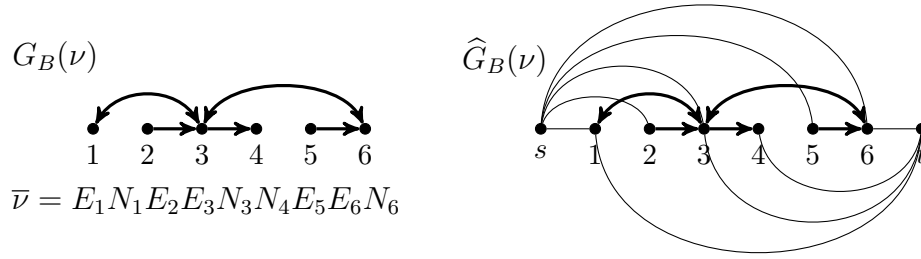


Figure 5.3: A graph $G_B(\nu)$ with its partially augmented counterpart $\widehat{G}_B(\nu)$.

Recall that the partial augmentation of G , denoted \widehat{G} , is obtained from the full augmentation \widetilde{G} by removing edges (s, i) where i has out-degree one, and any edges (j, t) where j has in-degree one. See Figure 5.3 for an example of a graph $G_B(\nu)$ and its partial augmentation $\widehat{G}_B(\nu)$.

Lemma 5.2.2. *Let ν be a lattice path from $(0, 0)$ to (a, b) . The flow polytope $\mathcal{F}_{\widehat{G}_B(\nu)}$ is integrally equivalent to the product of simplices $\Delta_a \times \Delta_b$.*

Proof. By construction, an inner edge of $\widehat{G}(\nu)$ is either idle or bidirectional. Thus contracting the idle inner edges and bidirectional edges yields the graph on vertex set $\{s, 1, t\}$ with $a + 1$ edges of the form $(s, 1)$ and $b + 1$ edges of the form $(1, t)$. The flow polytope of this resulting graph is $\Delta_a \times \Delta_b$. \square

5.2.2 The simplex subdivision

We can now subdivide $\mathcal{F}_{\widehat{G}_B(\nu)}$ into a union of w interior disjoint polytopes. Let v_i denote the index of the i -th valley in $\bar{\nu}$, which is also the i -th element in $I \cap J$ when read in increasing order. In Figure 5.3 for example, $I \cap J = \{1, 3, 6\}$, so $v_1 = 1$, $v_2 = 3$, and $v_3 = 6$. For $1 \leq i < w$, let \mathcal{Q}_i denote the convex hull of the routes in $\widehat{G}_B(\nu)$ with the bidirectional edge (v_i, v_{i+1}, \pm) replaced with the backward edge $(v_i, v_{i+1}, -)$ such that if the route contains backward edges, then it contains the edge $(v_i, v_{i+1}, -)$. Additionally, we let $\mathcal{Q}_w = \widehat{G}(\nu)$.

Let C_ν denote the cycle graph on $I \cap J$ with edges $\{(v_1, v_2, +), (v_2, v_3, +), \dots, (v_{w-1}, v_w, +), (v_w, v_1, -)\}$. Let $C_\nu(i)$ denote the graph C_ν without the edge beginning at v_i , and let $G(\nu, i)$ denote the graph obtained by replacing the bidirectional path in $G_B(\nu)$ with $C_\nu(i)$. Note in particular that $G(\nu, w) = G(\nu)$ since $C_\nu(w)$ is the directed path from v_1 to v_w . See Figure 5.4 for an example.

Theorem 5.2.3. *The flow polytope $\mathcal{F}_{\widehat{G}_B(\nu)}$ can be written as*

$$\mathcal{F}_{\widehat{G}_B(\nu)} = \bigcup_{i=1}^w \mathcal{Q}_i$$

where the polytopes $\mathcal{Q}_1, \mathcal{Q}_2, \dots, \mathcal{Q}_w$ have pairwise disjoint interiors, and w is the number of valleys in $\bar{\nu} = E\nu N$. Furthermore, for any nonempty $S \subseteq [w]$ we have that $\bigcap_{i \in S} \mathcal{Q}_i \equiv \mathcal{F}_{\bigcap_{i \in S} \widehat{G}(\nu, i)}$.

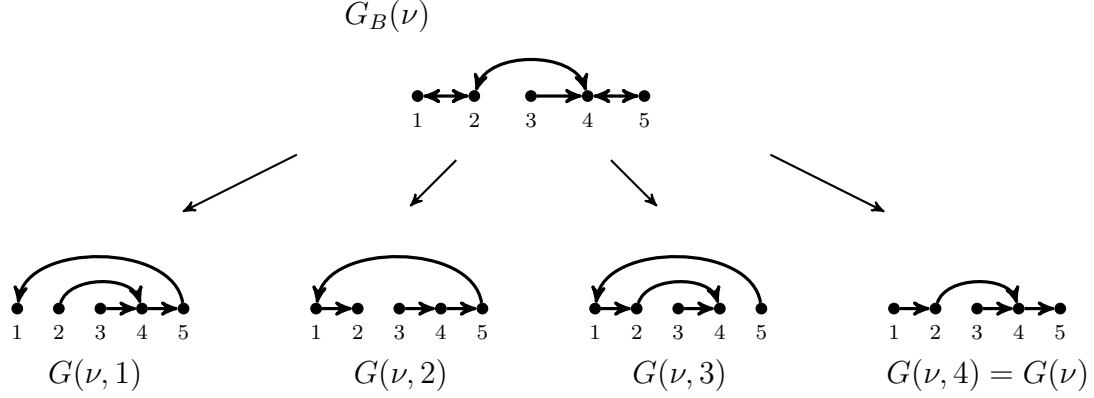


Figure 5.4: Decomposing $G_B(\nu)$ into the possible $G(\nu, i)$. The flow polytope $\mathcal{F}_{\widehat{G}_B(\nu)}$ decomposes into $\cup_{i \in [w]} \mathcal{Q}_i$, where $\mathcal{Q}_i \equiv \mathcal{F}_{\widehat{G}(\nu, i)}$ for each $i \in [w]$.

Proof. We begin by checking that $\mathcal{F}_{\widehat{G}_B(\nu)} = \bigcup_{i=1}^w \mathcal{Q}_i$. Let $\mathbf{x}_1 \in \mathcal{F}_{\widehat{G}_B(\nu)}$, we show that it can be written as a convex combination of routes in some \mathcal{Q}_i . Let I_1 denote the indices of the entries in \mathbf{x}_1 with negative flow, i.e. $I_1 = \{k \mid x_{1, e_k} < 0\}$. If $I_1 = \emptyset$, then $\mathbf{x}_1 \in \mathcal{F}_{\widehat{G}(\nu)} = \mathcal{Q}_w$. If $I_1 \neq \emptyset$, we choose edges $e_{j_1} = (v_{h_1}, v_{h_1+1}, -)$ and $e_{k_1} = (v_{\ell_1-1}, v_{\ell_1}, -)$ from $\{e_k \mid k \in I_1\}$ (not necessarily distinct) such that v_{h_1} is minimal and v_{ℓ_1} is maximal. Let R_1 be the route with edges $\{(s, v_{\ell_1}, +), (v_{\ell_1-1}, v_{\ell_1}, -), \dots, (v_{h_1}, v_{h_1+1}, -), (v_{h_1}, t, +)\}$, which exists since the bidirectional edges form a path. Now R_1 is the shortest route containing all edges with negative flow. By conservation of flow, the edges $(s, v_{\ell_1}, +)$ and $(v_{h_1}, t, +)$ must have positive flow. Furthermore, the flow in $(v_{h_1}, t, +)$ must be greater than or equal to $|x_{e_{k_1}}|$, and the flow in $(s, v_{\ell_1}, +)$ must be greater than or equal to $|x_{e_{j_1}}|$. Letting $\alpha_1 = |x_{e_{k_1}}|$, we have that $\mathbf{x}_2 = \mathbf{x}_1 - \alpha_1 \mathbf{x}_{R_1}$ is a $(1 - \alpha_1)\mathbf{u}$ -flow on $\widehat{G}_B(\nu)$ in which the edge e_{k_1} has zero flow, and the flow in the edges $(s, v_{\ell_1}, +)$ and $(v_{h_1}, t, +)$ is nonnegative.

Letting $I_2 = \{k \mid x_{2, e_k} < 0\}$, we now have $I_2 \subsetneq I_1$. If $I_2 \neq \emptyset$, we continue as before, choosing edges $e_{j_2} = (v_{h_2}, v_{h_2+1}, -)$ and $e_{k_2} = (v_{\ell_2-1}, v_{\ell_2}, -)$ from $\{e_k \mid x_{2, e_k} < 0\}$ with minimal v_{h_2} and maximal v_{ℓ_2} . Taking R_2 to be the route with edges $\{(s, v_{\ell_2}, +), (v_{\ell_2-1}, v_{\ell_2}, -), \dots, (v_{h_2}, v_{h_2+1}, -), (v_{h_2}, t, +)\}$, we obtain the shortest route containing all edges with negative flow. Letting $\alpha_2 = |x_{e_{k_2}}|$, we have that $\mathbf{x}_3 := \mathbf{x}_2 - \alpha_2 \mathbf{x}_{R_2}$ is a $(1 - \alpha_1 - \alpha_2)\mathbf{u}$ -flow on $\widehat{G}_B(\nu)$ in which the edge e_{k_2} has zero flow, and the flow in the edges $(s, v_{\ell_2}, +)$ and $(v_{h_2}, t, +)$ is nonnegative.

We proceed in this fashion until we obtain a $(1 - \sum_{k=1}^r \alpha_k)\mathbf{u}$ -flow \mathbf{x}_{r+1} with no negative entries, so $\emptyset = I_{r+1} \subsetneq I_r \subsetneq \dots \subsetneq I_1$. Let i be the index in I_{r-1} of the edge $(v_{\ell_r-1}, v_{\ell_r}, -)$. Necessarily, e_i is an edge with minimal flow in \mathbf{x}_1 , and by construction the routes R_1, \dots, R_r all share the edge e_i . As \mathbf{x}_{r+1} has no negative entries, we can write it as a convex combination of a set our routes R_r, \dots, R_u in $\widehat{G}(\nu) \setminus e_i$. In particular, $\mathbf{x}_{r+1} = \sum_{k=r}^u \alpha_k \mathbf{x}_{R_k}$ such that $\alpha_k \geq 0$ for all $r \leq k \leq u$ and $\sum_{k=r}^u \alpha_k = (1 - \sum_{k=1}^r \alpha_k)$. We can thus write \mathbf{x}_1 as the convex combination $\mathbf{x}_1 = \sum_{k=1}^u \alpha_k \mathbf{x}_{R_k}$, with $\alpha_k \geq 0$ for all k and $\sum_{k=1}^u \alpha_k = 1$. Since all routes R_1, \dots, R_u

are vertices in \mathcal{Q}_i , we have that $\mathbf{x} \in \mathcal{Q}_i$. It follows that $\mathcal{F}_{\widehat{G}_B(\nu)} \subseteq \cup_{i=1}^w \mathcal{Q}_i$, and the reverse inclusion is immediate.

To see that \mathcal{Q}_i and \mathcal{Q}_j have disjoint interiors for any $i, j \in [w]$ with $i \neq j$ we observe that \mathcal{Q}_i and \mathcal{Q}_j lie in the positive and negative half-spaces of the hyperplane determined by $x_{(v_i, v_{i+1})} = x_{(v_j, v_{j+1})}$. If $i = w$ and $j \neq w$, then \mathcal{Q}_i and \mathcal{Q}_j are cut by the hyperplane $x_{(v_j, v_{j+1})} = 0$.

It remains to show that for $S \subseteq [w]$ we have $\cap_{i \in S} \mathcal{Q}_i \equiv \mathcal{F}_{\cap_{i \in S} \widehat{G}(\nu, i)}$. As noted earlier, $\widehat{G}(\nu, w) = \widehat{G}(\nu)$, and so if $w \in S$, then $\cap_{i \in S} \mathcal{Q}_i = \mathcal{F}_{\cap_{i \in S} \widehat{G}(\nu, i)}$. In the case that $w \notin S$, we construct an integral equivalence φ as follows. First fix an ordering e_1, \dots, e_{m+1} on the set of edges in $\widehat{G}_B(\nu) \cup (v_1, v_w)$ (as undirected edges) so that $e_i = (v_i, v_{i+1})$ for each $i \in [w-1]$ and $e_w = (v_1, v_w)$. Then $\cap_{i \in S} \mathcal{Q}_i$ and $\mathcal{F}_{\cap_{i \in S} \widehat{G}(\nu, i)}$ both embed into \mathbb{R}^{m+1} , and we define $\varphi : \mathbb{R}^{m+1} \rightarrow \mathbb{R}^{m+1}$ to be the linear transformation

$$\mathbf{x} \mapsto \mathbf{x} + x_{\min(S)} \mathbf{e}_w - x_{\min(S)} \sum_{i=1}^{w-1} \mathbf{e}_i.$$

By construction, a route R in $\cap_{i \in S} \mathcal{Q}_i$ must contain all or none of the edges $(v_i, v_{i+1}, -)$ with $i \in S$. Thus, for a vertex \mathbf{x}_R , either $x_i = 0$ for all $i \in S$ or $x_i = -1$ for all $i \in S$. In both cases, R is uniquely determined by its edges e_s and e_t incident to the source and sink respectively. Now φ maps \mathbf{x}_R to the unique route in $\cap_{i \in S} \widehat{G}(\nu, i)$ determined by e_s and e_t . It follows that φ restricts to a bijection between $\text{aff}(\cap_{i \in S} \mathcal{Q}_i)$ and $\text{aff}(\cap_{i \in S} \widehat{G}(\nu, i))$, with inverse φ^{-1} given by $\varphi(\mathbf{x}) = \mathbf{x} - x_w \mathbf{e}_w + x_w \sum_{i=1}^{w-1} \mathbf{e}_i$. This restriction of φ is a bijection between $\cap_{i \in S} \mathcal{Q}_i$ and $\cap_{i \in S} \widehat{G}(\nu, i)$, while mapping lattice points to lattice points. \square

For any non-empty k -subset S of $[w]$, $\cap_{i \in S} \widehat{G}(\nu, i)$ has $k-1$ less edges than $\widehat{G}(\nu, i)$. In particular, $\mathcal{F}_{\cap_{i \in S} \widehat{G}(\nu, i)}$ is a codimension $k-1$ inner face of the subdivision. Since this holds for all non-empty k -subsets of $[w]$ where $1 \leq k \leq w$, we have the following corollary.

Corollary 5.2.4. *The dual to the subdivision $\cup_{i=1}^w \mathcal{Q}_i$ of $\mathcal{F}_{\widehat{G}_B(\nu)}$ is a w -simplex. \square*

For this reason, we refer to the subdivision of Theorem 5.2.3 as the **simplex-subdivision** of $\mathcal{F}_{\widehat{G}_B(\nu)}$. We refer to the subdivision of $\Delta_a \times \Delta_b$ induced by the integral equivalence in Lemma 5.2.2 as the **simplex-subdivision induced by ν** .

Remark 5.2.5. When $\nu = (NE)^n$, projecting the simplex-subdivision of $\Delta_n \times \Delta_n$ induced by ν along the span of the vectors $\{(\mathbf{e}_i, \mathbf{e}_i) \mid i \in [n]\}$ gives Cho's subdivision of the full root polytope of type A_n in [21] (also called the Legendre polytope in [32]).

5.3 A subdivision algebra for $\Delta_a \times \Delta_b$

Using the simplex subdivision in the previous section, we can now extend the subdivision algebra from Section 2.4 as a tool to encode subdivisions of $\Delta_a \times \Delta_b$. Relaxing

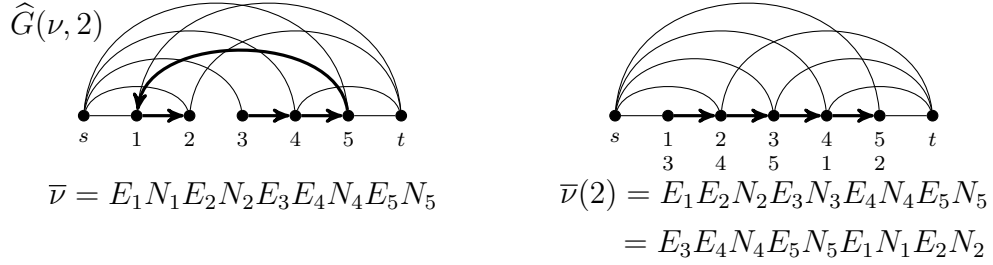


Figure 5.5: A reordering of the inner vertices of $\widehat{G}(\nu, 2)$ gives $\widehat{G}(\bar{\nu}(2), w)$ up to a relabeling of inner vertices.

the requirements on i , j , and k in the definition of the subdivision algebra (Definition 2.4.1), we obtain the following slight generalization.

Definition 5.3.1. The **subdivision algebra** $\mathcal{S}(\beta)$ is an associative and commutative algebra over the ring of polynomials $\mathbb{Z}[\beta]$, generated by the elements $\{x_{ij} \mid i \neq j\}$, subject to the relation $x_{ij}x_{jk} = x_{ik}x_{ij} + x_{jk}x_{ik} + \beta x_{ik}$, where $i \neq k$.

The terminology of reductions, reduced forms, reduction trees, basic reductions, etc. carry over naturally to this more general setting.

Given a digraph G with forward and backward edges, we associate a forward edge $(i, j, +)$ and a backward edge $(i, j, -)$ with the generators x_{ij} and x_{ji} in $\mathcal{S}(\beta)$ respectively. The graph G can then be encoded with the monomial

$$M(G) := \prod_{(i,j,+)\in E(G)} x_{ij} \prod_{(i,j,-)\in E(G)} x_{ji}.$$

Define a **cyclic peak** of a lattice path to be a consecutive NE pair in a cyclic reading of the steps in the path. In particular, the only cyclic peak which is not a peak occurs when the path begins with E and ends with N . Given a path ν , we define $\bar{\nu}(k)$ to be the path obtained by reading the steps of $\bar{\nu}$ beginning at the E step of the k -th cyclic peak. We begin counting from the first cyclic peak which is also a peak of $\bar{\nu}$. Since $\bar{\nu}$ begins with E and ends with N , the number of cyclic peaks is the same as the number of valleys in $\bar{\nu}$, with the first and last steps of $\bar{\nu}$ forming the w -th cyclic peak.

Consider the graph $G(\bar{\nu}(i), w)$, which necessarily only has forward edges. Now $\widehat{G}(\bar{\nu}(i), w)$ is the graph $\widehat{G}(\nu, i)$ up to relabeling of the inner vertices. Figure 5.5 gives an example. We also have that $\mathcal{F}_{\widehat{G}(\nu,i)} \equiv \mathcal{F}_{\widehat{G}(\bar{\nu}(i),w)}$ since changing the sign of the flow in the possible backward edge of $\mathcal{F}_{\widehat{G}(\nu,i)}$ is an integral equivalence (Lemma 5.1.2). Therefore, the reduction lemma holds for $\mathcal{F}_{\widehat{G}(\nu,i)}$, and reductions of the monomial $M(G(\nu, i))$ encode subdivisions of $\mathcal{F}_{\widehat{G}(\nu,i)}$. By the reordering of inner vertices, it is now also immediate that the reductions of $M(\cap_{i \in S} G(\nu, i))$ encode subdivisions of $\cap_{i \in S} \mathcal{Q}_i$ for any $S \subseteq [w]$. Therefore, multiplying monomials encoding faces of codimension k by β^k , we obtain the following.

Theorem 5.3.2. *The simplex-subdivision of $\mathcal{F}_{\widehat{G}_B(\nu)}$ is encoded in the polynomial*

$$p_\nu = \sum_{\substack{S \subseteq [w] \\ S \neq \emptyset}} \beta^{|S|-1} M(\cap_{i \in S} G(\nu, i))$$

where w is the number of valleys in $\bar{\nu}$. Furthermore, reducing p_ν in the subdivision algebra encodes subdivisions of $\mathcal{F}_{\widehat{G}_B(\nu)}$.

Proof. By Theorem 5.2.3, each $S \subseteq [w]$ determines a face $\cap_{i \in S} \mathcal{Q}_i$ in the simplex-subdivision of $\mathcal{F}_{\widehat{G}_B(\nu)}$ which is integrally equivalent to $\mathcal{F}_{\cap_{i \in S} \widehat{G}(\nu, i)}$. A monomial $M(\cap_{i \in S} G(\nu, i)) \beta^{|S|-1}$ then encodes a codimension $|S| - 1$ face in the subdivision. A reduction at a pair $x_{ij} x_{jk}$ encodes the cutting of the simplex subdivision of $\mathcal{F}_{\widehat{G}_B(\nu)}$ with the hyperplane determined by $x_{(i,j)} = x_{(j,k)}$. Therefore, reductions of p_ν encode subdivision of $\mathcal{F}_{\widehat{G}_B(\nu)}$. \square

By the integral equivalence in Lemma 5.2.2 we then have the following.

Corollary 5.3.3. *For a lattice path ν from $(0, 0)$ to (a, b) , reducing p_ν encodes subdivisions of $\Delta_a \times \Delta_b$.*

For each ν we have a simplex subdivision of $\Delta_a \times \Delta_b$, for which reductions of the polynomial p_ν encode refinements. Since all triangulations of a product of simplices are unimodular [27, Proposition 6.2.11], the triangulations obtained via Theorem 5.3.2 are unimodular. Triangulating each \mathcal{Q}_i separately with the subdivision algebra gives regular triangulations [46, Theorem 3]. We therefore ask the following.

Question 5.3.4. Are all the triangulations of $\Delta_a \times \Delta_b$ encoded in reduced forms of p_ν regular triangulations?

We now give an example of applying the extended subdivision algebra directly to a product of two simplices $\Delta_a \times \Delta_b$.

Example 5.3.5. Let $a = 3$ and $b = 2$. To subdivide $\Delta_3 \times \Delta_2$, we first choose a path ν from $(0, 0)$ to $(3, 2)$, say $\nu = NEENE$, and consider the canonically indexed $\bar{\nu} = E_1 N_1 E_2 E_3 N_3 E_4 N_4$. We have $I = \{1, 2, 3, 4\}$ and $J = \{1, 3, 4\}$, and $I \cap J = \{1, 3, 4\}$. Cycling the path $\bar{\nu}$ to start at its cyclic peaks we have $\bar{\nu}(1) = E_2 E_3 N_3 E_4 N_4 E_1 N_1$, $\bar{\nu}(2) = E_4 N_4 E_1 N_1 E_2 E_3 N_3$, and $\bar{\nu}(3) = E_1 N_1 E_2 E_3 N_3 E_4 N_4$. From the resulting graphs $G(\nu, i)$ for $i \in [3]$ we read the monomials $M_1 = x_{23} x_{34} x_{41}$, $M_2 = x_{41} x_{13} x_{23}$, and $M_3 = x_{13} x_{23} x_{34}$. The simplex-subdivision of $\Delta_3 \times \Delta_2$ induced by ν is encoded with

$$p_\nu = \sum_{\substack{S \subseteq [3] \\ S \neq \emptyset}} \beta^{|S|-1} \gcd\{M_i \mid i \in S\},$$

which expands to

$$p_\nu = x_{23} x_{34} x_{41} + x_{41} x_{13} x_{23} + x_{13} x_{23} x_{34} + x_{23} x_{41} \beta + x_{23} x_{34} \beta + x_{13} x_{23} \beta + x_{23} \beta^2.$$

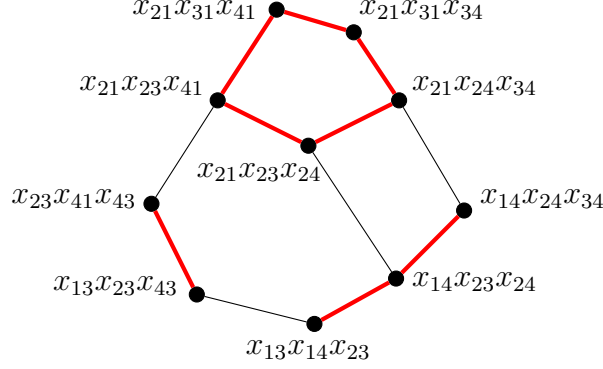


Figure 5.6: The dual graph of the triangulation obtained in Example 5.3.5. The three connected components induced by the bolded red edges are dual graphs of the triangulations of the three full dimensional cells in the simplex subdivision.

For simplicity, we consider only simple reductions by setting $\beta = 0$, and reduce $p_\nu(\beta = 0)$ as follows.

$$\begin{aligned}
p_\nu(\beta = 0) &= x_{23}x_{34}x_{41} + \mathbf{x}_{13}x_{23}\mathbf{x}_{41} + x_{13}x_{23}x_{34} \\
&= x_{23}x_{34}x_{41} + x_{13}x_{23}x_{43} + x_{23}x_{41}x_{43} + \mathbf{x}_{13}x_{23}\mathbf{x}_{34} \\
&= \mathbf{x}_{23}\mathbf{x}_{34}x_{41} + x_{13}x_{23}x_{43} + x_{23}x_{41}x_{43} + x_{13}x_{14}x_{23} + x_{14}\mathbf{x}_{23}\mathbf{x}_{34} \\
&= x_{23}\mathbf{x}_{24}\mathbf{x}_{41} + \mathbf{x}_{24}x_{34}\mathbf{x}_{41} + x_{13}x_{23}x_{43} + x_{23}x_{41}x_{43} + x_{13}x_{14}x_{23} + \\
&\quad x_{14}x_{23}x_{24} + x_{14}x_{24}x_{34} \\
&= x_{23}x_{24}x_{21} + x_{23}x_{21}x_{41} + x_{24}x_{34}x_{21} + x_{21}\mathbf{x}_{34}\mathbf{x}_{41} + x_{13}x_{23}x_{43} + \\
&\quad x_{23}x_{41}x_{43} + x_{13}x_{14}x_{23} + x_{14}x_{23}x_{24} + x_{14}x_{24}x_{34} \\
&= x_{23}x_{24}x_{21} + x_{23}x_{21}x_{41} + x_{24}x_{34}x_{21} + x_{21}x_{34}x_{31} + x_{21}x_{31}x_{41} + \\
&\quad x_{13}x_{23}x_{43} + x_{23}x_{41}x_{43} + x_{13}x_{14}x_{23} + x_{14}x_{23}x_{24} + x_{14}x_{24}x_{34}.
\end{aligned}$$

Each summand in the reduced form corresponds to a simplex, where each generator x_{ij} gives the vertex $(\mathbf{e}_i, \mathbf{e}_j)$ of the simplex, where \mathbf{e}_i and \mathbf{e}_j are the i -th and j -th standard basis vectors in \mathbb{R}^4 and \mathbb{R}^3 respectively. The simplex corresponding to the summand $x_{23}x_{24}x_{21}$ is the convex hull of vertices $(\mathbf{e}_2, \mathbf{e}_3)$, $(\mathbf{e}_2, \mathbf{e}_4)$, and $(\mathbf{e}_2, \mathbf{e}_1)$, along with the cone points of the triangulation, which are $(\mathbf{e}_k, \mathbf{e}_k)$ where $k \in I \cap J = \{1, 3, 4\}$. From the reduced form we also obtain the dual graph of the triangulation, with an edge between monomials differing by a single generator. The dual graph is shown in Figure 5.6.

We also observe the following identity.

Proposition 5.3.6. *Let ν be a lattice path from $(0,0)$ to (a,b) such that $\bar{\nu}$ has w cyclic peaks. Then*

$$\binom{a+b}{a} = \sum_{i=1}^w \text{Cat}(\nu(i)).$$

Proof. Since the volume of $\mathcal{F}_{\widehat{G}_B(\nu)}$ is $\binom{a+b}{a} = \sum_{i=1}^w \text{vol}\mathcal{Q}_i$, it suffices to show that $\text{vol}\mathcal{Q}_i$ is $\text{Cat}(\nu(i))$. However, this follows from

$$\mathcal{Q}_i \equiv \mathcal{F}_{\widehat{G}(\nu,i)} \equiv \mathcal{F}_{\widehat{G}(\bar{\nu}(i),w)} = \mathcal{F}_{\widehat{G}(\nu(i))} \equiv \mathcal{F}_{\text{car}(\nu(i))},$$

since $\text{vol}\mathcal{F}_{\text{car}(\nu(i))} = \text{Cat}(\nu(i))$ by Theorem 4.1.6. \square

Example 5.3.7. Continuing Example 5.3.5 with $a = 3$, $b = 2$, and ν being the path $NEENE$, we have $\nu(1) = ENENE$, $\nu(2) = NENEE$, and $\nu(3) = NEENE$. Thus $\text{Cat}(\nu(1)) = 5$, $\text{Cat}(\nu(2)) = 2$, and $\text{Cat}(\nu(3)) = 3$. Indeed, $\binom{2+3}{2} = 10 = 5 + 2 + 3$.

5.3.1 The ν -cyclohedron triangulations of $\mathcal{F}_{\widehat{G}_B(\nu)}$

In this section, we use the subdivision algebra to obtain a particular interesting triangulation of $\mathcal{F}_{\widehat{G}_B(\nu)}$, and thus also of a product of two simplices via the integral equivalence of Lemma 5.2.2. The triangulation in question is a geometric realization of the cyclic ν -Tamari complex (see Definition 2.6.3) and is known as the ν -cyclohedron triangulation.

We rely on the knowledge from Section 4.3.3 that the ν -Tamari complex can be obtained with the length reduction order, which reduces longer pairs first. In the cyclic setting we define the length of an edge (i,j) to be $i + n - j \pmod{n}$. A pair $x_{ij}x_{jk}$ forms a **longest pair at vertex j** if x_{ij} and x_{jk} respectively correspond with the longest incoming and outgoing edges at j . As in the non-cyclic case, the **length reduction order** is the reduction order induced by successively reducing the longest pair $x_{ij}x_{jk}$ with minimal j at each reduction step.

An arc (i,j) is said to be **maximal** if $i = 1$ and $j = n$, or $j < i$ and there is no $k \in I \cup J$ with $j < k < i$. Every cyclic (I,J) -tree has a maximal arc (i,j) where i and j are the indices of an E step and N step of cyclic peak of $\bar{\nu}$. In this way the set of cyclic peaks of $\bar{\nu}$ naturally partition the set of cyclic (I,J) -trees into $w = |I \cap J|$ disjoint sets, where each set consists of the cyclic (I,J) -trees with the same maximal arc. Furthermore, note that these w sets of cyclic (I,J) -trees can be considered as the sets of increasing (I,J) -trees induced by the paths $\bar{\nu}(i)$ for $1 \leq i \leq w$.

Theorem 5.3.8. *The triangulation of $\mathcal{F}_{\widehat{G}_B(\nu)}$ induced by reducing p_ν in the length reduction order is a geometric realization of the cyclic ν -Tamari complex.*

Proof. The monomials in p_ν are in correspondence with the graphs $G(\nu,1)$, $G(\nu,2)$, \dots , $G(\nu,w)$, along with their intersections. By Lemma 4.3.12, the reduced form of each $M(G(\nu,i))$ according to the length reduction order encodes the (I,J) -trees with maximal arc determined by the i -th cyclic peak of ν . Since any reduction order reducing longest pairs first yields the same reduced form by Lemma 4.3.13,

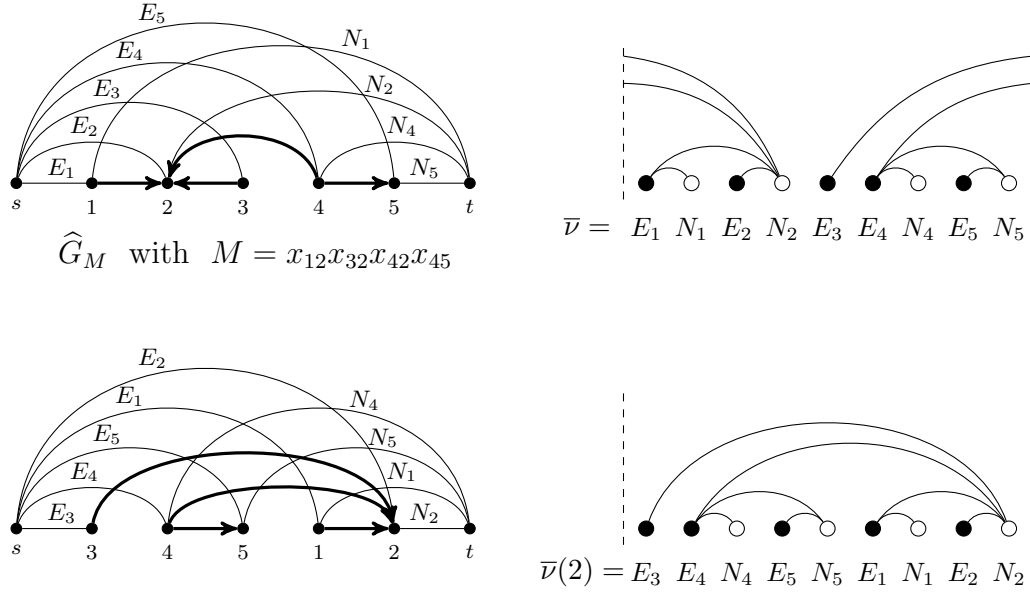


Figure 5.7: A cyclic reorientation of inner vertices corresponds with a cyclic shift of a cyclic (I, J) -tree. A route through edges labeled E_i and N_j corresponds with the arc (E_i, N_j) in the (I, J) -tree.

the simultaneous reduction of each $M(G(\nu, i))$ in the length reduction order encodes all cyclic (I, \bar{J}) -trees determined by ν . Thus the triangulation of $\mathcal{F}_{\widehat{G}_B(\nu)}$ encoded by the reduced form of p_ν has facets given by the set of cyclic (I, J) -trees determined by ν . \square

Remark 5.3.9. In the case that $\nu = (NE)^n$, Ehrenborg, Hetyei, and Readdy [32] introduced objects closely related to (I, J) -trees, which they called *valid digraphs*. The graphs corresponding to the monomials in the reduced form of p_ν under the length reduction order are a generalization of their valid graphs.

Corollary 5.3.10. *Reducing p_ν in the length reduction order gives a triangulation of $\mathcal{F}_{\widehat{G}_B(\nu)}$ whose dual graph is the Hasse diagram of the cyclic ν -Tamari poset.*

The reduction order in Example 5.3.5 was the length reduction order, and hence the dual graph of the resulting triangulation in Figure 5.6 is the Hasse diagram of the cyclic ν -Tamari poset for $\nu = NEENE$.

In the case that $\nu = E^a N^b$, there is only one valley in $\bar{\nu}$, and $G_B(\nu) = G(\nu)$. Thus $p_\nu = M(G(\nu))$, and by Theorem 4.3.14 the reduced form of p_ν in the length reduction order encodes the ν -Tamari complex (and also the cyclic ν -Tamari complex as they are the same in this case). By Proposition 4.2.11 the dual graph of this triangulation is the Hasse diagram of both $\text{Tam}(\nu)$ and the principal order ideal $I(\nu)$ of Young's lattice. The triangulation of $\Delta_a \times \Delta_b$ induced by ν in this case is a staircase triangulation of $\Delta_a \times \Delta_b$.

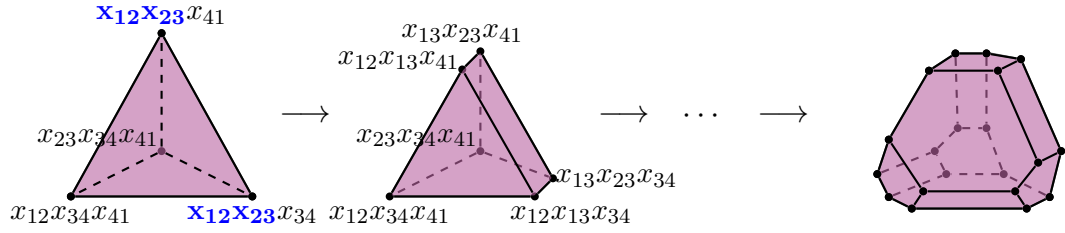


Figure 5.8: When ν is the staircase path $(NE)^n$, the cylcohedron is obtained by reducing the monomial p_ν in the length reduction order.

Remark 5.3.11. When ν is the path $(NE)^n$, reductions of p_ν can be viewed as successive truncations of an n -simplex. The truncation order induced by the length reduction order yields the cylcohedron, as shown in Figure 5.8.

Chapter 6 Future directions

There are several interesting avenues for future research which arise naturally from the work in the previous chapters. We conclude this dissertation by identifying three potentially fruitful future directions to explore.

6.1 Maximal clique posets

In Chapter 4 the ν -caracol flow polytope was the central object of study, with its length-framed and planar-framed triangulations yielding interesting dual structures. The planar framing can be described by ordering incoming edges from longest to shortest, and ordering the outgoing edges from shortest to longest. With this description of the planar framing, it naturally extends to general graphs, as does the length framing. Hence one can consider other flow polytopes arising from different graphs, and investigate the dual structures obtained with these two framed triangulations. The dual graphs of the two triangulations for the ν -caracol flow polytope have natural lattice structures, although these lattice structures were not directly induced by the triangulation in our presentation. However, it is possible to give a poset structure on maximal cliques of routes of $\text{car}(\nu)$ which induce the ν -Tamari lattice and the principal order ideal generated by ν . Let R_1 and R_2 be two routes in a framed graph (G, \prec) . Let i be the smallest vertex after which the routes differ. We order $R_1 < R_2$ if $iR_1 \prec_{\sigma(i)} iR_2$. This induces a linear order on the routes in \mathcal{R}_G . We can then define a cover relation \triangleleft on the set of maximal cliques of (G, \prec) as follows. Let C_1 and C_2 be two maximal cliques of routes which differ by a single route, that is, the symmetric difference of C_1 and C_2 is $\{R_1, R_2\}$, where $R_1 \in C_1$ and $R_2 \in C_2$. The cover relation \triangleleft is then given by $C_1 \triangleleft C_2$ if and only if $R_1 < R_2$.

Definition 6.1.1. The **maximal clique poset of (G, \prec)** is the poset of maximal cliques of routes induced by the transitive closure of the cover relation \triangleleft .

It would be interesting to study these maximal clique posets arising from different graphs. In the case of $\text{car}(\nu)$ these posets were lattices, and it would be natural to ask what properties of the underlying graph or its framing give rise to lattices. Even in the case of $\text{car}(\nu)$, it may be possible to obtain new lattice structures on ν -Catalan objects by considering different framings.

6.2 ν -Permutohedra

The associahedron and cyclohedron are both examples of generalized permutohedra, which were introduced by Postnikov in [54], and can be described as polytopes whose normal fan refine the braid fan [55]. Having encountered ν -generalizations of both associahedra and cyclohedra in this work, one can ask the following.

Question 6.2.1. Are ν -associahedra and ν -cyclohedra captured by a general theory of ν -permutohedra?

Both the associahedron and cyclohedron are also examples of graph associahedra introduced by Carr and Devadoss [14], which arise from collections of tubings on graphs. The classical associahedron is obtained from tubings on the path graph, while the cyclohedron is obtained from tubings of the cycle graph. In the setting of graph associahedra, the ν -generalizations of the classical associahedron and cyclohedron can be interpreted as arising from colorful tubings on the path graph and cycle graph respectively. This gives an avenue for considering ν -generalizations of the permutohedron, namely, as colorful tubings of the complete graph.

6.3 Applications of the subdivision algebra for $\Delta_a \times \Delta_b$

As we saw in Chapter 5, the subdivision algebra can be used to obtain triangulations of a product of two simplices. The use of this new tool for the study of products of simplices has not yet been explored. It would be interesting to know which classes of triangulations are obtainable in this way, and which ones cannot. As discussed in Section 5.3, the triangulation given by a reduced forms of p_ν restricts to regular triangulations of the subpolytopes \mathcal{Q}_i , however, the regularity of the triangulation obtained as their union remains unknown. It would be interesting to know the answer to Question 5.3.4, namely, whether the triangulations of $\Delta_a \times \Delta_b$ encoded in reduced forms of p_ν in the subdivision algebra are regular triangulations. The regularity of the triangulations of each \mathcal{Q}_i obtained by the subdivision algebra hinge on the fact that they are framed triangulations of flow polytopes. It may be possible to extend the notion of framings to the graph $G_B(\nu)$ with bidirectional edges, and then extend the regularity results of [24] to this larger setting.

Since the dual graph structure of the triangulations can easily be obtained from the monomials in a basic reductions of p_ν , the subdivision algebra provides a way to generate dual graphs of these triangulations. It could be interesting to study the class of graphs which arise as dual graphs of a product of two simplices.

As mentioned above, the associahedron and cyclohedron are both examples of generalized permutohedra, and both can now be obtained via the subdivision algebra by reductions of a polynomial. It is therefore natural to ask the following.

Question 6.3.1. Which generalized permutohedra can be obtained using the cyclic subdivision algebra?

As discussed in the beginning of Chapter 5, triangulations of a product of simplices have connections to algebraic geometry, optimization, and game theory, and they serve as building blocks for triangulations of products of polytopes more generally. Applications of the subdivision algebra in these settings remains to be explored.

Bibliography

- [1] M. Aguiar and W. Moreira. Combinatorics of the free Baxter algebra. *Electronic Journal of Combinatorics*, 13(1):Research Paper 17, 38, 2006.
- [2] F. Ardila, M. Beck, S. Hoşten, J. Pfeifle, and K. Seashore. Root polytopes and growth series of root lattices. *SIAM Journal on Discrete Mathematics*, 25(1):360–378, 2011.
- [3] F. Ardila and S. Billey. Flag arrangements and triangulations of products of simplices. *Advances in Mathematics*, 214(2):495–524, 2007.
- [4] F. Ardila and M. Develin. Tropical hyperplane arrangements and oriented matroids. *Mathematische Zeitschrift*, 262(4):795–816, 2009.
- [5] N. Arkani-Hamed, Y. Bai, S. He, and G. Yan. Scattering forms and the positive geometry of kinematics, color and the worldsheet. *Journal of High Energy Physics*, 2018(5):1–78, 2018.
- [6] D. Armstrong, N. A. Loehr, and G. S. Warrington. Rational parking functions and Catalan numbers. *Annals of Combinatorics*, 20(1):21–58, 2016.
- [7] D. Armstrong, B. Rhoades, and N. Williams. Rational associahedra and non-crossing partitions. *Electronic Journal of Combinatorics*, 20(3):Paper 54, 27, 2013.
- [8] W. Baldoni and M. Vergne. Kostant partitions functions and flow polytopes. *Transformation Groups*, 13(3-4):447–469, 2008.
- [9] M. Beck and S. Robins. *Computing the continuous discretely*, volume 61. Springer, 2007.
- [10] M. von Bell, R. S. González D’León, F. A. Mayorga Cetina, and M. Yip. A unifying framework for the ν -Tamari lattice and principal order ideals in Young’s lattice. arXiv:2101.10425, 2021.
- [11] M. von Bell and M. Yip. Schröder combinatorics and ν -associahedra. *European Journal of Combinatorics*, 98:103415, 2021.
- [12] C. Benedetti, R. S. González D’León, C. R. H. Hanusa, P. E. Harris, A. Khare, A. H. Morales, and M. Yip. A combinatorial model for computing volumes of flow polytopes. *Transactions of the American Mathematical Society*, 372(5):3369–3404, 2019.
- [13] J. Bonin, L. Shapiro, and R. Simion. Some q -analogues of the Schröder numbers arising from combinatorial statistics on lattice paths. *Journal of Statistical Planning and Inference*, 34(1):35–55, 1993.

- [14] M. Carr and S. Devadoss. Coxeter complexes and graph-associahedra. *Topology and its Applications*, 153(12):2155–2168, 2006.
- [15] C. Ceballos and R. S. González D’León. Signature Catalan combinatorics. *Journal of Combinatorics*, 10(4):725–773, 2019.
- [16] C. Ceballos, A. Padrol, and C. Sarmiento. Geometry of Tamari lattices in types A and B . *Transactions of the American Mathematical Society*, 371(4):2575–2622, 2019.
- [17] C. Ceballos, A. Padrol, and C. Sarmiento. The ν -Tamari lattice via ν -trees, ν -bracket vectors, and subword complexes. *Electronic Journal of Combinatorics*, 27(1), 2020.
- [18] C. Ceballos, F. Santos, and G. M. Ziegler. Many non-equivalent realizations of the associahedron. *Combinatorica*, 35(5):513–551, 2015.
- [19] P. Cellini and M. Marietti. Root polytopes and abelian ideals. *Journal of Algebraic Combinatorics*, 39(3):607–645, 2014.
- [20] C. S. Chan, D. P. Robbins, and D. S. Yuen. On the volume of a certain polytope. *Experimental Mathematics*, 9(1):91–99, 2000.
- [21] S. Cho. Polytopes of roots of type A_n . *Bulletin of the Australian Mathematical Society*, 59(3):391–402, 1999.
- [22] A. Conca, S. Hosten, and R. R. Thomas. Nice initial complexes of some classical ideals. *Algebraic and Geometric Combinatorics*, 423:11–42, 2006.
- [23] M. Conforti, G. Cornuéjols, and G. Zambelli. *Integer programming*, volume 271. Springer, 2014.
- [24] V. I. Danilov, A. V. Karzanov, and G. A. Koshevoy. Coherent fans in the space of flows in framed graphs. In *24th International Conference on Formal Power Series and Algebraic Combinatorics (FPSAC 2012)*, Discrete Math. Theor. Comput. Sci. Proc., AR, pages 481–490. Assoc. Discrete Math. Theor. Comput. Sci., Nancy, 2012.
- [25] J. A. De Loera. Nonregular triangulations of products of simplices. *Discrete & Computational Geometry*, 15(3):253–264, 1996.
- [26] J. A. De Loera, E. D. Kim, S. Onn, and F. Santos. Graphs of transportation polytopes. *Journal of Combinatorial Theory, Series A*, 116(8):1306–1325, 2009.
- [27] J. A. De Loera, J. Rambau, and F. Santos. *Triangulations*, volume 25 of *Algorithms and Computation in Mathematics*. Springer-Verlag, Berlin, 2010. Structures for algorithms and applications.
- [28] E. Deutsch. A bijection on Dyck paths and its consequences. *Discrete Mathematics*, 179(1-3):253–256, 1998.

- [29] S. Devadoss. Combinatorial equivalence of real moduli spaces. *Notices of the AMS*, 51:620–628, 2004.
- [30] M. Develin and B. Sturmfels. Tropical convexity. 2003. arXiv:math/0308254.
- [31] R. S. González D’León, C. R. Hanusa, A. H. Morales, and M. Yip. Column convex matrices, g -cyclic orders, and flow polytopes. arXiv:2107.07326, 2021.
- [32] R. Ehrenborg, G. Hetyei, and M. Readdy. Simion’s type B associahedron is a pulling triangulation of the Legendre polytope. *Discrete & Computational Geometry*, 60(1):98–114, 2018.
- [33] E. Ehrhart. Sur les polyèdres rationnels homothétiques à n dimensions. *Comptes rendus de l’Académie des Sciences*, 254:616–618, 1962.
- [34] P. Galashin. Poset associahedra. arXiv:2110.07257, 2021.
- [35] I. M. Gelfand, M. I. Graev, and A. Postnikov. Combinatorics of hypergeometric functions associated with positive roots. In *The Arnold-Gelfand mathematical seminars*, pages 205–221. Birkhäuser Boston, Boston, MA, 1997.
- [36] I. Gessel. Schröder numbers, large and small. CanaDAM2009 talk slides, 2009.
- [37] I. Gessel and G. Viennot. Binomial determinants, paths, and hook length formulae. *Advances in mathematics*, 58(3):300–321, 1985.
- [38] B. Grünbaum. *Convex polytopes*, volume 221. Springer Science & Business Media, 2013.
- [39] M. Haiman. A simple and relatively efficient triangulation of the n -cube. *Discrete & Computational Geometry*, 6(3):287–289, 1991.
- [40] G. Hetyei. Delannoy orthants of Legendre polytopes. *Discrete & Computational Geometry*, 42(4):705–721, 2009.
- [41] L. Hille. Quivers, cones and polytopes. *Linear Algebra and its Applications*, 365:215–237, 2003. Special Issue on Linear Algebra Methods in Representation Theory.
- [42] D. Kozlov. *Combinatorial algebraic topology*, volume 21 of *Algorithms and Computation in Mathematics*. Springer, Berlin, 2008.
- [43] C. W. Lee. The associahedron and triangulations of the n -gon. *European Journal of Combinatorics*, 10(6):551–560, 1989.
- [44] K. Mészáros. Root polytopes, triangulations, and the subdivision algebra I. *Transactions of the American Mathematical Society*, 363(8):4359–4382, 2011.
- [45] K. Mészáros. Root polytopes, triangulations, and the subdivision algebra, II. *Transactions of the American Mathematical Society*, 363(11):6111–6141, 2011.

- [46] K. Mészáros. h -polynomials via reduced forms. *Electronic Journal of Combinatorics*, 22(P4.18), 2015.
- [47] K. Mészáros. Product formulas for volumes of flow polytopes. *Proceedings of the American Mathematical Society*, 143(3):937–954, 2015.
- [48] K. Mészáros. Pipe dream complexes and triangulations of root polytopes belong together. *SIAM Journal on Discrete Mathematics*, 30(1):100–111, 2016.
- [49] K. Mészáros and A. H. Morales. Volumes and Ehrhart polynomials of flow polytopes. *Mathematische Zeitschrift*, 293(3):1369–1401, 2019.
- [50] K. Mészáros, A. H. Morales, and B. Rhoades. The polytope of Tesler matrices. *Selecta Mathematica*, 23(1):425–454, 2017.
- [51] K. Mészáros, A. H. Morales, and J. Striker. On flow polytopes, order polytopes, and certain faces of the alternating sign matrix polytope. *Discrete & Computational Geometry*, 62(1):128–163, 2019.
- [52] K. Mészáros and A. St. Dizier. From generalized permutahedra to Grothendieck polynomials via flow polytopes. *Algebraic Combinatorics*, 3(5):1197–1229, 2020.
- [53] D. Orden and F. Santos. Asymptotically efficient triangulations of the d -cube. *Discrete & Computational Geometry*, 30(4):509–528, 2003.
- [54] A. Postnikov. Permutahedra, associahedra, and beyond. *International Mathematics Research Notices*, 2009(6):1026–1106, 2009.
- [55] A. Postnikov, V. Reiner, and L. Williams. Faces of generalized permutahedra. 2006. arXiv math/0609184.
- [56] L.-F. Prévaille-Ratelle and X. Viennot. The enumeration of generalized Tamari intervals. *Transactions of the American Mathematical Society*, 369(7):5219–5239, 2017.
- [57] F. Santos. A point set whose space of triangulations is disconnected. *Journal of the American Mathematical Society*, 13(3):611–637, 2000.
- [58] F. Santos. Personal communication. 2021.
- [59] R. Simion. A type- b associahedron. *Advances in Applied Mathematics*, 30(1-2):2–25, 2003.
- [60] C. Song. The generalized Schröder theory. *Electronic Journal of Combinatorics*, 12:Research Paper 53, 10, 2005.
- [61] R. P. Stanley. Decompositions of rational convex polytopes. *Annals of Discrete Math*, 6(6):333–342, 1980.
- [62] R. P. Stanley. Two poset polytopes. *Discrete & Computational Geometry*, 1(1):9–23, 1986.

- [63] R. P. Stanley. A monotonicity property of h-vectors and h*-vectors. *European Journal of Combinatorics*, 14(3):251–258, 1993.
- [64] R. P. Stanley. *Enumerative combinatorics. Volume 1*, volume 49 of *Cambridge Studies in Advanced Mathematics*. Cambridge University Press, Cambridge, second edition, 2012.
- [65] R. P. Stanley. *Catalan numbers*. Cambridge University Press, 2015.
- [66] R. P. Stanley and J. Pitman. A polytope related to empirical distributions, plane trees, parking functions, and the associahedron. *Discrete & Computational Geometry.*, 27(4):603–634, 2002.
- [67] J. D. Stasheff. Homotopy associativity of h-spaces. i. *Transactions of the American Mathematical Society*, 108(2):275–292, 1963.
- [68] B. Sturmfels. *Gröbner bases and convex polytopes*, volume 8. American Mathematical Soc., 1996.
- [69] M. Yip. A Fuss-Catalan variation of the caracol flow polytope. arxiv:1910.10060.
- [70] D. Zeilberger. Proof of a conjecture of Chan, Robbins, and Yuen. *Electronic Transaction on Numerical Analysis*, 9(147-148):1–2, 1999.
- [71] G. M. Ziegler. *Lectures on polytopes*, volume 152. Springer Science & Business Media, 2007.

Vita

Matias Kaspar von Bell

Place of Birth:

- Espoo, Finland

Education:

- University of Kentucky, Lexington, KY
M.A. in Mathematics, Dec. 2019
- University of Helsinki, Helsinki, Finland
M.S. in Mathematics, May 2016
eximia cum laude
- Asbury University, Wilmore, KY
B.A. in Mathematics, May 2012
cum laude

Professional Positions:

- Graduate Teaching Assistant, University of Kentucky
Fall 2016 – Spring 2022

Honors

- Carl Lee Excellence in Teaching Award, University of Kentucky
- Cliff Swauger Jr. Summer Graduate Fellowship, University of Kentucky
- Max Steckler Fellowship, University of Kentucky

Publications & Preprints:

1. *Schröder combinatorics and ν -associahedra* (with M. Yip), *European Journal of Combinatorics* 98 (2021): 103415.
2. *On framed triangulations of flow polytopes, the ν -Tamari lattice, and Young's lattice* (with R. S. González D'León, F. Mayorga Cetina, and M. Yip). *Séminaire Lotharingien de Combinatoire. Proceedings of the 33rd international conference on Formal Power Series and Algebraic Combinatorics*, Ramat-Gan, Israel (2021).
3. *A unifying framework for the ν -Tamari lattice and principal order ideals in Young's lattice* (with R. S. González D'León, F. Mayorga Cetina, and M. Yip). arXiv ID: 2101.10425. (2021)

4. *Triangulations, order polytopes, and generalized snake posets* (with B. Braun, D. Hanely, K. Serhiyenko, J. Vega, A. Vindas-Meléndez, M. Yip).
arXiv ID: 2102.11306. (2021)
5. *Triangulations of flow polytopes, ample framings, and gentle algebras* (with B. Braun, K. Bruegge, D. Hanely, Z. Peterson, K. Serhiyenko, and M. Yip).
arXiv ID: 2203.01896. (2022)